UNIVERSIDADE DE LISBOA
FACULDADE DE CIÊNCIAS
DEPARTAMENTO DE ENGENHARIA GEOGRÁFICA, GEOFÍSICA E ENERGIA

THE ROLE OF REMOTE SENSING IN ASSESSING THE IMPACT OF CLIMATE VARIABILITY ON VEGETATION DYNAMICS IN EUROPE

Célia Marina Pedroso Gouveia

Doutoramento em Ciências Geofísicas e da GeoInformação

(Detecção Remota)

2008

UNIVERSIDADE DE LISBOA
FACULDADE DE CIÊNCIAS
DEPARTAMENTO DE ENGENHARIA GEOGRÁFICA, GEOFÍSICA E ENERGIA

THE ROLE OF REMOTE SENSING IN ASSESSING THE IMPACT OF CLIMATE VARIABILITY ON VEGETATION DYNAMICS IN EUROPE

Célia Marina Pedroso Gouveia

Doutoramento em Ciências Geofísicas e da GeoInformação

(Detecção Remota)

Tese orientada pelo Professor Doutor Carlos da Camara,
Professor Associado do Departamento de Física da
Faculdade de Ciências da Universidade de Lisboa
e pelo Professor Doutor Ricardo Machado Trigo,
Investigador Auxiliar do Instituto D. Luiz

2008

to my father

ACKNOWLEDGEMENTS

My first words of acknowledgment are for my supervisors. To Prof. Carlos da Camara I am grateful for accepting being my supervisor and for introducing me into Remote sensing; indeed, I have learned more than advanced techniques of colouring! His words of friendship, never-ending optimism and senses of humour made this work much more interesting. Our science-related discussions, his advices and suggestions, made me 'grow up'.

I am especially indebted to Prof. Ricardo Trigo to whom I thank the support, dedication, involvement and suggestions; that without them this work would not have ever arrived to a safe harbour. His words and friendship in crucial moments of this long way showed me the light at the end of the tunnel.

To my PhD colleague and friend, Margarida L. R. Liberato, I thank her unconditional friendship, patience and support, our long and fruitful scientific discussions, which helped overcoming difficulties.

I may not forget Teresa Calado, to whom I thank her suggestions, friendship and support, which eased this work. To Dulce Lajas I thank for her friendship and support, so important at the initial stage of this research. To Renata Libonati and Leonardo Peres I thank our scientific discussions so important that proved that friendship is at the distance of a click. I also would like to thank Alexandre Ramos, Joana Freire, Telmo Frias and David Barriopedro for their friendship.

I am grateful to Escola Superior de Tecnologia and Instituto Politécnico de Setúbal, where I have been teaching since 1999, for granting a six-month leave for full time scientific research, so important at the final stage of this work, as well as for supporting my participation at International Scientific Conferences and Workshops where I have presented scientific results from this research. A word of acknowledgment is also due to my colleagues at the Departamento de Energia Mecânica who have always motivated

me to pursue these studies, in particular Fernando Cunha, Luis Ferro, Luis Coelho and Miguel Cavique. To Margarida Lopes I thank for her precious teaching collaboration.

Last, but not the least, a very special word of acknowledgement to my family and close friends for their understanding and help provided during this long path. To Débora and Miguel for the time we did not spend together, during which they grow and became adults. To my sister and my parents, for all the motivation incentive encouragement, help and support they have always provided; without it this work would have been impossible. A very special thought towards my mother who taught me to dream and also showed me that depending on our will dreams may become true.

To my husband, Rogério, who has always accompanied me along this course, as along the other paths, and with whom I have been sharing good and bad moments of all these years, I wish to thank for all his support, help and love without which all this effort would not make sense. This work is also a bit of him! To Duarte, who cannot understand yet why mummy likes doing "such things" so much, I want to thank his patience, understanding and care for what we could not do together, but mainly for what we managed to do. These prove that, after all, he has been my master piece (once again shared with my husband).

Finally, to my Father, who has always believed that I would accomplish this goal and would certainly have a smile of proud on his lips. Unfortunately he did not live to see this day. To him, that I miss so much, I dedicate this work.

The Portuguese Foundation of Science and Technology (FCT) partially supported this research (Grant SFRH / BD / 32829 / 2006).

ABSTRACT

The study aims at investigating the relationship between climate variability and vegetation dynamics by combining meteorological and remote-sensed information. The vegetation response to both precipitation and temperature in two contrasting areas (Northeastern Europe and the Iberian Peninsula) of the European continent is analysed and special attention is devoted to the impact of the North Atlantic Oscillation (NAO) on the vegetative cycle in the two regions which is assessed taking into account the different land cover types and the respective responses to climate variability.

An analysis is performed of the impact of climate variability on wheat yield in Portugal and. the role of NAO and of relevant meteorological variables (net solar radiation, temperature and precipitation) is investigated. Using spring NDVI and NAO in June as predictors, a simple regression model of wheat yield is built up that shows a general good agreement between observed and modelled wheat yield values.

The severity of a given drought episode in Portugal is assessed by evaluating the cumulative impact over time of negative anomalies of NDVI. Special attention is devoted to the drought episodes of 1999, 2002 and 2005. While in the case of the drought episode of 1999 the scarcity of water in the soil persisted until spring, the deficit in greenness in 2005 was already apparent at the end of summer. Although the impact of dry periods on vegetation is clearly noticeable in both arable land and forest, the latter vegetation type shows a higher sensitivity to drought conditions.

Persistence of negative anomalies of NDVI was also used to develop a procedure aiming to identify burned scars in Portugal and then assess vegetation recovery over areas stricken by large wildfires. The vulnerability of land cover to wildfire is assessed and a marked contrast is found between forest and shrubland vs. arable land and crops. Vegetation recovery reveals to strongly depend on meteorological conditions of the year following the fire event, being especially affected in case of a drought event.

Keywords: Remote sensing, Vegetation dynamics, Wheat yield, Vegetation recovery, Burned areas, Climate Variability, North Atlantic Oscillation, Drought persistence.

RESUMO

Os ecossistemas terrestres têm vindo a ser objecto de interesse crescente devido ao papel que desempenham no controlo e forçamento do sistema climático à escala global. Responsáveis pelo armazenamento e libertação de diversos gases com efeito de estufa, tais como o dióxido de carbono (CO_2), o metano e o óxido nitroso, os ecossistemas terrestres encontram-se, por sua vez, sujeitos localmente à influência do clima. Tais interacções traduzem-se numa multiplicidade de mecanismos de *feedback* entre o ciclo do carbono e o clima, os quais podem ser atenuados ou amplificados pela variabilidade climática às escalas regional e global. Neste contexto, destaca-se o papel da vegetação, dada a quantidade elevadíssima de carbono que é armazenada na própria vegetação e na matéria orgânica.

Recentemente, um número crescente de trabalhos tem vindo a pôr em evidência a resposta das componentes terrestres do ciclo do carbono às variações e tendências do sistema climático à escala global. Heimann e Reichstein (2008) mostraram que a forte variabilidade interanual da taxa global de crescimento médio de CO_2 atmosférico está correlacionada fortemente com o índice El-Niño-Oscilação do Sul. Este controlo parece estar relacionado com o impacto de eventos extremos na vegetação da Amazónia ocidental e do sudeste da Ásia, conduzindo a uma perda do carbono pela floresta devido à diminuição da produtividade fotossintética e/ou ao aumento da respiração.

Ao estudar o impacto do clima no balanço do carbono assume-se que a sequestração de CO_2, pela fotossíntese, é estimulada pelo aumento de temperatura e pelo próprio aumento de CO_2 (Davidson e Janssens, 2006), tendo-se que estes processos – que ocorrem essencialmente nas florestas da região boreal e das regiões temperadas – devem atingir a saturação para valores elevados da temperatura e da concentração de CO_2. Acontece, porém, que a respiração responde de forma exponencial às variações da temperatura, mas não é sensível aos níveis do CO_2. Assim, parece ser a própria biosfera que fornece um mecanismo de *feedback* negativo para o aumento da temperatura e do CO_2, o qual permanecerá activo enquanto o efeito de estimulação da temperatura exceder o efeito de fertilização do CO_2 (Denman et al., 2007). Por outro lado, numa terra aquecida, será de esperar um aumento da evaporação, conducente a um balanço

negativo da água, o qual será mitigado pela diminuição da perda da água nos estomas das plantas, característica de um mundo com excesso de CO_2. Desta forma, o resultado líquido dependerá essencialmente da capacidade de armazenamento de água pelo solo, da distribuição vertical do carbono e das raízes no solo e da sensibilidade geral da vegetação às condições de stress hídrico (Heimann e Reichstein, 2008), tendo-se que as limitações em água podem até suprimir a resposta da respiração à temperatura. (Reichstein et al., 2007). Sob condições de seca severa, alguns cenários climáticos apontam para um aumento do sequestro do carbono através da supressão da respiração, bem como da redução da perda de carbono devido à diminuição da actividade fotossintética (Ciais et al., 2005; Saleska et al., 2003).

Acontece que a biosfera não responde unicamente às variações das variáveis climáticas médias, mas também – e sobretudo – às flutuações e à variabilidade dessas variáveis, as quais, por sua vez, se encontram relacionadas com a ocorrência de eventos extremos. Um bom exemplo desta dependência foi a recente onda de calor que assolou a Europa durante o Verão de 2003; tendo-se que a acumulação de carbono durante os cinco anos precedentes, foi anulada em apenas alguns dias de condições atmosféricas extremas. Ciais et al. (2005) mostraram que a respiração, em vez de aumentar com a temperatura, diminuiu juntamente com a produtividade, tendo aqueles autores destacado ainda que as secas e as ondas de calor podem modificar a produtividade da vegetação e transformar, por curtos períodos, sumidouros em fontes, conduzindo, desta forma, a um mecanismo de *feedback* positivo do sistema climático. Os efeitos prejudiciais de tais eventos extremos podem mesmo ser amplificados por meio de impactos retardados, tais como aqueles associados à morte das árvores e à recuperação lenta da vegetação em caso de incêndios florestais (Heimann e Reichstein, 2008; Le Page et al., 2008).

Nas latitudes elevadas, as variações na sazonalidade da temperatura têm vindo a induzir Invernos amenos e Primaveras antecipadas, conduzindo a um derretimento dos gelos e a um florescimento da vegetação prematuros e, portanto, a uma maior vulnerabilidade às geadas (Myneni et al., 1997; Zhou et al., 2001). Por outro lado, os aumentos de temperatura observados, na Primavera e no Outono das latitudes elevadas do Hemisfério Norte, conduzem a um aumento da extensão da estação de crescimento e a uma maior actividade fotossintética, a qual poderá afectar o ciclo sazonal do carbono. Enquanto que na Primavera a fotossíntese prevalece sobre a respiração, já no Outono acontece o oposto e, por conseguinte, será na Primavera que se espera a ocorrência do sequestro de CO_2 (Piao et al., 2008). No futuro – e caso se verifique um aquecimento

mais acelerado no Outono – a capacidade de sequestro do carbono pelos ecossistemas do Norte poderá diminuir mais rapidamente do que se previa (Sitch et al., 2008).

Por sua vez, as variações temporais na velocidade de vento, na temperatura do ar, no stress hídrico e na humidade podem induzir variações na frequência e na severidade dos fogos florestais e, consequentemente, originar a libertação para a atmosfera, em apenas alguns minutos, de enormes quantidades do carbono, que foram acumuladas no solo e na vegetação durante séculos (Shakesby et al., 2007; Michelsen et al., 2004). Acresce que fogos florestais mais frequentes e mais intensos reduzem a biomassa e a produtividade da camada superficial do solo, o que leva à erosão e à diminuição do biodiversidade e, em última análise, conduzirá à degradação dos solos. Por outro lado, em regiões áridas e semi-áridas, e durante períodos secos, as espécies herbáceas altamente combustíveis tendem a competir com a vegetação nativa, tornando estas áreas mais vulneráveis ao fogo, devido à acumulação de biomassa seca altamente inflamável. Por sua vez, a reincidência de incêndios pode induzir alterações na estrutura do coberto vegetal, convertendo a vegetação nativa em espaços florestais degradados.

A detecção remota afigura-se presentemente como uma ferramenta muito útil para a monitorização, à escala global e a custo relativamente baixo, da dinâmica e do stress da vegetação, bem como da desflorestação e das alterações na utilização do solo. O aparecimento de novas plataformas, sensores e satélites tem vindo a suscitar um esforço notável com vista ao desenvolvimento de métodos mais sofisticados e de algoritmos mais aperfeiçoados com o objectivo de proceder a uma homogeneização das séries temporais e de integrar observações da natureza diferente. Um bom exemplo é dado pelo *Global Inventory Monitoring and Modelling System* (GIMMS), que proporciona actualmente à comunidade científica mais de vinte anos de dados com 8 km de resolução, baseados na informação proveniente dos satélites da série AVHRR/NOAA. A Europa, por sua vez, encetou uma iniciativa complementar, através do sistema VEGETATION que, desde o final de 1998, tem vindo a fornecer dados acerca das características da superfície do solo, com 1 km de resolução, baseada na informação proveniente do sensor VEGETATION a bordo dos satélites SPOT. De referir, ainda, o esforço adicional que tem vindo a ser efectuado no sentido de se proceder ao desenvolvimento de diversos índices da vegetação – de que merece destacar-se o NDVI – elaborados especificamente para quantificar diversos aspectos relacionados com as concentrações da vegetação verde e a identificação de locais onde a vegetação é saudável ou se encontra sujeita a stress térmico ou hídrico.

A presente tese tem por objectivo contribuir para uma melhor compreensão do impacto da variabilidade climática na dinâmica da vegetação à escala europeia, com especial ênfase nos aspectos particulares que ocorrem em Portugal continental e dando-se especial atenção à análise da relação entre a actividade fotossintética e a Oscilação do Atlântico Norte (NAO) já que esta constitui o modo principal de variabilidade climática do Hemisfério Norte. Assim – e no seguimento de diversos estudos que abordaram alguns aspectos da relação da NAO com a dinâmica da vegetação à escala europeia (D'Odorico et al., 2002; Cook et al., 2004; Stöckli and Vidale, 2004; Vicente Serrano and Heredia Laclaustra, 2004) – procedeu-se a uma análise sistemática de duas regiões com comportamentos contrastantes, a saber a Península Ibérica e o Nordeste da Europa. A análise, que abarcou um período de 21 anos (1982-2002), foi efectuada a partir de compósitos mensais de NDVI e da temperatura do brilho da série de dados GIMMS, bem como da precipitação mensal disponibilizada pelo *Global Precipitation Climatology Centre* (GPCC). Para o referido período de 21 anos, procedeu-se a um estudo sistemático dos campos de correlação pontual entre os valores de Inverno da NAO e os correspondentes valores da Primavera e do Verão do NDVI, tendo-se ainda analisado, nas duas regiões referidas, a resposta da vegetação às condições de precipitação e de temperatura de Inverno. No caso da Península Ibérica, os resultados do estudo efectuado evidenciaram que valores (negativos) positivos da NAO de Inverno induzem (elevada) baixa actividade da vegetação na Primavera e no Verão seguintes, estando este comportamento associado ao impacto da NAO na precipitação do Inverno, conjuntamente com a forte dependência da vegetação da Primavera e do Verão da disponibilidade de água durante o Inverno precedente. Já no Nordeste da Europa se observou um comportamento diferente, com valores (negativos) positivos da NAO de Inverno a induzirem valores (baixos) elevados de NDVI na Primavera e valores (elevados) baixos de NDVI no Verão, comportamento este resultante principalmente do forte impacto da NAO na temperatura do Inverno, associado com a dependência do crescimento da vegetação do efeito combinado de condições amenas e da disponibilidade de água ocorridas no Inverno. Na Península Ibérica, observou-se ainda que o impacto da NAO é maior nas zonas não florestadas, já que estas respondem mais rapidamente às variações espaço-temporais da humidade do solo e da precipitação. No Nordeste da Europa, o impacto da NAO é especialmente notório durante os primeiros meses do ano, sugerindo que o crescimento da vegetação verde tende a ocorrer mais

cedo e intensamente nos anos de fase positiva da NAO, devido às condições relativamente mais amenas associadas a um derretimento prematuro do coberto de gelo.

Os resultados obtidos – em particular aqueles que respeitam à relação entre a NAO de Inverno e o NDVI da Primavera e do Verão – representam um importante valor acrescentado, na medida em que proporcionam uma antevisão global do estado da vegetação, passível de diversas aplicações que incluem a formulação de previsões a curto prazo da produtividade de culturas e a previsão a longo prazo de risco de incêndios florestais. Neste contexto – e no seguimento de diversos estudos em que se procede ao estudo de relações entre o rendimento de culturas e a distribuição espaço-temporal de variáveis meteorológicas relevantes (Maytelaube et al. 2004; Atkinson et al., 2005; Iglesias and Quiroga, 2007, Rodríguez-Puebla et al., 2007) – analisou-se a produtividade de trigo no Alentejo e suas relações com o regime meteorológico do ano agrícola. O estudo foi suscitado pelo facto de se terem encontrado no Alentejo, para o período 1982-1999, correlações fortemente negativas entre a produtividade do trigo e o NDVI da Primavera obtido a partir da base de dados GIMMS. O impacto dos factores meteorológicos na produtividade do trigo naquela região foi, por sua vez, avaliado através do cálculo de correlações mensais das anomalias da produtividade do trigo com a radiação solar, a temperatura e a precipitação, bem como com a NAO. Os resultados obtidos indicam que temperaturas frias durante o Inverno e uma Primavera antecipada, juntamente com a ocorrência de precipitação em Fevereiro e Março e a disponibilidade de radiação solar em Março, têm um impacto positivo durante a fase de crescimento, tendo-se ainda que um valor elevado do índice NAO em Junho é benéfico para o estádio de maturação do grão. Com base nas relações obtidas, procedeu-se à elaboração de um modelo simples (de regressão linear multivariada) da produção de trigo, utilizando como predictores os valores de NDVI da Primavera e da NAO de Junho. Os resultados da validação cruzada confirmaram o bom desempenho do modelo, que se antevê possa vir a ser melhorado quando estendido a um período mais alargado.

Os campos de NDVI derivados do sensor VEGETATION foram, por sua vez, utilizados para monitorizar episódios de seca em Portugal continental, estudo este motivado pelo recente reconhecimento da existência de uma forte dependência da dinâmica da vegetação, na região do Mediterrâneo, da disponibilidade em água (Eagleson, 2002, Rodríguez-Iturbe and Porporato, 2004, Vicente-Serrano and Heredia-Laclaustra, 2004, Vicente-Serrano, 2007). Nesta conformidade, a severidade de um dado episódio de seca foi avaliada através da persistência temporal das condições de

stress hídrico da vegetação – traduzida pelo número de meses em que se observa uma anomalia negativa do NDVI num determinado período de tempo – tendo-se dado atenção especial ao episódio de seca de 2005, bem como aos episódios ocorridos em 1999 e em 2002. O impacto da humidade do solo na dinâmica da vegetação foi ainda avaliado através do estudo do ciclo anual do *Soil Water Index* (SWI) em função do NDVI, tendo-se observado que, no caso do ano de 1999, a escassez de água no solo persistiu até à Primavera, enquanto que, no episódio de 2005, o stress da vegetação já era visível no final do Verão. Igualmente se avaliou o impacto dos períodos secos nos diferentes tipos de coberto vegetal, tendo-se observado, em particular, que a terra arável apresenta maior sensibilidade do que a floresta.

O problema da recuperação da vegetação após um episódio de fogo florestal tem vindo a ser objecto de um considerável número de estudos realizados para as regiões do Mediterrâneo e baseados em informação proveniente de detecção remota (Jakubauskas et al., 1990; Viedma et al., 1997; Díaz-Delgado et al., 1998; Henry and Hope, 1998; Ricotta et al., 1998). Seguindo o exemplo de alguns autores que têm utilizado o NDVI para proceder à monitorização da recuperação do coberto vegetal (Paltridge and Barber, 1988; Viedma et al., 1997; Illera et al., 1996), novamente se recorreu à persistência das anomalias negativas de NDVI para simultaneamente desenvolver uma metodologia que permitisse a identificação de áreas queimadas e avaliasse a capacidade de recuperação da vegetação nas áreas ardidas. A metodologia desenvolvida revelou-se adequada para ambos os propósitos no caso de áreas afectadas por incêndios florestais de grandes dimensões, tendo os resultados obtidos apontado para uma muito maior vulnerabilidade ao fogo das zonas de floresta e de mato, em contraste com o observado nas zonas de terra arável e culturas. No que respeita à recuperação da vegetação nas áreas afectadas por fogos florestais, observou-se que a recuperação depende em larga medida das condições meteorológicas durante o ano que se segue ao fogo, em particular das condições de aridez. De facto, verificou-se que a recuperação da vegetação foi especialmente lenta em 2003, por causa da seca que se seguiu em 2004/2005, sobretudo nas áreas ardidas na região do Algarve onde os efeitos da seca foram mais severos.

Palavras chave: Detecção Remota, Dinâmica da Vegetação, Produtividade do Trigo em Portugal, Recuperação da Vegetação, Áreas Ardidas, Variabilidade Climática, Oscilação do Atlântico Norte, Secas, Severidade, Persistência de Secas

TABLE OF CONTENTS

LIST OF FIGURES

LIST OF TABLES

LIST OF ACRONYMS

AVHRR	Advanced Very High Resolution Radiometer
CLC2000	Corine Land Cover 2000
CNES	Centre National d'Etudes Spatiales
CORINE	COoRdinate INformation on the Environment
CRU	Climate Research Unit
DFRF	Direcção Geral dos Recursos Florestais
EEA	European Environment Agency
EMD	Empirical Mode Decomposition
ERS	European Remote Sensing
FAO	Food and Agriculture Organization
GAC	Global Area Coverage
GEWEX	Global Energy and Water Cycle Experiment
GIMMS	Global Inventory Monitoring and Modelling System
GIS	Geographical Information System
GLAM	Global Agriculture Monitoring
GLC2000	Global Land Cover 2000
GPCC	Global Precipitation Climatology Centre
HRPT	High Resolution Picture Transmission
HRV	High Resolution Visible
HRVIR	High Resolution Visible and Infrared
IB	IBerian peninsula
IFOV	Instantaneous Field of View
INE	Instituto Nacional de Estatística
ISEGI	Instituto Superior de Estatística e Gestão da Informação
JRC	Joint Research Center
LAC	Local Area Coverage
LST	Local Solar Time
MAM	March, April and May

MODIS	MODerate Resolution Imaging Spectroradiometer
MS	MultiSpectral mode
MSU	Microwave Sounding Unit
MVC	Maximum Value Composite
NASA	National Aeronautics and Space Administration
NDVI	Normalised Difference Vegetation Index
$NDVI_{SPR}$	SPRing NDVI
$NDVI_{SUM}$	SUMmer NDVI
NE	Northeastern Europe
NHCP	NAO High Correlated Pixels
NAO	North Atlantic Oscillation
NIMA	United States National Imagery and Mapping Agency
NIR	Near InfraRed
NOAA	US National Oceanic and Atmospheric Administration
PAN	PANchromatic mode
PDSI	Palmer Drought Severity Index
P_{NAO}	Precipitation corresponding to the winter NAO index
SPOT	Satellite Pour l'Observation de la Terre
SWI	Soil Water Index
SWIR	ShortWave InfraRed
TIR	Thermal InfraRed
T_{NAO}	Temperature corresponding to the winter NAO index
TOVS	TIROS Operational Vertical Sounder
USDA/FAS	United States Department of Agriculture/Foreign Agricultural Service
UTM	Universal Transverse Mercator
VGT	VEGETATION
VGT-NDVI	NDVI using VGT
VGT-P	VGT Physical products
VGT-S	VGT Synthesis products
VI	Vegetation Index
VIS	VISible
WCRP	World Climate Research Program
WMO	World Meteorological Organization

1. INTRODUCTION

Terrestrial ecosystems are of primary importance as they exert control and can partially drive the climate system at the global scale. Among other climate related impacts, terrestrial ecosystems are responsible for the storage and release of greenhouse gases, such as carbon dioxide (CO_2), methane and nitrous oxide. However terrestrial ecosystems themselves are subject to the influence of local climate, leading to a multiplicity of feedback mechanisms between carbon cycle and climate, which may in turn be attenuated or intensified by regional and global climate variability. The role played by vegetation becomes decisive in this context because of the large quantities of carbon that are stored in vegetation and organic matter. When released into the atmosphere, in CO_2 form, stored carbon may have strong impacts on global climate. Since carbon discharges, such as those resulting from the combustion of fossil fuel and in land-use changes, are mainly due to human activities, forest has become a major carbon source either in a direct or in an indirect way.

As carbon changes are a major driver of climate change, it has become essential to understand in detail how terrestrial ecosystems may gain carbon through photosynthesis and lose it via autotrophic and heterotrophic respiration (as well as by volatile organic compounds, methane and dissolved carbon, in less but not neglected amounts). Quantifying and predicting the carbon cycle and modelling climate feedbacks is not an easy task, mainly because of the present limited knowledge about the geobiochemical processes that transform/recycle the carbon inside the climate system (Heimann and Reichstein, 2008).

In recent years a growing number of works has provided strong evidence that the terrestrial components of the carbon cycle are responding to global climate changes and trends. Heimann and Reichstein (2008) have shown that the strong interannual variability of globally averaged growth rate of atmospheric CO_2 is highly correlated with the El-Niño-Southern Oscillation index. This control appears be related with the

impact of extreme events on the health of vegetation of Western Amazonia and Southeastern Asia, leading to a loss of carbon by forest due to the decrease of photosynthetic productivity and/or increase in respiration. In this context, when studying the climate impact on carbon budget it is usually assumed that the CO_2 uptake, by photosynthesis, is stimulated by the increases in both the CO_2 itself and in temperature (Davidson and Janssens, 2006). These processes that essentially occur in boreal forests and temperate regions are expected to saturate at high values of CO_2 concentration and temperature. On the other hand, respiration responds exponentially to temperature changes, but is not sensitive to CO_2 levels. This may indicate that the biosphere provides a negative feedback to the increase of temperature and CO_2 until temperature is so high that the stimulation of respiration exceeds the fertilization effect of CO_2. However the full process may be even more complex if we take into account the complex mechanisms that occur in soil layers. Furthermore, other climatic and environmental factors may modify the carbon balance (Denman et al, 2007).

The primary productivity in the majority of the terrestrial ecosystems is limited by water availability, which means that significant changes in precipitation may have a strong impact on the dynamics of the carbon cycle. Changes in frequency and occurrence of precipitation (even without changes in the total annual amount) may be decisive to photosynthetic productivity because the precipitation regime determines when the water will be used and transpired by vegetation or just runoff and evaporate (Knapp et al., 2002). On other hand, in a warmer Earth, an increase of evaporation is expected, leading to a negative water balance, whereas the diminishing of loss of water by plant stomata in a world with a surplus of CO_2 will mitigate the previous effect. As a consequence, the net result will mainly depend on the water holding capacity of the soil, as well as on the vertical distribution of carbon and roots in the soil and on the general sensitivity of vegetation to drought (Heimann and Reichstein, 2008). Water limitations may even suppress the response of respiration to temperature (Reichstein et al., 2007). Under drier conditions, some climate change scenarios give an indication of an increasing of carbon sequestration, by respiration suppression, as well as of a reducing of carbon loss due to the decrease of photosynthetic productivity (Ciais et al., 2005; Saleska et al., 2003).

It is a well establish fact that the biosphere does not solely respond to changes in average climatic variables, but its changes are mainly associated to fluctuations and to variability of climatic variables, which in turn are related to the occurrence of extreme

events. A good example was the recent heat wave that stroke Europe during the summer of 2003; the carbon sequestration that occurred in the previous five years was annihilated in just a few days of extreme weather conditions. Ciais et al. (2005) have shown that, rather than accelerating with temperature rise, respiration has decreased together with productivity. These authors have highlighted that droughts and heat waves may modify the health and productivity of vegetation and transform, albeit for a short period, sinks into sources, leading to a short-term positive carbon-climate feedback. It may be noted that these mechanisms are related to the productivity rates of cultures, mainly in regions where artificial irrigation is not employed and for crops with vegetative cycles that do not coincide with the extreme heat. The negative effects of such extreme events may be even amplified by lagged impacts, such as those associated to tree death and the slow recovery of vegetation in case of wildfires (Holmgren et al., 2006; Heimann and Reichstein, 2008, Le Page et al., 2008).

Changes in temperature seasonality may have induced the occurrence of mild winters and early springs in high latitudes, leading to an early melting and flowering and, consequently, to a higher vulnerability to frost (Myneni et al., 1997; Zhou et al., 2001). On the other hand, the observed increases of temperature in spring and autumn over high latitude regions of the Northern Hemisphere leads inevitably to larger growing seasons and to higher photosynthetic activity and therefore strongly affecting the carbon seasonal cycle. However the processes that take place in spring and in autumn have a different nature. Whereas in spring photosynthesis dominates respiration, the opposite takes place in autumn and therefore it is in spring that an increase in CO_2 sequestration is expected to occur (Piao et al., 2008). Accordingly, in the future and in case the autumn warming occurs faster than the spring warming, the ability of carbon sequestration by Northern ecosystems may decrease faster than previously suggested (Sitch et al., 2008). However, changes in the seasonality of temperature and precipitation may have distinct impacts, depending on local characteristics.

Temporal changes in wind speed, air temperature, water stress and humidity may change the frequency and severity of wildfires with the consequent release, in a few minutes, of enormous quantities of carbon, into the atmosphere, that have been accumulated in soil and vegetation during centuries (Shakesby et al., 2007; Michelsen et al., 2004). More frequent and intense forest fires reduce biomass and productivity of the surface layer of soil, leading to erosion and decrease of biodiversity and finally to soil degradation. Recent observations in different regions have related fire severity to

summers drought; persistent droughts tend to intensify land degradation due to land use pressure, setting conditions, when rainfall starts, for the spreading and for a faster growing of highly flammable wild plants (Dube, 2007; Holmgren and Scheffer, 2001). In arid and semi-arid regions, and during dry periods, the highly flammable herbaceous species tend to compete with native vegetation. With the increase of meteorological fire risk, these areas tend to become more vulnerable to wildfires, due to the accumulation of highly flammable dry biomass. Repeated fires may in turn induce changes in vegetation structure, by converting the native vegetation into shrub-woodland vegetation (Brooks and Pyke, 2002; Sheuyange et al., 2005).

A solid understanding of vegetation dynamics and climate variability becomes therefore crucial for the integration of the carbon cycle into the climate system and for the establishment of links between land use changes and extreme events, namely droughts and wildfires. In such a wide and complex context, remote sensing has become a very useful tool to monitor, at the global scale and relatively low cost, vegetation dynamics and stress, as well as deforestation and land use changes. The emergence of new satellite platforms and sensors, has prompted a strong effort to develop more sophisticated methods and algorithms to homogenise time series and to integrate observation of different nature. A good example is the one provided by the Global Inventory Monitoring and Modelling System (GIMMS) group, that has supplied the user community with more than twenty years of remote-sensed data at 8 km resolution, based on original information from the successive satellites of the AVHRR/NOAA series. Europe has built another complementary important initiative, the VEGETATION system that, since the end of 1998, has been supplying data on earth surface characteristics, at 1 km resolution, based on remote sensed information from VEGETATION instrument on board of the French SPOT satellites. An effort has also been put into the development of several vegetation indices, specifically design to quantify concentrations of green leaf vegetation and identify places where vegetation is either healthy or under stress.

The aim of the present thesis is to further investigate the relationship between climate variability and vegetation dynamics in Europe by combining remote-sensed information and meteorological data. Special attention will be devoted to the Iberian

Peninsula and Portugal and the study will encompass different aspects of the problem, from the impact of NAO on the vegetative cycle to vegetation recovery after fire events.

The thesis is organised into three main parts; a first one dedicated to fundamentals, data and methods; a second one dealing with the impact of climate variability on vegetation dynamics in Europe and crop production in southern Portugal; and a third focusing on the effects of extreme events on Portuguese vegetation health.

The first part comprises Chapters 2 and 3. In Chapter 2 an overview is given on remote sensing and image correction techniques and a detailed description is provided about the major characteristics of NOAA and SPOT systems. Chapter 3 gives a thorough description of datasets used, namely remote-sensed (GIMMS, VITO, CLC2000, GLC2000) and meteorological (CRU, GPCC) data and presents an overview on the characteristics and the applicability of vegetation indices, namely on the Normalised Difference Vegetation Index (NDVI).

The second part comprises Chapters 4 and 5 and the goal is to assess the impact of climate variability on vegetation dynamics and crop production. Chapter 4 is dedicated to the analysis of the relation between vegetation phenology and climate variability over Europe and to characterizing the response of vegetation to both precipitation and temperature in two contrasting areas of Europe, respectively Northeastern Europe and the Iberian Peninsula. The impact of the Northern Atlantic Oscillation (NAO) on the vegetative cycle in the two regions is assessed and related to the different land cover types and to the respective responses to climate variability. Results of this chapter have been published in Gouveia at al. (2008). Chapter 5 gives a brief description of the impact of climate variability on wheat production and yield that is mostly relevant in southern Portugal. The role of relevant meteorological variables is investigated, namely net solar radiation, temperature and precipitation and the impact of NAO is evaluated. A simple regression model of wheat yield is built up using as predictors spring NDVI and NAO in June that are related to meteorological conditions during the growing and maturation stages of wheat. Parts of these results have been published in Gouveia and Trigo (2008).

The third part of the thesis which comprises Chapters 6 and 7 is related to the assessment of the impact of extreme events, such as drought episodes and wildfires, on vegetation health in Continental Portugal. Chapter 6 is dedicated to the spatial and temporal monitoring of heat and water stress of vegetation. The severity of a given episode is assessed and special attention is devoted to the drought episode of 2005, as

well as to those of 1999 and 2002. Parts of these results have been submitted in Gouveia et al.*, (2008). In Chapter 7 a simple methodology is presented that allows identifying burned areas based on the analysis of persistent negative anomalies of NDVI. The developed methodology allows evaluating the susceptibility to fire of different land cover types as well as assessing the distinct recovery profiles of vegetation after wildfire events.

Finally an overview of results is given in Chapter 8 and a summary of the most important conclusions are presented on the work that was performed.

*Gouveia, C., DaCamara, C.C. Trigo; R.M., 2008: Drought and Vegetation Stress Monitoring in Portugal using Satellite Data, *Natural Hazards and Earth System Sciences* (Submitted).

2. FUNDAMENTALS

2.1 Remote sensing

Following the American Society of Photogrammetry and Remote Sensing we will adopt a combined definition of photogrammetry and remote sensing (Colwell, 1997), that will be defined as

> "*the art, science, and technology of obtaining reliable information about physical objects and the environment, through the process of recording, measuring and interpreting imagery and digital representations of energy patterns derived from noncontact sensor systems*".

This is a complex and comprehensive sequence of processes involving the detection and measurement of electromagnetic radiation of different wavelengths reflected or emitted from distant objects or materials, with the aim of estimating their physical and biophysical properties and/or organising them in terms of class/type, substance, and spatial distribution. A device such as a camera or a scanner that is able to detect the electromagnetic radiation reflected or emitted from an object is called a "remote sensor" or "sensor". The vehicle, such as an aircraft or a satellite that carries the sensor is called a "platform".

Remote sensing aims therefore at identifying and describing objects and/or environmental conditions by analysing the respective signatures on the reflected and emitted spectra of electromagnetic radiation (Figure 2.1). Because of the unique view it provides of the Earth, remote sensing has come to be a very important method to analyse the environment. In this sense, remote sensing is an exploratory science, as it provides images of areas in a fast and cost efficient way, and attempts to uncover the properties of the observed elements.

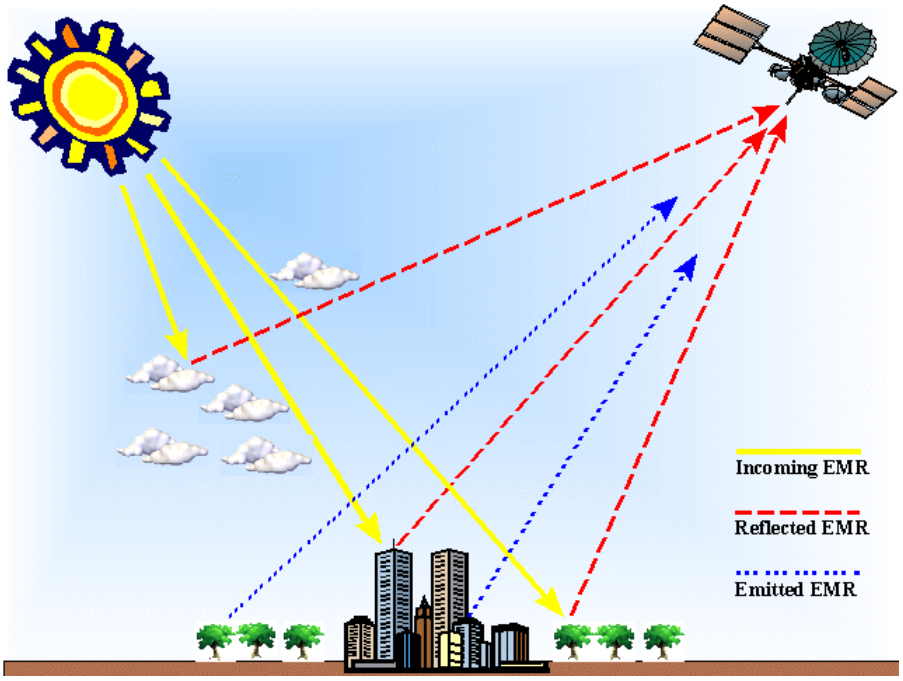

Figure 2.1 Data collection by remote sensing (from http://www.cla.sc.edu/geog/cgisrs/).

2.2 Radiometric concepts

All matter reflects, absorbs and emits electromagnetic radiation in a unique way. For example, the reason why a leaf looks green is that the chlorophyll absorbs blue and red and reflects green radiation. Such unique characteristics of matter are usually called spectral characteristics.

The flux of electromagnetic radiation is usually characterised by the so-called radiance, L, which is defined as the flux per unit projected area (at the specific location in the plane of interest) per unit solid angle (in the direction specified relative to the reference plane). The SI units of radiance are therefore $Wm^{-2}sr^{-1}$.

In general, we may consider that:

$$L = f\left(\lambda, s_{x,y,z}, t, \theta, P, \Omega\right)$$

where:

L is the radiance recorded within the Instantaneous Field of View (IFOV) of the considered optical remote sensing system, i.e., the area from which radiation impinges on the detector (e.g. a picture element or pixel in a digital image)

and where:

λ denotes wavelength (i.e. the spectral response measured in various bands or at specific frequencies);

$s_{x,y,z}$ denotes the size of the picture element (or pixel) whose location is at (x,y,z);

t refers to temporal information (i.e., when and how often the information is acquired);

θ denotes the set of angles that describe the geometric relationships among the radiation sources (e.g., the Sun), the target of interest (e.g., a corn field), and the remote sensing system (e.g., a satellite platform);

P denotes the polarization of back-scattered energy recorded by the sensor;

Ω denotes the radiometric resolution (precision) at which the data (e.g., reflected, emitted, or back-scattered radiation) are recorded by the remote sensing system.

As shown in Table 2.1, the electromagnetic radiation regions used in remote sensing are the near ultra-violet (0.3-0.4 μm), the visible (0.4-0.7 μm), the reflective infrared (0.7-3.0 μm), the thermal infrared (3.0-14 μm) and the microwave (1 mm-1 m). The spectral range of reflective infrared is more influenced by solar reflection than by the emission from the ground surface. The reflective infrared is usually subdivided into the near infrared (0.7-0.9 μm) and the shortwave infrared (0.9-3.0 μm). In the thermal infrared region, emission from the surface dominates the radiant energy with little influence from solar reflection.

Table 2.1 Regions used in remote sensing. (adapted from http://www.esa.int/esaEO/SEMLFM2VQUD_index_1_m.html).

Ultra-violet		Visible		Infrared		Microwave
0.30-0.40μm	Near ultra-violet	0.40-0.45 μm	Violet	0.7-3.0 μm	Reflective Infrared	1mm-1m
		0.45-0.50 μm	Blue	3.0-14 μm	Thermal Infrared	
		0.50-0.55 μm	Green	14.0- 1000 μm	Far Infrared	
		0.55-0.60 μm	Yellow			
		0.60-0.65 μm	Orange			
		0.65-0.70 μm	Red			

Meteorological, agricultural and environmental remote sensing in general is commonly performed in the visible (VIS), the near-infrared (NIR), the shortwave infrared (SWIR) and thermal infrared (TIR) portions of the spectrum.

Resolution is generally defined as the ability of an entire remote-sensing system to render a sharply defined image. Resolution involves the following specific types (Figure 2.2)

- Spatial resolution, defined as the size of the field-of-view (FOV), e.g., 10 × 10 m;
- Spectral resolution, defined as the number and size of spectral regions the sensor records data, e.g. blue (B), green (G), red (R), NIR, TIR, microwave;
- Temporal resolution which is related to how often the sensor acquires data, e.g. every 30 days;
- Radiometric resolution, defined as the sensitivity of detectors to small differences in electromagnetic energy.

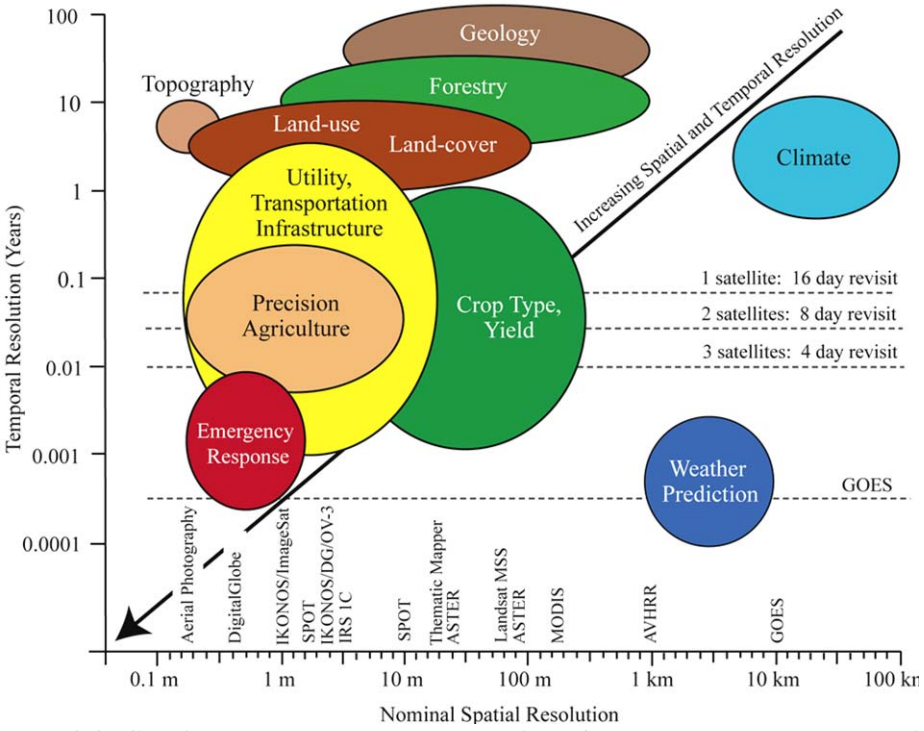

Figure 2.2 Spatial and temporal resolution for selected remote sensing applications (from Jensen, 2007).

It may be noted that the resolution determines how many pixels are available in measurement, but more importantly, higher resolutions are more informative, giving more data about more points. However, more resolution occasionally yields less data. For example, in thematic mapping to study plant health, imaging individual leaves of plants is actually counterproductive. Also, large amounts of high-resolution data can clog a storage or transmission system with useless data, when a few low-resolution images might be a better use.

Reflectance is defined as the ratio of incident flux on a sample surface to reflected flux from the surface and ranges between 0 and 1. Reflectance with respect to wavelength is called *spectral reflectance.* Figure 2.3 shows an example of spectral reflectance for vegetation. Spectral reflectance is assumed to be different with respect to the type of land cover. This feature in many cases allows the identification of different land covers types with remote sensing by observing the spectral reflectance or spectral radiance from the surface. Figure 2.4 shows three curves of spectral reflectance for typical land covers; vegetation, soil and water. As seen in the figure, vegetation has a very high reflectance in the near infrared region, though there are three low minima due to absorption.

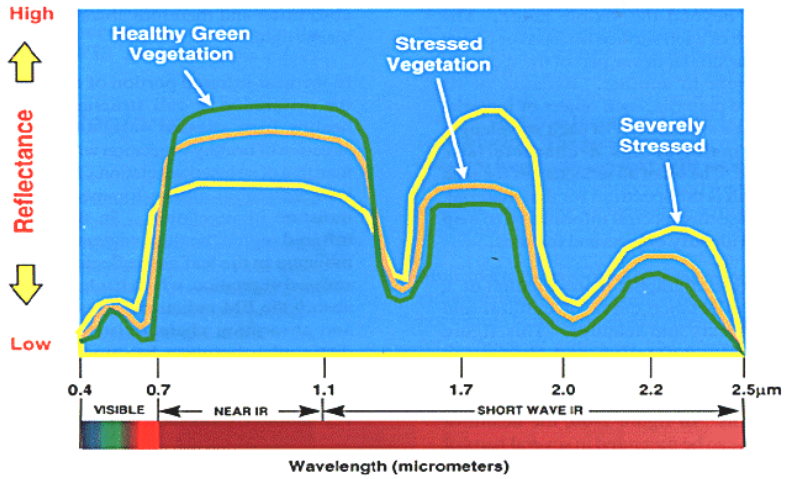

Figure 2.3 Spectral reflectance of vegetation (from http://www.csc.noaa.gov/products/sccoasts/html/images/reflect2.gif).

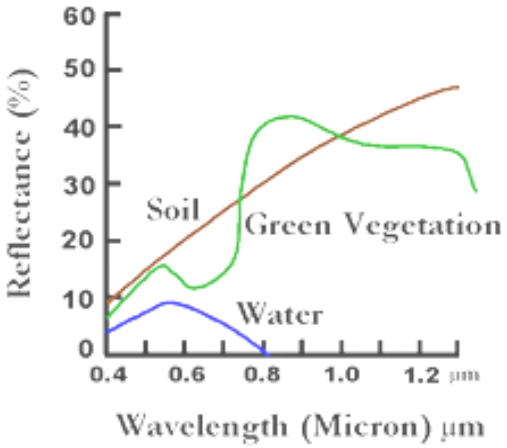

Figure 2.4 Spectral reflectance of vegetation, soil and water (from http://landsat.usgs.gov/resources/remote_sensing/remote_sensing_applications.php).

Soil has rather higher values for almost all spectral regions. Water has almost no reflectance in the infrared region. Chlorophyll, contained in a leaf, has strong absorption at B (0.45 μm) and R (0.67 μm), and high reflectance at NIR (0.7-0.9 μm). This characteristic reflects in the small peak at G (0.5-0.6 μm), which makes vegetation green to the human observer. NIR is very useful for vegetation surveys and mapping because such a steep gradient at 0.7-0.9 μm is produced only by vegetation. Because of the water content in a leaf, there are two absorption bands at about 1.5 μm and 1.9 μm. This is also used for surveying vegetation greenness.

2.3 Image correction

2.3.1 Atmospheric correction

Radiation from the Earth's surface undergoes significant interaction with the atmosphere before it reaches the satellite sensor. This interaction with the atmosphere can be severe, as in the case of cloud contamination, or minor, as in the case when the FOV is essentially a clear sky (Schott and Henderson-Sellers, 1984). Regardless of the

type of analysis that is performed on the remotely sensed data, it is important to understand the effects of the atmosphere upon the radiance response.

The propagation of electromagnetic radiation through the atmosphere is affected by two essential processes; absorption and scattering. Absorption occurs when a fraction of energy passing through the atmosphere is absorbed by some of the atmospheric constituents and is then re-emitted at different wavelengths. Scattering occurs when a fraction of energy passing through the atmosphere has its direction altered through a diffusion of radiation by small particles in the atmosphere. The type and significance of the scattering depends upon the size of the scattering element compared to the wavelength of the radiation (Schott and Henderson-Sellers, 1984; Drury, 1987).

At the shorter wavelengths, attenuation occurs by scattering due to clouds and other atmospheric constituents, as well as by reflection. The effect of scattering on the visible wavelengths is significant and must be compensated for when developing empirical relationships through time. The most significant interaction that thermal infrared radiation undergoes, as it passes through the atmosphere, is by absorption, primarily due to ozone and water vapour particles in the atmosphere.

The objective of atmospheric correction is to retrieve the surface reflectance (that characterizes the surface properties) from remotely sensed imagery by removing the atmospheric effects. Since atmospheric correction has been shown to significantly improve the accuracy of image classification, the problem has received considerable attention from researchers in remote sensing who have devised a number of approaches to its solution (Crippen, 1987). Most of them are sophisticated approaches (based on e.g. correlation with ground-based measurements, ground truth methods, in-scene methods, multiple view angle, multiple altitude techniques, atmospheric propagation models) but they are computationally challenging and have only been validated on a very small scale. Simplified approaches (e.g. use of a constant correction factor for each channel of the dataset) have also been adopted, especially in cases of operational applications over large areas. Atmospheric correction is beyond the scope of this work and an overview of methods is given e.g. in Chapter 6 of Schott (1997).

2.3.2 Radiometric correction

When the emitted or reflected electromagnetic energy is received by a sensor, the observed energy does not coincide with the energy emitted or reflected from the same object observed from a short distance. This is due to several factors which include the sun's azimuth and elevation, the topography, the atmospheric conditions (e.g. fog or aerosols) and the sensor response. All such factors influence the observed energy and radiometric correction is a pre-processing technique that aims at reconstructing the signal and getting physically-calibrated values. In such context, radiometric errors and inconsistencies are frequently referred to as noise, which may be defined as any undesirable spatial or temporal variations in image brightness not associated with variations in the imaged surface.

There are several others techniques aiming at minimizing the effects of the above-mentioned factors. One of the most common consists of adjusting the average and the standard deviation of recorded data. Another one is performing a conversion of data to a normalized index, e.g. the Normalized Difference Vegetation Index (NDVI), which will be described in detail in Chapter 3. Other techniques include the least square method and the histogram matching, i.e. histograms per band and/or per sensor are calculated and the cumulative histogram with cut-offs at 1% and 99% is then relatively adjusted to the reference histogram.

2.3.3 Geometric correction

Geometric distortions refer to errors between the actual image coordinates and the ideal image coordinates, which would be projected theoretically with an ideal sensor and under ideal conditions. Geometric distortions are classified into internal distortions that result from the geometry of the sensor (e.g. lens distortion, misarrangement of detectors, variations of sampling rate), and external distortions that arise from the position and the attitude of the sensor as well as from the shape of the object, the earth curvature, and the topographic relief. Geometric correction is therefore achieved by

establishing the relationship between the image coordinate system and the geographic coordinate system.

According to Schowengerdt (1997) various terms may be used to describe specific aspects related to the geometric correction of imagery:

- Registration, that is defined as the alignment of one image to another image of the same area such that two pixels at the same location in both images represent two samples at the same point on the Earth;
- Rectification or georeferencing, that is defined as the alignment of an image to a map so that the image is planimetric, just like the map;
- Geocoding, a special case of rectification, that includes scaling to a uniform, standard pixel, therefore allowing the "layering" of images from different sensors and maps in a Geographical Information System (GIS).

The correction of spatial distortions due to an incorrect positioning of the sensor requires adequate sensor and orbital models. The satellite position and velocity may be computed by means of complex numerical models or most commonly by simple analytical orbit extrapolation models that ingest a set of orbital elements that usually include the position-velocity of the satellite at a given instant in time as well as the elliptical parameters of the satellite orbit and ephemeris data, i.e., the times of various events (e.g. ascending and descending nodes, start and end of data acquisition).

Once positional distortions have been corrected, deviations due to spacecraft attitude have to be considered. Errors in the platform attitude are expressed by means of three angles (Figure 2.5) that define the platform rotation; the roll, the pitch and the yaw, which may be corrected by using distortion models, followed by an adequate coordinate transformation and a resampling process. These processes are briefly described below.

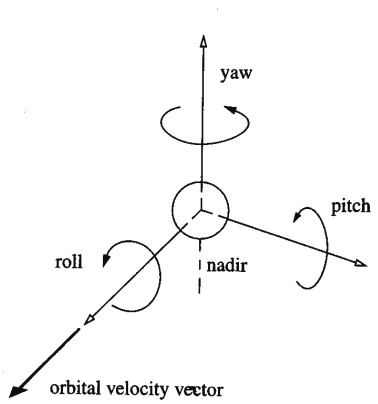

Figure 2.5 Conventional definitions for the three attitude axes of a sensor platform (source: Schowengerdt, 1997).

2.3.3.1 Distortion models

Polynomial models are the most common among mathematical distortion model. A polynomial model of order N relates the coordinates (x,y) in the distorted image to those in the reference image or map (x_{ref},y_{ref}), i.e.

$$x = \sum_{i=0}^{N}\sum_{j=0}^{N-i} a_{ij}\left(x_{ref}\right)^i\left(y_{ref}\right)^j$$

$$y = \sum_{i=0}^{N}\sum_{j=0}^{N-i} b_{ij}\left(x_{ref}\right)^i\left(y_{ref}\right)^j$$

In general a quadratic polynomial (N=2) is adequate, i.e.

$$x = a_{00} + a_{10}x_{ref} + a_{01}y_{ref} + a_{11}x_{ref}y_{ref} + a_{20}\left(x_{ref}\right)^2 + a_{02}\left(y_{ref}\right)^2$$

$$y = b_{00} + b_{10}x_{ref} + b_{01}y_{ref} + b_{11}x_{ref}y_{ref} + b_{20}\left(x_{ref}\right)^2 + b_{02}\left(y_{ref}\right)^2$$

a_{00} and b_{00} are shifts in x and y, respectively; a_{10} and b_{01} are scales in x and y, respectively; a_{01} and b_{10} are shears in x and y, respectively; a_{11} and b_{11} are a y-dependent scale in x and an x-dependent scale in y, respectively; and a_{20} and b_{02} are non-linear scales in x and y, respectively.

In case the image has been processed accurately for systematic distortions, a linear polynomial usually gives satisfactory results

$$x = a_{00} + a_{10} x_{ref} + a_{01} y_{ref}$$

$$y = b_{00} + b_{10} x_{ref} + b_{01} y_{ref}$$

This linear transformation is known as an affine transformation (Wolf, 1983) and includes six kinds of distortion, i.e. a translation (or shift) in x, a translation in y, a scale change in x, a scale change in y, a skew and a rotation.

Coefficients of the polynomial models are usually determined by means of Ground Control Points (GCPs). Examples of GCPs include natural features (e.g. along coastlines and rivers), small islands and man-made features (e.g. dams and road intersections). Once a suitable set of GCPs has been found then coefficients of the polynomial model may be retrieved by the least-squares technique. However it should be noted that the goodness-of-fit of the solution does not indicate the validity of the polynomial model as a model for the physical distortion (Schowengerdt, 1997). Accordingly, a number of GCPs should be kept for validation but this procedure is seldom used.

2.3.3.2 Coordinate transformations

Unlike local scale analyses, which treat the Earth as a plane, the precise determination of the position of points over a broad area must take into account the actual shape of the Earth that may be approximated by an ellipsoid of revolution or spheroid, i.e. the geometric figure defined by an ellipse rotated round its minor axis. The ellipsoid is very important to GIS because heights are measured with respect to the ellipsoid.

National mapping agencies in different countries around the world use different ellipsoids, adjusting the lengths of the polar and equatorial radii to get the best fit within their region of interest (Table 2.2). However recent work based on satellite data has seen the development of ellipsoids that are used worldwide (e.g. GRS80).

Horizontal and vertical measurements made on the earth are made in the earth's gravitational field, which can distort those measurements. In fact, the gravity field is

dependent on the distribution of the earth mass and some parts of the earth are more massive than others. If there is a dense mass to one side, "up" will be deflected in the direction of the mass and "down" will not necessarily be directed toward the centre of the earth with enough precision for intercontinental distance measurements. Elevation with respect to mean sea level is therefore measured in respect to the geoid, which is defined as an equipotential surface derived from the earth's gravity field and the outward centrifugal force of the earth's rotation. Gravity is accordingly perpendicular to the geoid at every point. Generally, the geoid is higher over continents and lower over the oceans (Figure 2.6). Because the geoid is dependent on the irregular distribution of masses in the earth, the shape of the geoid can not be calculated, only measured.

Table 2.2 Table of Ellipsoids (Adapted from http://ltpwww.gsf.nasa.gov/IAS/handbook/hamdbook_htmls/chapter1/chapter1.html).

Name	Date	Semi-major Axis(a)	Semi-minor Axis(b)	Use
Airy	1830	6377563.396	6356256.91	Great Britain
Bessel	1841	6377397.155	6356078.963	Chile, most parts of Central Europe, and Indonesia
Clarke	1866	6378206.4	6356583.8	North America and Philippines
Clarke	1880	6378249.145	6356514.87	France, and most of Africa
Everest	1956	6377301.243	6356100.228	India and Nepal
Everest	1969	6377295.664	6356094.668	
Hayford	1909	6378388	6356911.946	
Helmert	1906	6378200	6356818.17	Egypt
Hough		6378270	6356794.343	
Modified Everest	1948	6377304.063	6356103.039	W. Malaysia and Singapore
Sphere		6370997	6370997	
Walbeck		6376896	6355834.847	
WGS66	1966	6378145	6356759.769	
WGS72	1972	6378135	6356750.52	World wide
WGS84	1984	6378137	6356752.31	World wide

The process of converting image coordinates (e.g. lines and columns of pixels) into positions on Earth requires the adoption of a Coordinate Reference System which consists of a Coordinate System (i.e. a set of mathematical rules for specifying how coordinates are to be assigned to points) together with a Datum (EPSG, 2002) that relates the Coordinate System to the Earth.

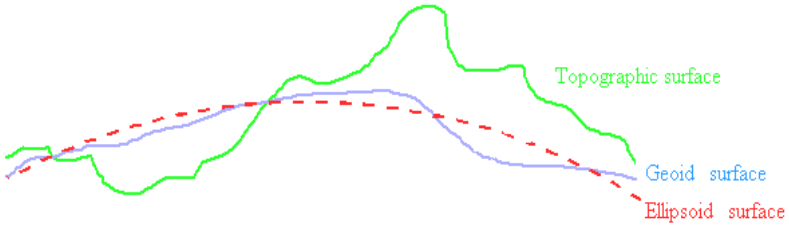

Figure 2.6 Ellipsoid, geoid and topographic surfaces (source: http://www2.uefs.br/geotec/topografia/apostilas/topografia(1).htm).

Among the different Coordinate Systems, map projections are worth mentioning since they constitute the framework for analysis of remote-sensing imagery (Schowengerdt, 1997). There is a very wide variety of projection schemes that constitute trade-offs between different types of distortions (e.g. Gilbert, 1974; Snyder, 1987). Examples of several commonly used map projections are given in Table 2.3 and an extensive survey on currently used map projections may be found e.g. in EPSG (2002).

In most maps meridians of longitude and parallels of latitude appear as curved lines and, to avoid the inconvenience of pinpointing locations on curved reference lines, cartographers superimpose on the map a rectangular grid consisting of two sets of straight, parallel lines, uniformly spaced, each set perpendicular to the other. This grid is designed so that any point on the map can be designated by its latitude and longitude or by its grid coordinates. Such grids are usually identified by the name of the particular projection for which they are designed.

The United States National Imagery and Mapping Agency (NIMA) adopted a special grid for military use throughout the world called the Universal Transverse Mercator (UTM) grid (USGS, 2001). In this grid, the world is divided into 60 north-south zones (Figure 2.7), each covering a strip 6° wide in longitude.

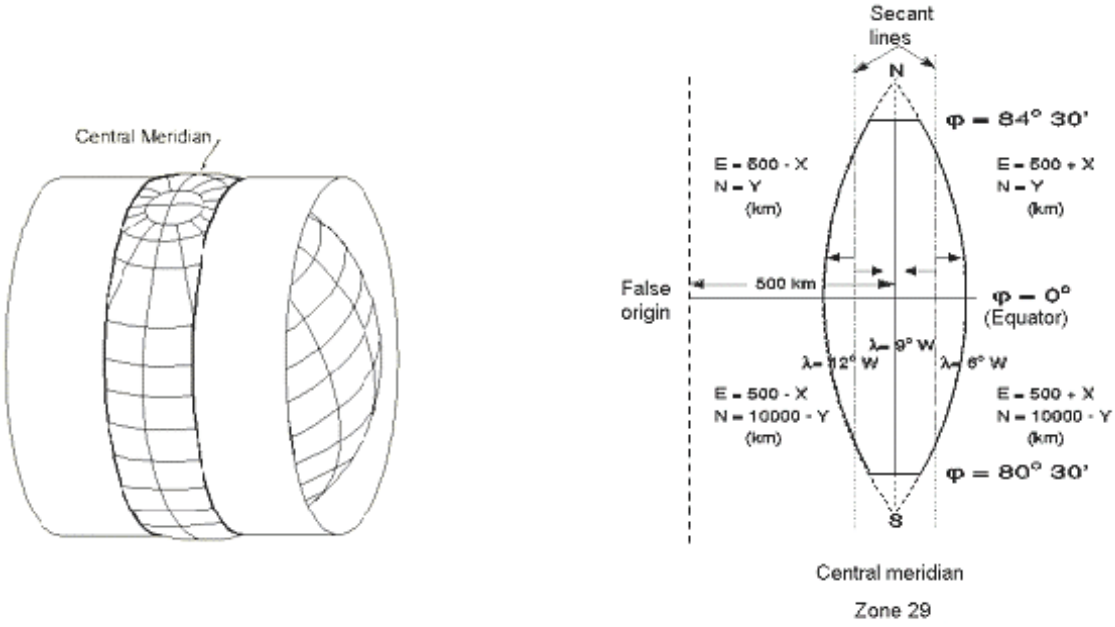

Figure 2.7 The UTM Zone 29 (source: www.isa.utl.pt/der/Topografia /cartografia2.ppt).

These zones are numbered consecutively beginning with Zone 1, between 180° and 174° west longitude, and progressing eastward to Zone 60, between 174° and 180° east longitude. In each zone, coordinates are measured north and east in meters. The northing values are measured continuously from zero at the Equator, in a northerly direction. To avoid negative numbers for locations south of the Equator, NIMA's cartographers assigned the Equator an arbitrary false northing value of 10,000,000 meters. A central meridian through the middle of each 6° zone is assigned an easting value of 500,000 meters. Grid values to the west (east) of this central meridian are less (more) than 500,000.

Table 2.3 Projection plane equations for several common map projections (Moik, 1980). The latitude of a point on the Earth is φ and its longitude is λ. The projected map coordinates, *x* and *y*, are called "easting" and "northing", respectively. *R* is the equatorial radius of the Earth and ε is the Earth's eccentricity. The subscripted values of latitude and longitude pertain to the definition of a particular projection (*source*: Schowengerdt, 1997).

Projection	***X***	***Y***
Polar stereographic	$2R\tan\left(\frac{\pi}{2}-\varphi\right)\sin\lambda$	$2R\tan\left(\frac{\pi}{2}-\varphi\right)\cos\lambda$
Mercator	$R\lambda$	$R\lambda\ln\left[\tan\left(\frac{\pi}{4}+\frac{\varphi}{2}\right)\left(\frac{1-\varepsilon\sin\varphi}{1+\varepsilon\sin\varphi}\right)^{\varepsilon/2}\right]$
Oblique Mercator	$Ra\tan\left[\frac{\cos\varphi\sin(\lambda-\lambda_p)}{\sin\varphi\cos\varphi_p-\beta\sin\varphi_p}\right]$ $\beta=\cos\varphi\cos(\lambda-\lambda_p)$	$\frac{R}{2}\ln\left[\frac{1+\alpha+\beta\cos\varphi_p}{1-\alpha+\beta\cos\varphi_p}\right]$ $\alpha=\sin\varphi\sin\varphi_p$
Transverse Mercator	$Ra\tan\left[\cos\varphi\sin(\lambda-\lambda_p)\right]$	$\frac{R}{2}\ln\left[\frac{1+\beta}{1-\beta}\right]$
Lambert normal conic	$\rho\sin\theta$	$\rho_0-\rho\cos\theta$ $\rho=\frac{R\cos\varphi_1}{\sin\varphi_0}\left[\frac{\tan\left(\frac{\pi}{4}-\frac{\varphi}{2}\right)}{\tan\left(\frac{\pi}{4}-\frac{\varphi_1}{2}\right)}\right]^{\sin\varphi_0}$ $\theta=\lambda\sin\varphi_0$ $\sin\varphi_0=\frac{\ln\left(\frac{\cos\varphi_1}{\cos\varphi_2}\right)}{\ln\left[\frac{\tan\left(\frac{\pi}{4}-\frac{\varphi_1}{2}\right)}{\tan\left(\frac{\pi}{4}-\frac{\varphi_2}{2}\right)}\right]}$

2.4 Resampling

Once the coordinate transformation from (x_{ref}, y_{ref}) to (x,y) has been determined then the transformation is applied by stepping through the reference coordinates and computing the corresponding distorted coordinates (x,y). Computed values of (x,y) will not usually match the values of the pixels of the image and therefore there is the need to proceed to the interpolation of the "new" pixels between the existing pixels in the image. This procedure is usually referred to as resampling.

There are several interpolation schemes to compute the value of a resampled pixel; these include:

- the nearest neighbour method;
- the bilinear interpolation method;
- the cubic convolution method.

A) Nearest neighbour method

In this method, also called zero-order interpolation, each new pixel at (x_{ref}, y_{ref}) gets the value of the original pixel whose location (x,y) is the nearest to it.

The nearest neighbour method (e.g. Cracknell, 1998) does not require any computations and therefore has the advantage of being very fast to use. Besides, it does not lead to any loss of information due to smoothing and no new values are introduced in the statistical distribution. However, the "round-off" property that is inherent to the method may cause geometric discontinuities of the order of ± ½ pixel, which may be the cause of spurious effects (e.g. omission or repetition of pixels).

B) Bilinear interpolation method

In this method, also called first-order interpolation, the estimate of the value of the output pixel located at (x_{ref}, y_{ref}) is based on the values of the four surrounding input pixels located in the original space (x,y). The method consists in performing two linear

interpolations, one along the lines (x direction) that creates a new resampled column (y direction), the final value at (x,y) being again obtained by linear interpolation.

Bilinear resampling is computationally much more expensive and produces a much smoother interpolating surface than the nearest-neighbour method. This smoothing effect is especially conspicuous in sharp boundaries that become blurred after bilinear interpolation.

C) Cubic convolution method

The cubic convolution method, also called bicubic or third-order interpolation, avoids the excessive smoothing of bilinear resampling. The method involves fitting third-degree polynomials using the 16 nearest pixels located in the original space (x,y) that surround the output pixel (x_{ref},y_{ref}). However, unlike bilinear resampling, the method may create values outside the original range.

In the case of thematic maps (e.g. land cover maps) resampling is usually performed by using either the already described nearest neighbour method or the so-called majority rule, where the output pixel (x_{ref},y_{ref}) is assigned to the most frequent class as observed in a given window of pixels in the original space (x,y). The majority rule will be described in detail in section 3.2.3.

2.5 The SPOT and the NOAA systems

2.5.1 The SPOT Program

The SPOT (Satellite Pour l'Observation de la Terre) program consists of a series of optical remote sensing satellites with the primary mission of obtaining Earth imagery for land use, agriculture, forestry, geology, cartography, regional planning, water resources and GIS applications. The program is committed to commercial remote sensing on an international scale and has established a global network of control centres, receiving stations, processing centres and data distributors. SPOT satellites are operated by the French Space Agency, the Centre National d'Etudes Spatiales (CNES).

SPOT 1 was first launched in February, 1986, with successors following every three or four years. SPOT 2 was launched in January, 1990 and SPOT 3 was launched in September 1993; SPOT 4 was launched on March 1998 and SOPT 5 followed on May 2002. The orbit of SPOT 1 was lowered in 2003 and the satellite will gradually loose its altitude and break up on the atmosphere. The recorders on-board SPOT 2 are not working but the satellite is still able to provide imagery. SPOT 3 is not working anymore but SPOT 4 and SPOT 5 are fully functional.

All satellites are in sun-synchronous, near-polar orbits at altitudes of about 830 km above the Earth, and have orbit repetitions of 26 days. The SPOT system provides global coverage between the latitudes of 87ºN and 87ºS. The loads of SPOT 1, SPOT 2 and SPOT 3 were the same, each satellite carrying two identical High Resolution Visible (HRV) imaging instruments. As shown in Table 2.4, the HRV instrument is able to operate in two modes; the panchromatic (PAN) mode and the multispectral (MS) mode. In PAN, imaging is performed in a single spectral band that covers the visible part of the electromagnetic spectrum. In MS, imaging is performed in three spectral bands, green, red and NIR.

Table 2.4 HRV Spectral Bands. (from http://www.spotimage.fr/html/_167_224_230_.php).

Mode	Band	Wavelength (µm)	Resolution (m)
Multispectral	XS1	0.50 - 0.59 (Green)	20
Multispectral	XS2	0.61 - 0.68 (Red)	20
multispectral	XS3	0.79 - 0.89 (Near IR)	20
Panchromatic	P	0.51 - 0.73 (Visible)	10

In the case of SPOT 4 (Figure 2.8) the two imaging instruments were upgraded, becoming the High Resolution Visible and Infrared (HRVIR) instrument. As shown in Table 2.5 the HRVIR is similar to the HRV, except that HRVIR has an additional SWIR band, and the wavelength bandwidth of the panchromatic mode is narrower than that for HRV.

Figure 2.8 Picture of the satellite SPOT 4. (from http://medias.obs-mip.fr/www/Reseau/Lettre/11/en/systemes/vegetation.html).

In the field of environment and agriculture, the sensitivity of the SWIR band to variations in canopy or soil water content produces a high contrast between soil and vegetation reflectances, leading to an easier detection of variations in the canopy structure. The SWIR band is therefore especially interesting for the discrimination of wet areas, the identification of water stress in plants, the classification of some crops and vegetation areas. In particular, the SWIR enables to obtain a better characterisation of arid and semi-arid areas and reveals to be also useful to study forest areas. In

particular, it provides increased precision for the mapping of forests types, with special interest for areas poorly mapped (e.g. tropical environment), as well as for the estimation of cover rate and the relative humidity of plant communities.

Table 2.5 HRVIR Spectral Bands (from http://www.spotimage.fr/html/_167_224_230_.php).

Mode	Band	Wavelength (µm)	Resolution (m)
Multispectral	XI1	0.50 - 0.59 (Green)	20
Multispectral	XI2	0.61 - 0.68 (Red)	20
Multispectral	XI3	0.79 - 0.89 (Near IR)	20
Multispectral	XI4	1.53 - 1.75 (SWIR)	20
Monospectral	M	0.61 - 0.68 (Red)	10

As shown in Figure 2.9, the two HRV (or HRVIR) sensors operate in a cross-track direction. The position of each HRV (or HRVIR) entrance mirror can be commanded by ground control to observe a region of interest not necessarily vertically beneath the satellite. Thus, each HRV (or HRVIR) offers an oblique viewing capability, the viewing angle being adjustable through ±27º relative to the vertical. This off-nadir viewing enables the acquisition of stereoscopic imagery and provides a short revisit interval of 1 to 3 days (Figure 2.10). Moreover, due to the parallax thus created, the oblique viewing capacity of SPOT makes it possible to produce “stereopairs” by combining two images of the same area acquired on different dates and at different angles, due to the parallax thus created.

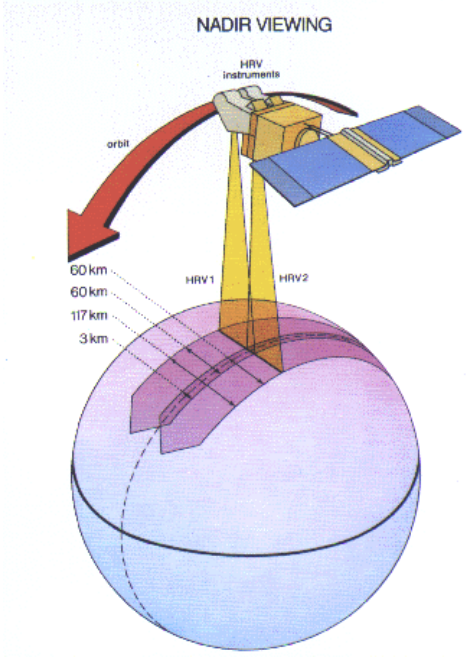

Figure 2.9 The cross-track direction operating mode of the two HRV sensors. (from http://www.spotimage.fr/html/_167_224_230_.php)

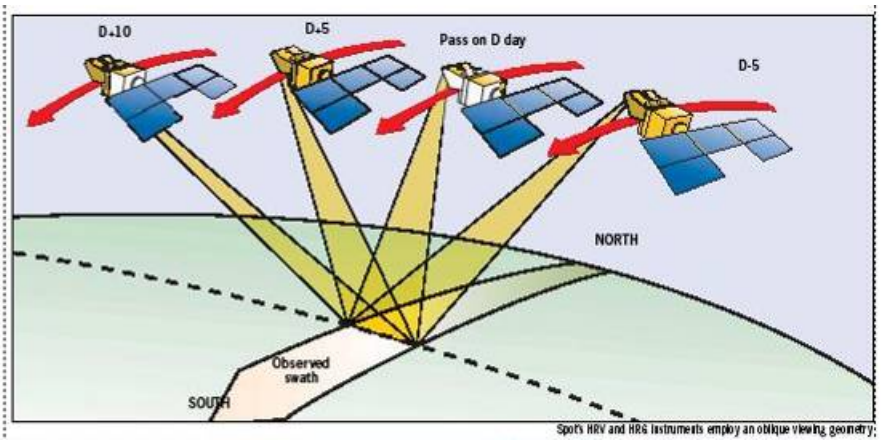

Figure 2.10 Repeated observation by SPOT. (from http://www.spotimage.fr/html/_167_224_230_.php)

Both the HRV and the HRVIR instruments were constructed with multilinear array detectors. In particular, the HRVIR instrument was designed to acquire, instantaneously, one complete line of pixels at a time covering the entire field of view. This is attained using a charged-couple device (CCD) linear array. The CCD linear arrays operate in the so-called "push-broom" mode (Figure 2.11). A wide-angle telescope forms an instantaneous image of adjacent "ground patch areas" on a row of detectors in the instrument's focal plane. Column-wise scanning is a direct result of the

satellite's motion along its orbit. The signals generated by the detectors (photodiodes) are read out sequentially at a predetermined clock rate. Thus, although the linear arrays do not "scan" in the line-wise direction to gather light, the detectors are scanned electronically to generate the output signal. The telescope has a field of view of 4°, corresponding to 60 km on the ground covered instantaneously by a line of 6000 detectors. Each HRVIR is thus said to offer a "strip width" of 60 km (Figure 2.12).

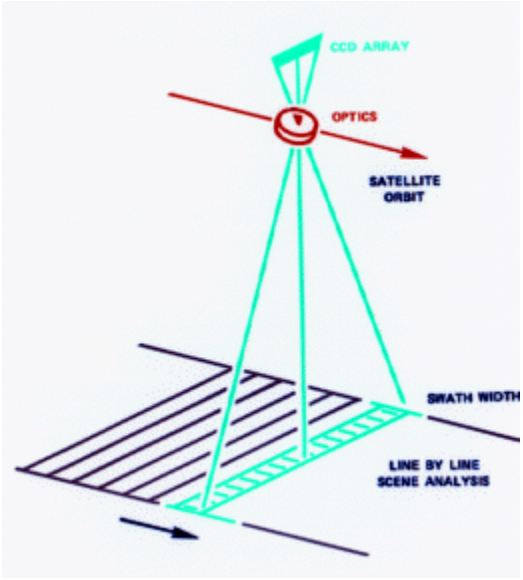

Figure 2.11 The push broom principle (http://spot4.cnes.fr/spot4_gb/index.htm).

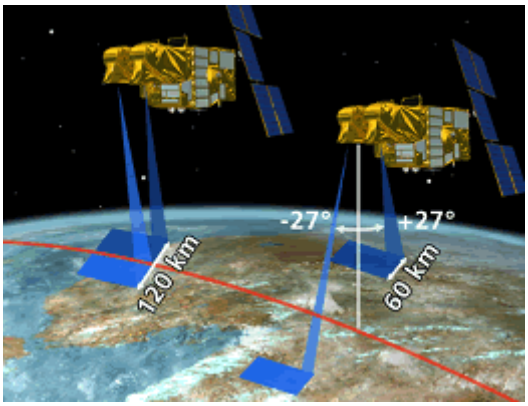

Figure 2.12 SPOT's Field of view. (from http://spot5.cnes.fr/gb/satellite/42.htm)

As a complement to the two HRVIR instruments, SPOT 4 takes on board the VEGETATION instrument that is part of the so-called VEGETATION system.

The VEGETATION system is the result of a co-operation between the European Union, France, Sweden, Belgium and Italy. It aims at ensuring a regional and global continuous monitoring of the continental biosphere and of crops. It observes the Earth at a resolution of 1.15 km, quite invariable in the swath width of nearly 2250 km (Figure 2.13). This gives almost daily access to any point on the earth surface. Taking into account the measurements which have to be discarded due to cloud coverage or bad atmospheric conditions, this feature minimises the probability to get one useful measurement per ten-day periods, the multitemporal spatial resolution being of about 1 km. These characteristics allow the observation and study of seasonal evolutions in the biosphere and its processes. Moreover, SPOT enables to lead these studies and observations in a multi-scale context, as the spectral bands and geometrical references of the VEGETATION instrument are the same for the two HRVIR instruments, the three instruments being inter-calibrated.

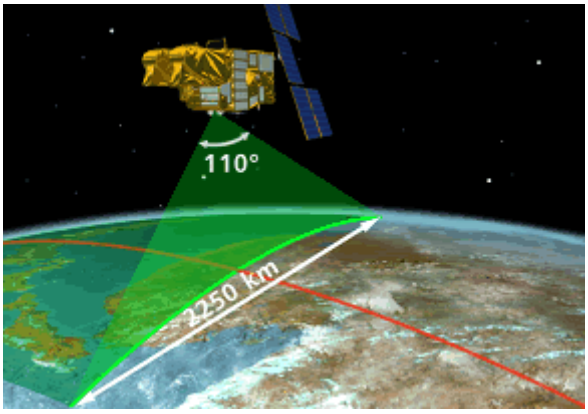

Figure 2.13 The VEGETATION field of view. (from http://spot5.cnes.fr/gb/satellite/42.htm)

The new SPOT 5 satellite is designed to ensure SPOT data users with continuity of service, enhanced image quality and improved services. Derived from the HRVIR instruments on SPOT 4, the two new HRG instruments offer higher resolution: 2.5 metres to 5 metres in panchromatic mode and 10 metres in multispectral mode. Imagery at a resolution of 2.5 metres is generated using a new sampling concept dubbed "Supermode". SPOT 5 features a new HRS imaging instrument operating in panchromatic mode. SPOT 5 is also carrying the recurrent VEGETATION 2 instrument. Tables 2.6 and 2.7 respectively show the orbit characteristics for SPOT 5 and the VEGETATION characteristics, for the four multi-spectral bands.

Table 2.6 Orbit characteristics for SPOT 5.

Repeat coverage interval:	26 days nominally but 4 - 5 days
Orbit	Polar Sun-synchronous
Altitude:	832 km
Inclination:	98.7 degrees
Equatorial crossing:	10.30 a.m.
Launch date:	May 2002

Table 2.7 SPOT 5 sensor characteristics.

Name	Band Type	Wavelength (µm)	Resolution (m)
BO	**Multispectral**	0.430 - 0.470 (Blue)	1165
B1	**Multispectral**	0.61 - 0.68 (Red)	1165
B2	**Multispectral**	0.78 - 0.89 (Near IR)	1165
SWIR	**Multispectral**	1.58 - 1.75 (SWIR)	1165

Finally, it is worth mentioning that the VEGETATION central system supplies two levels of enhanced products, namely the so-called physical products (VGT-P) and the so-called synthesis products (VGT-S). All VGT-P and VGT-S products are provided according to map projections previously defined, preserving the 1 km raw data resolution and corresponding to the existing needs of potential users.

VGT-P products are mostly directed to physicists for methodological development that may be embedded into applications using VEGETATION data. Accordingly, VGT-P products correspond to images of viewing segments without atmospheric correction (radiometry and geometry), which enable to compute the reflectance at the top of the atmosphere.

VGT-S, on the contrary, are products where some synthesis is applied on the "Core Archive" data with the aim of providing users with ground reflectances as well as with some simply derived parameters. Mostly intended for operational projects, VGT-S are geocoded products with atmospheric correction, and for which daily syntheses (S1) or 10-day syntheses (S10) are established. For instance, the normalised difference vegetation index (NDVI) is systematically included in these products and synthesis has been performed through selection of the best measurement acquired during one day or

one decade. As described in the next chapter, such selection is based on the Maximum Value Composite (MVC) technique where the retained measurement simply corresponds to the highest NDVI value computed on top of atmosphere reflectances.

2.5.2 The NOAA series

Starting with TIROS-1 in 1960, the first and the second generations of the US National Oceanic and Atmospheric Administration (NOAA) polar orbiting satellites reached the third generation of meteorological satellites with the launch of TIROS-N in 1978. The first generation was the TIROS series (1960-1965), while the second generation was ITOS series (1970-1976). TIROS-N has been followed by NOAA-6 through NOAA-18 (Table 2.8).

Table 2.8 General time coverage by satellite. (from http://www.ngdc.noaa.gov/stp/NOAA/noaa_poes.html)

TIROS-N	1978 - 1981
NOAA-6	1979 - 1986
NOAA-7	1981 - 1985
NOAA-8	1983 - 1985
NOAA-10	1986 - 1991
NOAA-12	1991 - 2002
NOAA-14	1994 - 2004
NOAA-15	1998 - present
NOAA-16	2001 - present
NOAA-17	2002 - present
NOAA-18	2005 - present

NOAA satellites operate at an altitude of approximately 850 km with slight inclined orbits of approximately 98.8º and an orbital period of about 101.5 min (i.e. 14.2 orbits per day). Since the number of daily orbits is not an integer, the sub-orbital tracks do not repeat on a daily basis, although the Local Solar Time (LST) of the satellite's passage is essentially unchanged for any latitude. However, the satellite's orbit drifts over time, causing a systematic change of illumination conditions and local time of

observation, which is the major source of non-uniformity in multi-annual satellite time series.

NOAA has two types of satellites operating in complementary orbits, one crossing the Equator around 0730 and 1930 LST and the other one around 0230 and 1430 LST. For reasons of convention, even satellites cover the "morning orbit" (0730), while the odd ones cover the "afternoon orbit" (1430). Table 2.9 shows the orbit characteristics for several NOAA satellites covering the "afternoon orbit".

Table 2.9 NOAA Satellites Orbital Characteristics. (Adapted from http://www.crisp.nus.edu.sg/~research/tutorial/noaa.htm)

	NOAA-12	NOAA-14	NOAA-16	NOAA-18
Launch date	14 May 1991	30 Dec 1994	21 Sep 2000	20 May 2005
Date operations began	17 Sep 1991	10 Apr 1995	20 Mar 2001	30 Oct 2005
Orbit inclination	98.5	99.1	98.8	98.8
Mean altitude (km)	808	847	851	833
Equator crossing time (A: Northbound, B: Southbound)	16:49A, 04:49D	17:52A, 05:52D	13:54A, 01:54D	
Period (min.)	101.2	101.9	102.1	101.35

One of the main instruments carried on-board the NOAA satellites is the Advanced Very High Resolution Radiometer (AVHRR) with a 1.1 km instantaneous field of view (IFOV) for a swath of 2,800 km in the visible and infrared wavelength regions. The earlier AVHRR instrument on-board NOAA 9, 10, 11, 12 had 5 bands, respectively in the visible (band 1), NIR (band 2), MIR (band 3) and TIR (bands 4, 5) regions. Starting from NOAA-14, the newer AVHRR instrument (AVHRR/2) has an extra band in the SWIR. This band shares the same transmission channel with the MWIR band which is designated Band 3A, while the SWIR band is Band 3B. Only one of the 3A or 3B bands is activated at any instant. Table 2.10 presents the AVHRR Sensor Characteristics of each band.

Table 2.10 AVHRR Sensor characteristics. (from http://www.crisp.nus.edu.sg/~research/tutorial/noaa.htm)

	Band	Wavelength (μm)	Applications
Visible	1	0.58-0.68	cloud, snow and ice monitoring
Near IR	2	0.725-1.10	water, vegetation and agriculture surveys
Short Wave IR	3A	1.58-1.64	snow, ice and cloud discrimination
Medium Wave IR	3B	3.55-3.93	sea surface temperature, volcano, forest fire activity
Thermal IR	4	10.3-11.3	sea surface temperature, soil moisture
Thermal IR	5	11.3-12.5	sea surface temperature, soil moisture

There is another important sensor on-board NOAA satellites, namely the TIROS Operational Vertical Sounder (TOVS) which consists of three units; the High Resolution Infrared Sounder; model 2 (HIRS/2) with 20 km IFOV, for a 2,200 km swath, the Stratospheric Sounding Unit (SSU) with 147 km IFOV, for a 736 km swath and the Microwave Sounding Unit (MSU) with 110 km IFOV, for a 2,347 km swath.

AVHRR data are acquired in three formats: High Resolution Picture Transmission (HRPT), Local Area Coverage (LAC) and Global Area Coverage (GAC). HRPT data are full resolution image data which are transmitted to a local ground station as they are being collected. Many weather stations around the world operate ground stations that routinely receive real-time HRPT data. LAC data are also full resolution, but they are recorded in an on-board tape for subsequent transmission during a station overpass. Since the on-board tape facility is limited, only a number of scenes are archived. GAC data are subsampled on-board to about 4-km pixel separation at nadir and provide daily global coverage. GAC data are also recorded on tape and then transmitted to a ground station. LAC and GAC data are available from NOAA's Satellite Active Archive (SAA) through the world-wide web (http://www.saa.noaa.gov).

3. BASIC DATA AND PRE-PROCESSING

3.1 Vegetation Indices

3.1.1 Introduction

Changes in vegetation have a strong impact on human activities around the globe. For instance, over the last 50 years deforestation in South America has left vast areas uncultivated and has destroyed many species. One of the major advantages of remote sensing data is its capability of detecting and quantifying green vegetation. Satellite data may for instance be used to detect vegetative changes from one growing season to the next, from year to year, or from decade to decade.

The principle behind the detection of green vegetation is connected with the use of blue and red radiation as energy sources for actively photosynthesizing plants. On the other hand, and as already pointed out in the previous chapter, near-infrared radiation is highly reflected by vegetation (Figure 3.1). Several algorithms have been developed which combine the measured radiances reflected by land surface in different spectral bands of the atmospheric window in order to obtain the so-called "Vegetation Indices" (VIs), that are able to discriminate green vegetation.

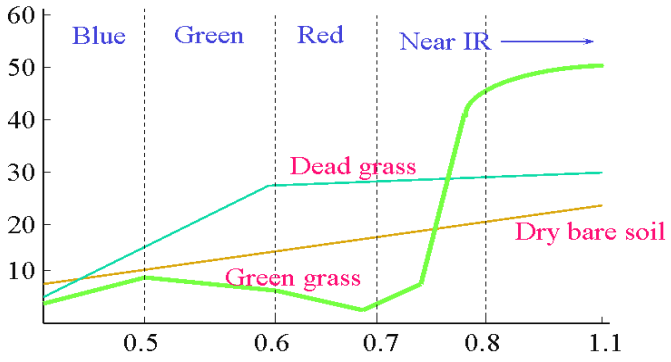

Figure 3.1 Reflectance from different wavelengths and different surfaces.

A VI may therefore be used to quantify concentrations of green leaf vegetation and identify those places where vegetation is either green or under stress due to the absence of water. In fact, several authors have shown that VIs are well correlated with vegetation amount, unstressed vegetation and photosynthetic capacity (Tucker, 1979; Sellers et al., 1992) as well as with other parameters, such as the Leaf Area Index (LAI) and the Fraction of Absorbed Photosynthetically Active Radiation (FAPAR), that quantify biomass and physiological functioning. For instance, LAI may be derived based on a regression model derived from a vegetation index and ground measurements of the considered type of vegetation (Holben et al. 1980; Li et al. 1993; Chen and Cihlar, 1996).

Other models based on indices have been designed to both detect sparse green vegetation and minimize the effects of soil background brightness, topographical distortion and atmospheric "noise".

In general terms, VIs may be divided into two main groups, referred to as Empirical Vegetation Indices and Optimised Vegetation Indices. The most commonly used VI, the so-called Normalized Difference Vegetation Index (NDVI), belongs to the first group. NDVI was introduced by Rouse et al. (1974) and is defined as:

$$NDVI = \frac{\rho_{nir} - \rho_{red}}{\rho_{nir} + \rho_{red}}$$

NDVI ranges between –1.0 and +1.0 and assumes positive values for areas with vegetation. Very low values of NDVI (0.1 and below) are characteristic of barren areas of rock, sand, or snow. Moderate values are associated to shrub and grassland (0.2 to 0.3), while high values indicate temperate and tropical rainforests (0.6 to 0.8). As already pointed out, healthy green leaves commonly have larger reflectances in the near infrared than in the visible range. As the leaves come under water stress, become diseased or die back, they become more yellow and reflect significantly less in the near infrared range. Additionally, unhealthy or sparse vegetation reflects more visible light and less near-infrared light (Figure 3.1).

Clouds, water, and snow have larger reflectances in the visible than in the near infrared whereas the difference is almost zero for rock and bare soil. However, actual vegetation status cannot be observed under cloudy sky conditions. Tropical areas, for instance, are often covered with clouds, becoming very hard to obtain cloud-free data at once for entire areas. In order to overcome this difficulty, NDVI data with little influence of cloud are usually produced by extracting the maximum value of NDVI from data series covering a long enough period, e.g. one month at each grid point. However, values of NDVI may still be low when cloud or ice covers the vegetation for the whole considered period. In the case of water bodies, such class of pixels is usually masked by assigning a conventional value (e.g. zero).

3.1.2 Performance and limitations of empirical vegetation indices

Vegetation indices were introduced over more than 25 years ago as a simple remote sensing tool. Still largely used today, their usage requires however a good understanding of their respective advantages and drawbacks when analysing remote sensing data. For instance, and in what respects to NDVI, it is important to understand that NDVI holds only a fraction of the information available in the original spectral reflectance data. Users of NDVI have in fact tended to estimate a large number of vegetation properties (e.g., LAI, FAPAR, chlorophyll concentration in leaves, plant productivity, fractional vegetation cover and accumulated rainfall). However, if correctly used, an appropriate VI may be converted into a useful product and is also an important tool to estimate the likelihood that vegetation is actively growing at a particular location. The correct usage and interpretation of an index generally depends on how it was designed, but there is no single and definite meaning.

It is worth stressing that NDVI turns out to be sensitive to a number of perturbing factors induced by clouds, atmospheric conditions and soil type. NDVI is also sensitive to anisotropic and spectral effects. Accordingly, in the case of quantitative applications that require a given level of accuracy, the perturbing factors may lead to errors or uncertainties of the same order of magnitude of the quantities to be evaluated. In such cases, special care must be taken to remove perturbations from the data and this may require extensive processing based on ancillary data and other sources of information.

Optimized vegetation indices represent an alternative to the use of empirical VIs. Such indices are 'optimized' in the sense that they are specifically designed to physically estimate a given geophysical or biological variable. During the last decades, a new generation of spectral indices has been developed in order to estimate a specific environmental variable on the basis of data from a specific instrument. The rationale behind the design of optimized vegetation indices is described e.g. in Verstraete and Pinty (1996) and Govaerts et al. (1999). This approach has been developed and applied in the context of a wide range of sensors, including SeaWiFS, VEGETATION, MIRS and MERIS (Gobron et al.; 2000; 2001; 2002). The design of optimized vegetation indices is based on exploiting combinations of spectral bands that have a maximal sensitivity to the presence and to changes in the properties of healthy green vegetation. In addition indices should have a minimal sensitivity to atmospheric scattering and absorption effects, to soil color and brightness changes, and to temporal and spatial variations in the geometry of illumination and observation.

Besides the simplicity and low computational cost, NDVI presents the advantage of the availability and continuity of the datasets (25 years of AVHRR NDVI), which represents an invaluable feature for climatic studies. In fact, when the aim is to study the status of vegetation due to climate variability, namely droughts and extreme events (e.g. heat waves), results based on the analysis of NDVI time series have brought some satisfactory insights. An example is shown in Figures 3.2 and 3.3 that present the results obtained during the extreme heat wave that has stricken Europe in August 2003. Results shown in Figure 3.2 were obtained using NDVI data as obtained from the VEGETATION instrument on board SPOT4, whereas those in Figure 3.3 are based on FAPAR as derived from the MERIS instrument on board ENVISAT platform. It may be noted that FAPAR is a physically-based quantity, defined as the fraction of photosynthetically active radiation (400 -700 nm) absorbed by vegetation canopies. Figure 3.2 presents monthly anomalies of NDVI during August 2003 and the anomaly was calculated with respect to a base period as obtained for the years 1999-2004 (excluding 2003). Negative (positive) anomalies correspond to lower (higher) than average NDVI. Figure 3.3 presents monthly FAPAR anomalies for August 2003 over Europe (Gobron et al., 2005). The anomaly is calculated with respect to a base period taken over the years of 1998 to 2002. In both cases the base period does not include the year of 2003 and it may be noted that anomaly fields of NDVI and FAPAR are

remarkably similar, a feature that points out that, despite its simplicity, NDVI is still useful to characterise the spatial and temporal variability of vegetation status, dynamics and behaviour.

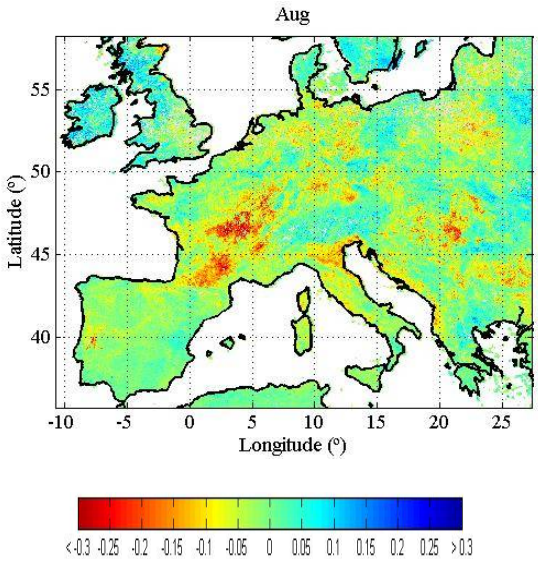

Figure 3.2 Monthly anomalies of NDVI over Europe for August 2003. Anomalies were computed with respect to the base period 1999-2004 (excluding 2003).

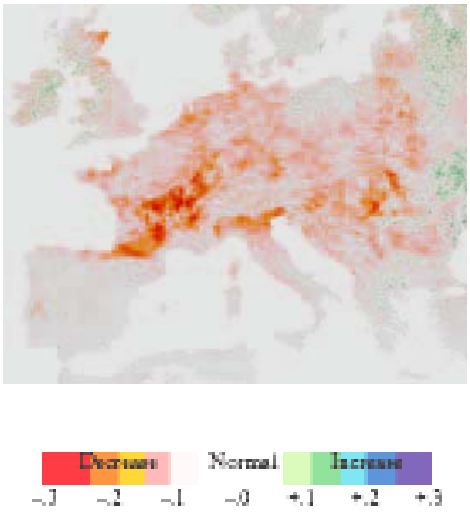

Figure 3.3 As in Figure 3.2 but respecting to FAPAR anomalies. Anomalies were computed with respect to the base period 1998-2002. (from Gobron et al, 2005)

In the present work we will use, for climatological purposes, two datasets of NDVI, respectively derived from VEGETATION/SPOT and NOAA/AVHRR. The two databases will be described in the following two sections.

3.1.3 NDVI from AVHRR/NOAA

The NDVI database as derived from AVHRR/NOAA has been widely used in studying vegetation and ecosystems, especially in semi-arid environments where vegetation cover is less than 30% (Huete and Tucker, 1991; Karnieli et al., 1996). In particular, NOAA-AVHRR derived NDVI and other related indices have been successfully used to identify and monitor areas affected by drought at the regional and the local scales (Malingreau, 1986; Bayarjargal et al., 2006, Vicente-Serrano, 2007). Relationships have also been found between NDVI and other vegetation indicators such as Leaf Area Index (LAI) (Myneni and Williams, 1994) and green biomass production, as well as with rainfall or soil moisture in semi-arid environments (Schmidt and Karnieli, 2000).

In our study we have used monthly values of NDVI and of channel 4 brightness temperature, at 8-km resolution, from the Advanced Very High Resolution Radiometers (AVHRR), as provided by the Global Inventory Monitoring and Modelling System (GIMMS) group (Pinzon et al., 2005; Tucker et al., 2005). The GIMMS NDVI datasets were generated with the aim of providing a 22-year satellite record (1982-2003) of monthly changes in terrestrial vegetation. Such long-term series of NDVI may be used in climate and biogeochemical models to calculate photosynthesis, the exchange of CO2 between the atmosphere and the land surface, the land-surface evapotranspiration and the absorption and release of energy by the land surface (Tucker et al., 2005).

It is worth emphasizing that several factors have to be taken into account when building up a long-term time series of NDVI. For instance, band calibrations have changed substantially during considered 22 years (five NOAA/AVHRR instruments). Natural variability in atmospheric aerosols and column water vapour has also affected the NDVI record. Over the acquisition period there were two major volcanic eruptions, El Chichon in May-July 1982 and Mount Pinatubo in July-September 1991, which injected large quantities of aerosols into the Earth's stratosphere. These aerosols, along

with smoke from biomass burning and dust from soil erosion and other sources, may have introduced significant variability in the AVHRR/NDVI dataset.

The pre-processing of satellite data involved cloud screening and calibration for sensor degradation and inter-sensor variations (Los, 1998). Cloud screening was provided by a channel 5 thermal mask of 0ºC for all continents except Africa, where a cloud mask of 10ºC was used. In addition, the bimonthly composites significantly reduced cloud contamination. The data from April 1982 to December 1984 and from June 1991 to December 1993 were corrected to remove the effects of stratospheric aerosol from El Chichon and Mount Pinatubo eruptions (Tanré et al., 1992), as well as NOAA-9 descending node data from September 1994 to January 1995 (Los, 1998). In fact, in 1992, NOAA-13 has failed to achieve orbit and NOAA-11 continued to supply global afternoon/early morning AVHRR data. From September 1994, the GIMMS group began to use NOAA-9 descending node AVHRR data for the global NDVI data set and continued using these data until NOAA-14 became operational in late January 1995. This feature constitutes a fundamental difference between the GIMMS NDVI and other AVHRR NDVI datasets, such as the Pathfinder AVHRR Land (PAL) data and the Global Vegetation Index (GVI) datasets. In the case of GIMMS the gap of data from September 1994 to January 1995 was filled using the NOAA-9 data while the other datasets present missing data (Pettorelli at al., 2005).

NDVI is also sensitive to the periodic variations in solar illumination angle and to sensor viewing angles induced by the NOAA orbits. The polar, sun-synchronous orbits of the NOAA series allow daily coverage of each point on earth, although at time-varying viewing and illumination geometry. The GIMMS NDVI dataset has a satellite overpass time drift correction that largely eliminates the variation of NDVI due to changes in solar zenith angle.

The GIMMS group uses the so-called Empirical Mode Decomposition (EMD) to identify and remove parts of the NDVI signal that are most related to the satellite drift (Pinzon 2002; Pinzon et al. 2004). The EMD is empirical, intuitive, direct, a posteriori, and adaptive, with the decomposition functions based on and derived from the data (Huang et al. 1998; Huang et al. 1999). Pinzon et al. (2001) showed that EMD was applicable to NDVI time series from the AVHRR sensor to isolate orbital drift effects from the NDVI signal. Further details on the quality of the AVHRR dataset may be found in Kaufmann et al. (2000) and Zhou et al. (2001).

The GIMMS data set is originally defined on an Alberts Conical Equal-area projection, using the Clarke ellipsoid. Data used in our study respects to a window covering the Eurasian and the North Atlantic regions, from 30º W to 60º E and from 30º to 75º N, over the 21-year long period, from 1982 to 2002. This dataset will be used in Chapters 4 and 5 and it is worth mentioning that NDVI values were re-projected to geographic coordinates, using a nearest neighbour scheme (Chapter 2).

3.1.4 NDVI data fromVEGETATION/SPOT

As pointed out in Chapter 2, VEGETATION on board SPOT 4 and SPOT 5 is an optical multi-spectral instrument that performs an almost complete cover of the Earth surface in four spectral bands (Hagolle et al., 2005), on a daily basis. NDVI data were extracted from the S10 products of the VITO database (http://free.vgt.vito.be), which are supplied at the resolution of 0.008928º (i.e., about 1 km^2 resolution at equator) in geographic coordinates (Lat/Lon), using the WGS84 ellipsoid It may be noted that supplied values of NDVI were derived from atmospherically corrected and geometrically calibrated data and that we have restricted to the period from September 1998 to July 2006 over the region extending from 37º N to 42º N and from 9º W to 6º E.

NDVI fields are given on a 10-day basis as derived using the Maximum Value Composite method (MVC, Holben, 1986), which simply consists in selecting, for each pixel, the date of maximum NDVI among 10 consecutive daily images. Despite some problems, time series of MVC-NDVI composites have proven to be a source of valuable information for monitoring surface vegetation dynamics at the global and the regional scales (Zhou et al., 2001; Lucht et al., 2002; Nemani et al., 2003). Remaining problems are related with contamination by clouds, shadows and snow, with sun/view directional dependence of the spectral response as well as with the dependence of phenological changes both on time of observation and on geographical location.

In order to create a consistent dataset of vegetation phenology, the yearly time-series of VGT-NDVI were analysed and corrected, following the method proposed by Stockli and Vidale (2004) that has been successfully applied to the Pathfinder NDVI data in order to create a continuous European vegetation phenology dataset of 10-day temporal and 0.1º spatial resolution. The approach involves two steps in the spatio-temporal interpolation process; i) a replacement of no-data values in the dataset by

spatial interpolation and ii) an adjustment of the NDVI time-series by using a temporal interpolation procedure.

The methodology relies on the application of an adjustment algorithm based on a weighted second-order Fourier analysis of the data, as previously described by Sellers et al. (1996) and Los (1998). This approach uses different correction procedures for the growing and the non-growing season and therefore requires a precise definition of the growing season, which in Portugal usually starts with the hydrological year, i.e. year N starts in the second decade of August of year N-1 and ends in the first decade of August of year N).

The correction method was applied to VGT-NDVI 10-day composites with 1 km spatial resolution for the period from September of 1998 to July 2006. Figure 3.4 shows four representative examples of corrected (red line) and non-corrected (green dots) monthly time-series of NDVI for different land cover types.

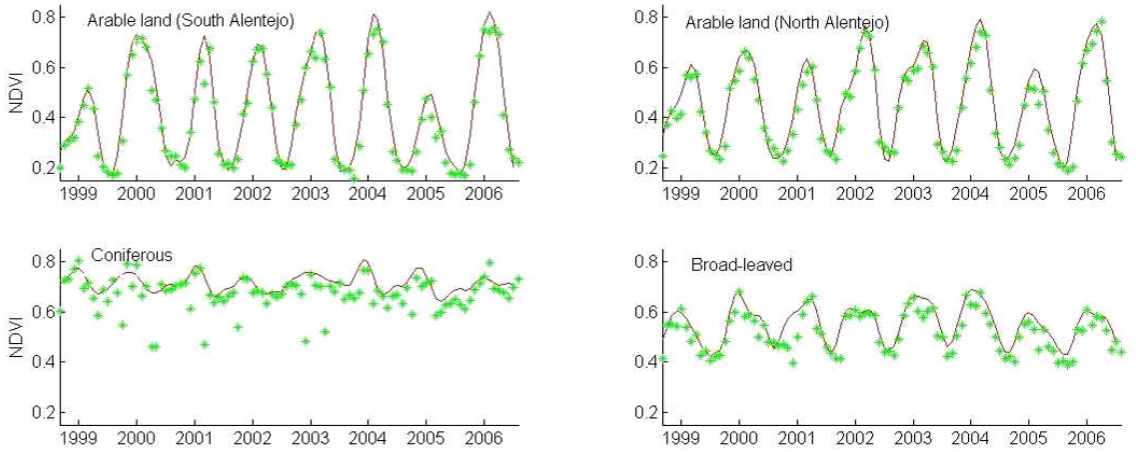

Figure 3.4 Monthly time-series of NDVI for the period 1999–2006 and respecting to four different land cover types; an arable land pixel located in South Alentejo (left top panel), an arable land pixel located in North Alentejo (right top panel), a coniferous forest pixel (left bottom panel) and a broad-leaved forest pixel (right bottom panel). Green dots and the solid curve respectively represent the time series of corrected and non-corrected NDVI monthly values.

With the exception of the coniferous type, the years of 1999 and 2005 are conspicuous in the time series because of the low photosynthetic activity. This is especially apparent in the case of the pixels associated to arable land (Figure 3.4, top panels). In particular, in the case of the arable land pixel located in South Alentejo (top

left panel) the years of 1999 and 2005 reveal marked signs of stress in the vegetation, which presents shorter vegetation cycles together with lower values of NDVI. In the case of forest pixels (low panels), the coniferous forest, as expected, presents a high photosynthetic activity along the year (high NDVI values) together with low interannual variability, while the broad-leaved type presents a pronounced year cycle of NDVI.

Figure 3.5 shows the results that were obtained when applying to non-corrected (left panel) and to corrected (right panel) NDVI pixels a technique aiming to detect years affected by drought conditions. The technique that will be described in Chapter 6, is based on the number of months characterised by negative anomalies below a given threshold. In the case of 2002, results are dramatically different when applied to non-corrected and to corrected NDVI. In the first case, pixels associated to a high number of months with strong negative anomalies present a rather noisy spatial structure and the year would not be classified as stricken by drought. However when corrected pixels are used, a large region of strong negative anomalies is well apparent in the Northeast of Portugal, indicating that the area was in fact under drought conditions, in good agreement with climatological records.

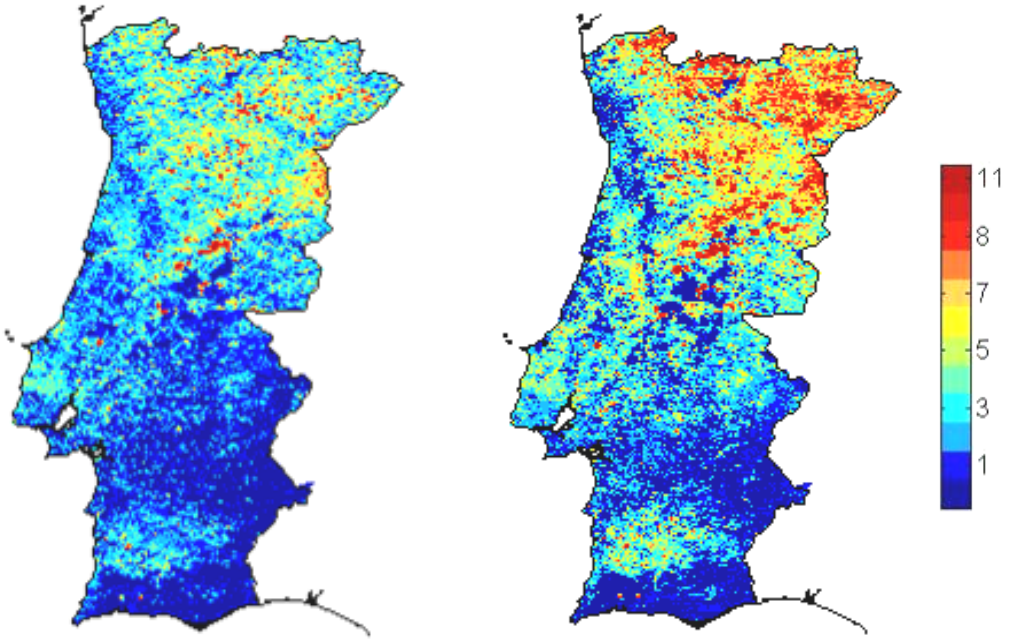

Figure 3.5 Number of months between September 2001 and August 2002 that are characterised by NDVI anomaly values below -0.025, using non-corrected (left panel) and corrected (right panel) NDVI data.

3.2 Land Cover Maps

3.2.1 Introduction

Land cover and land use mapping based on remote sensing data are becoming more and more important at both national and continental scales. In fact, the continuous monitoring of crop fields, paddy fields and deforested areas require land cover and land use data providing an extensive coverage with relatively high accuracy. Land cover relates to the physical condition of the surface (e.g. forest, grassland, water), whereas land use reflects human activities (e.g. industries, urban areas, agricultural fields). Land cover maps are always associated to a given land cover classification system, which is usually defined in terms of levels and classes. Land use may not necessarily coincide with land cover and may even be composed of several land cover classes.

3.2.2 The Global Land Cover 2000 Project

The Global Land Cover 2000 (GLC2000) project was designed to provide information to the International Conventions on Climate Change, the Convention to Combat Desertification, the Ramsar Convention and the Kyoto Protocol. The GLC2000 land cover database has also been chosen as a core dataset for the Millennium Ecosystems Assessment playing, in such context, a key role to define the boundaries of the different ecosystems, e.g. forest, grassland, and cultivated areas. In fact, reliable information about land cover is becoming essential in a wide range of fields, from an accurate specification of boundary conditions in climate and land surface process models, to the assessment of the impact and effectiveness of management actions associated with sustainable development policies.

In contrast to former global mapping initiatives, the GLC2000 project is a bottom up approach to global mapping (Figure 3.6), where more than 30 research teams have been involved, contributing to 19 regional windows. The fact that the mapping was carried out by regional experts has several benefits. First, as regional experts have a high level of knowledge about their particular region, a certain level of quality can be guaranteed. Second, each partner has the freedom to apply their own methods of

mapping and define their own regional legend, which allows them to apply the classification techniques they find as most appropriate for land cover mapping in their respective region. Third, the regional mapping approach ensures that access could be gained to reference material. However in order to guarantee the necessary consistency, the two following conditions had to be fulfilled by the regional experts; i) the data had to be based on SPOT-4 VEGETATION VEGA2000 dataset, which was made freely available by CNES, ii) the partners had to use the Land Cover Classification System which was adopted by FAO (Di Gregorio and Jansen, 2000).

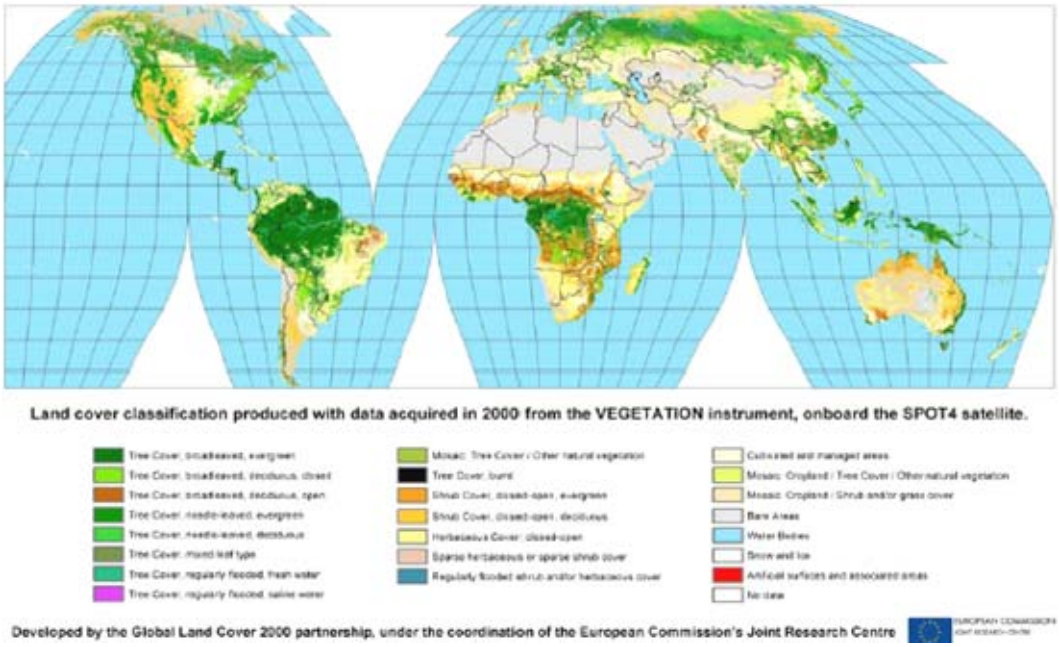

Figure 3.6 The Global Land Cover 2000 Project.

The Central European window was mapped by the Department of Environmental Sciences and Land Use Planning, at Catholic University of Louvain (Universite Catholique de Louvain, UCL), Belgium. In the classification process, fifteen land cover classes have been determined and labelled using a combination of reference information from the CORINE landcover database (see next sub-section), the interpretation of high resolution satellite imagery (Landsat TM) and the knowledge of the local experts. In 2006 the European window classification was updated and the result is presented in Figure 3.7.

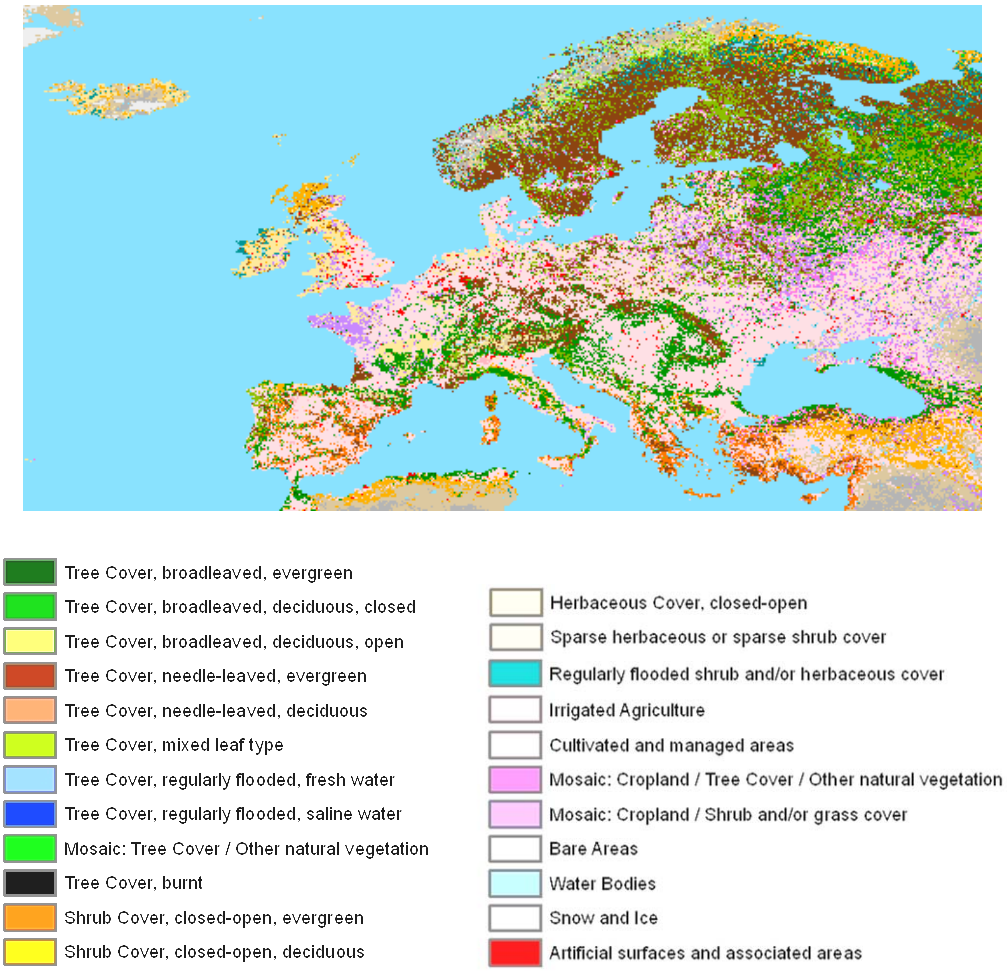

Figure 3.7 The updated version of the GLC2000 map for the European Window. (http://www-gvm.jrc.it/glc2000)

3.2.3 The Corine Land Cover 2000 project

The Corine Land Cover 2000 (CLC2000) project is based on the interpretation of satellite images and aims at providing comparable digital maps of land cover for most countries of Europe. The first CLC database was finalised in the early 1990s as part of the European Commission programme to COoRdinate INformation on the Environment (CORINE). It provides consistent information on land cover changes during the past decade across Europe. CLC has revealed to be particularly useful for environmental analysis and comparisons as well as for policy making and assessment. No other land cover information programme in the world covers such a wide geographical area in such

detail. CLC is recognised by decision-makers as a fundamental thematic reference data set for spatial and territorial analyses.

At the end of the 1990s several users at national and European levels expressed a need for its update. The European Environment Agency (EEA) and the Joint Research Center (JRC) launched the IMAGE2000 and CLC2000 projects, which consisted in the update of the Corine Land Cover 90 database. Image2000 is a related project to Corine Land Cover 2000 that provided the necessary Landsat 7 imagery (Figure 3.8) for the updating of the European Land Use/ Land Cover database.

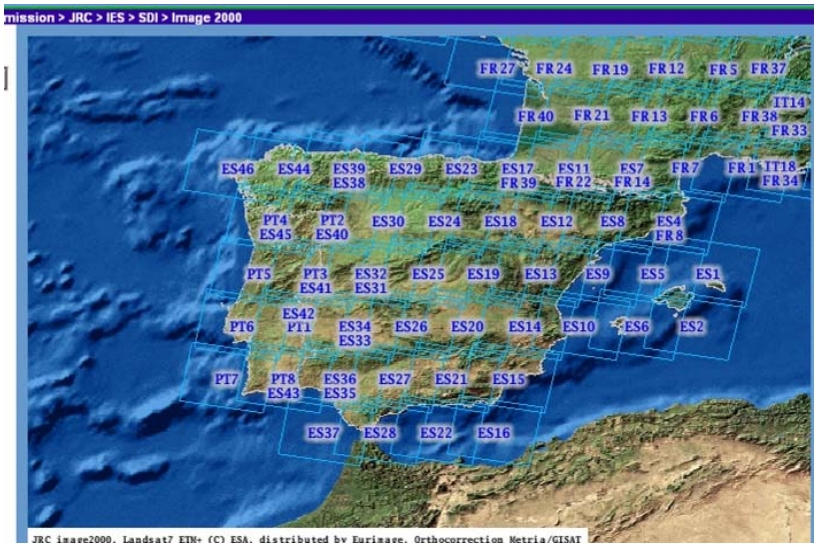

Figure 3.8 Landsat 7 imagery for the updating CLC, using the IMAGINE2000 software. (http://image2000.jrc.it/)

CLC is therefore a key database for integrated environmental assessment studies, namely those related with agricultural issues, and provides a pan-European inventory of biophysical land cover, using a 44 class-nomenclature. In Portugal, the development of this thematic map was made under the responsibility of Instituto Superior de Estatística e Gestão da Informação (ISEGI). This Corine Land Cover 2000 for Portugal (Figure 3.9) is originally provided on a 250m by 250m grid, using a Transverse Mercator projection with the Hayford spheroid. However, the majority of remote sensing imagery used in this work is defined on geographic coordinates, with 1000m at resolution. Therefore, in order to enable comparisons of images which had different spatial resolutions, it was necessary to resample the CLC2000 map to the coarser resolution of 1000m.

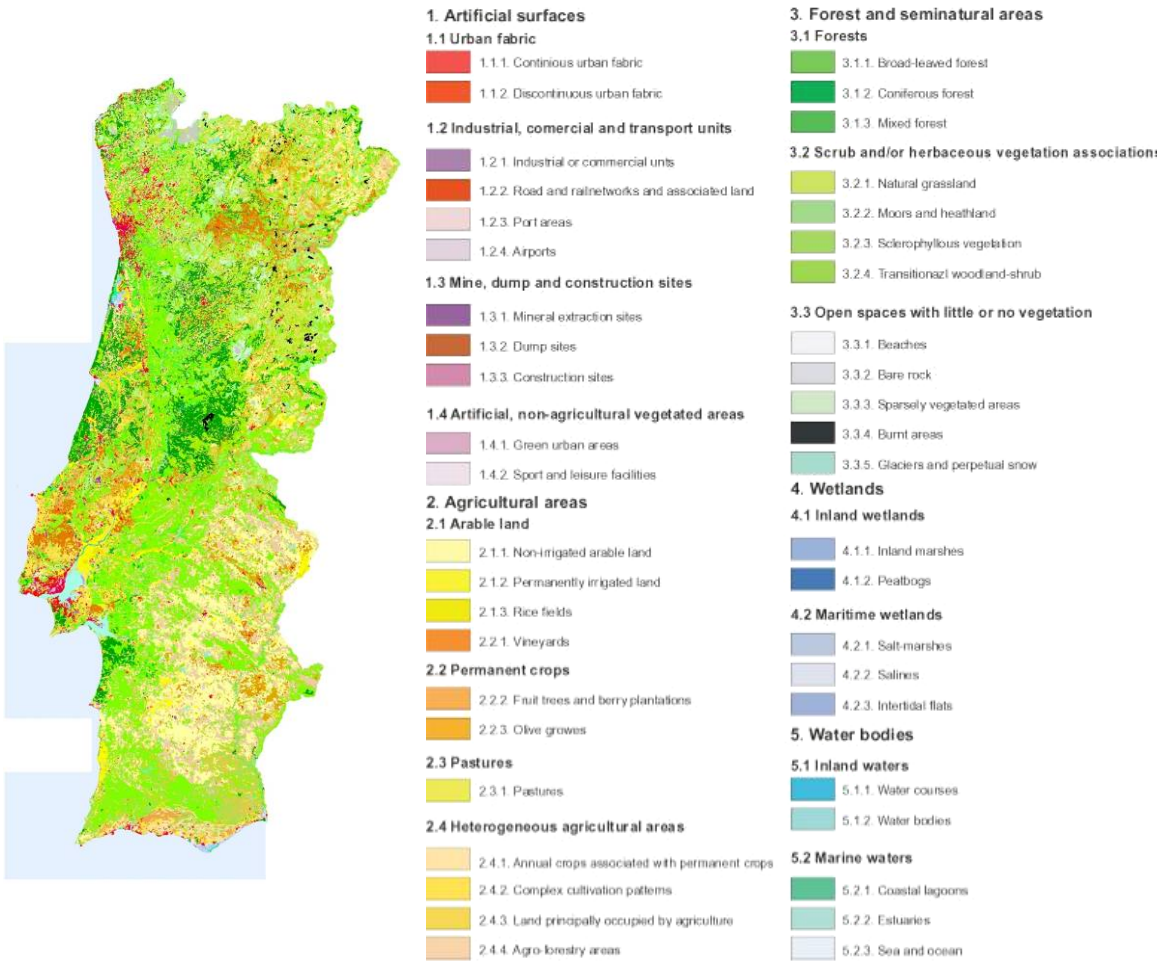

Figure 3.9 Corine Land Cover 2000 map for Portugal, as developed by ISEGI and the adopted 44 class-nomenclature (http://terrestrial.eionet.europa.eu/CLC2000).

We started by using the nearest neighbour re-sampling technique because of the expected good results for less populated classes (Schowengerdt, 1997). Results obtained for Portugal and for a box centred on the Tagus estuary are shown respectively in Figures 3.10 and 3.11. When comparing the original maps (left panels of Figures 3.10 and 3.11) with the ones obtained using the nearest neighbour technique (central panels), it may be observed that some of the classes, e.g. water courses (code 5.1.1) are correctly resampled, whereas some other classes, e.g. urban areas (codes from 1.1.1 up to 1.4.2) are less correctly represented.

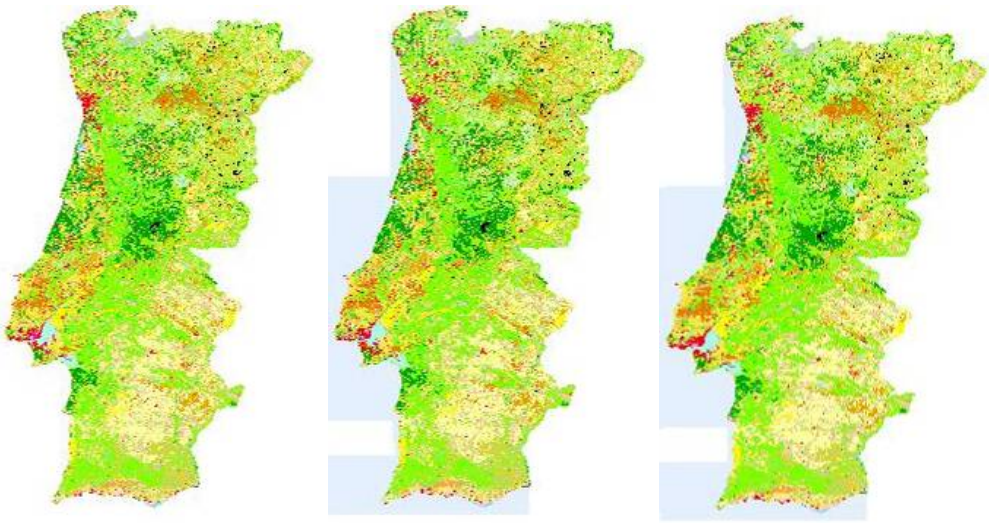

Figure 3.10 Corine Land Cover 2000 map for Portugal; the original map at 250m resolution (left panel), the degraded map at 1000m resolution using the nearest neighbour technique (central panel), the degraded map at 1000m resolution using the majority rule (right panel).

We have also tested a degradation procedure based on the majority rule that is commonly applied when degrading thematic maps, namely land cover maps (Turner et al., 1989; Benson and Mackenzie, 1995; Wu et al., 2002; Saura, 2004). The underlying assumption is that when applying the majority rule (i.e. the degraded image pixels are assigned to the most frequent class) similar patterns are produced at coarser resolutions. Majority rules assign to the degraded image the most frequent class in windows of F×F pixels, where F, the aggregation factor represents the relation between the length of a pixel in the degraded and in the original image. When applying this criterion to the CLC2000 map for Portugal at 250m of resolution in order to obtain a degraded map at 1000m resolution, the procedure involves degradation by a scale factor of 4 in each direction. The obtained maps, for Continental Portugal and for the box centred in the Tagus estuary are also shown in Figures 3.10 and 3.11 (right panels). In general, and independently of the aggregation method used, there is an under representation of the less frequent classes in the original map. In the case of water courses (code 5.1.1), the results obtained when using the majority rule were slightly worse than when using the nearest neighbour technique. However, other equally less frequent classes, e.g. the urban areas (codes from 1.1.1 up to 1.4.2) present higher spatial consistency when the majority rule is used.

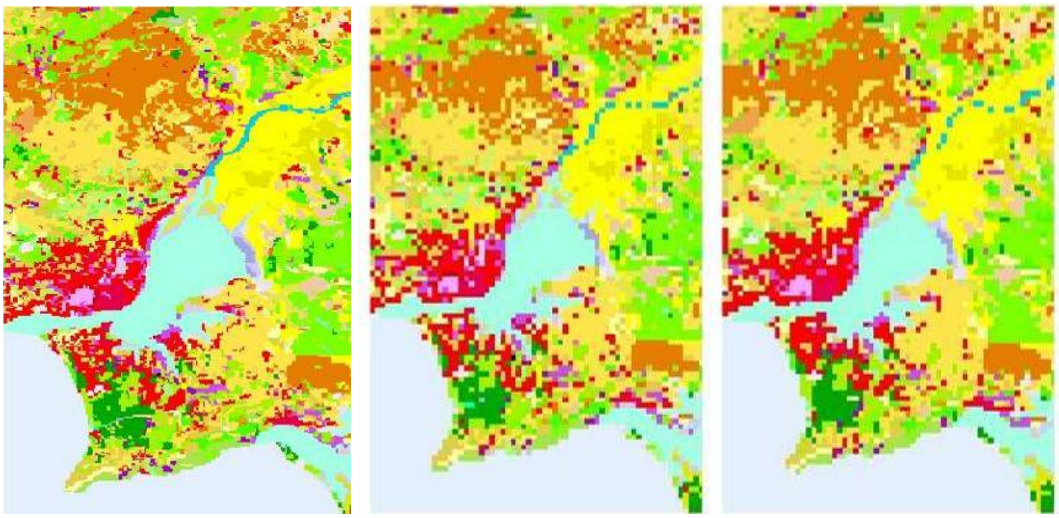

Figure 3.11 As in Figure 3.10 but respecting to a box centred in the Tagus estuary.

Figure 3.12 presents an histogram of relative frequencies of pixels over Portugal that belong to each CLC2000 class as obtained from the original map (blue bars) and from the two independently degraded maps using the nearest neighbour technique (green bars) and the majority rule (red bars). It may be noted that, when using the nearest neighbour technique there is an overall agreement between relative frequencies of original and degraded classes. In the case of the majority rule, homogeneously distributed classes, e.g., non irrigated arable land (code 2.1.1) and forest (codes 3.1.1 and 3.1.2) are overestimated, whereas scattered classes, e.g., land occupied by agriculture (code 2.4.3) and transitional woodland-shrubland (code 3.2.4) tend to be underestimated.

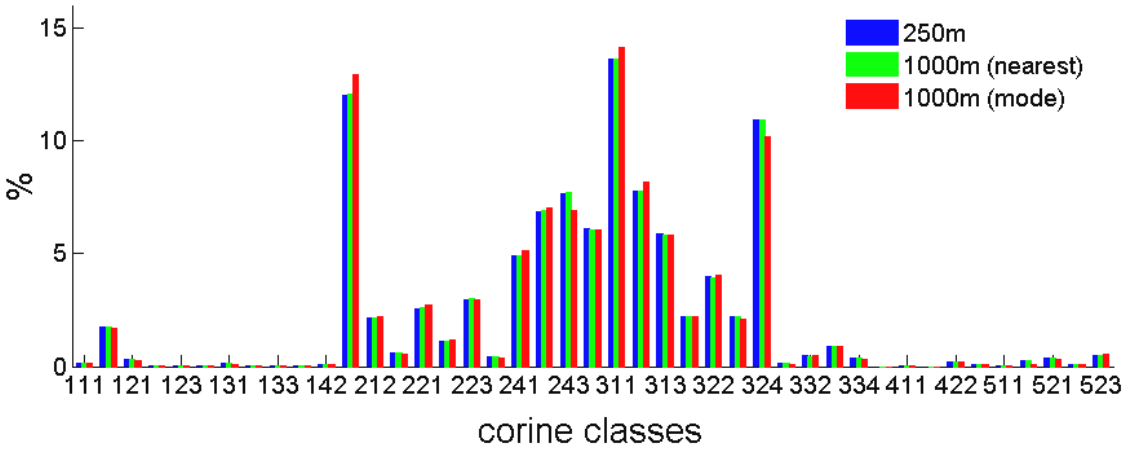

Figure 3.12 Histogram of relative frequencies of pixels in the 250m original map (blue), and in the 1000m degraded maps as obtained using the nearest neighbour technique (green) and the majority rule (red). Labels in bars identify classes referred to in the text.

The majority rule has however the advantage of assessing the relative presence of the most frequent class within the 4×4 pixel windows. In fact, when there is the need to assign pixels to a given class, specific thresholds (e.g. 50%, 75% or 90%) may be defined in such a way that a pixel is considered as representative of that class when the relative presence of that class is above the specified threshold. This procedure has the advantage of providing predefined levels of confidence for each class label, while maintaining a sufficiently large sample in each class (Lotsch et al., 2003).

Figure 3.13 presents several examples of the obtained spatial distribution of relative presence for a set of five GLC2000 classes, respectively urban areas (code 1.1.2), non irrigated arable land (code 2.1.1), broad-leaved forest (code 3.1.1), water courses (code 5.1.1) and estuaries (code 5.2.2). For instance, if there is the need to mask pixels contaminated by the presence of urban areas or water courses, a low threshold, e.g. 20%, has to be chosen in order to assure that contamination is adequately prevented. On the other hand, if the aim is to identify pixels associated to arable land or to forest a moderate threshold, e.g. 50%, may be appropriate. Finally a high threshold, e.g. 90% may be chosen if the aim is to study very specific areas, such as estuaries.

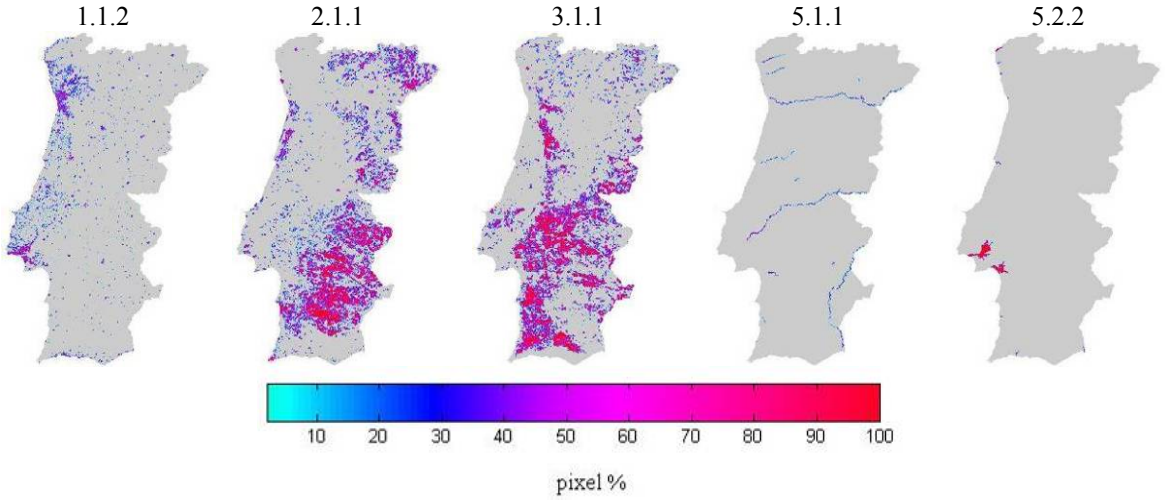

Figure 3.13 Spatial distribution of relative presence for a set of five GLC2000 classes for the 1000m degraded maps using the majority rule, respectively urban areas (code 1.1.2), non irrigated arable land (code 2.1.1), broad-leaved forest (code 3.1.1), water courses (code 5.1.1) and estuaries (code 5.2.2).

In the present work, the majority rule was used to degrade CLC2000 to 1000m resolution in order to identify land cover classes that were affected by drought (Chapter 6) and by wildfires (Chapter 7). In Chapter 5 we have defined a threshold of 50% to produce a 8000 m degraded map of non irrigated arable land (code 2.2.1) in order to identify areas with wheat crops and monitor the vegetation cycle using GIMMS-NDVI at 8 km resolution.

3.3 Climate data

3.3.1 Meteorological Data

Meteorological data used in this study are large-scale gridded data as retrieved from the Climate Research Unit (CRU) datasets, for the period 1982-1999. A complete description of the methodology used to derive this monthly high-resolution (10' resolution) climatic database may be found in Mitchell and Jones (2005). This high resolution dataset replaces the coarser resolution CRU dataset (0.5º x 0.5º) widely used in many climatic variability studies over Europe (e.g. Trigo et al., 2004; Paredes et al., 2006). This dataset was built based on an optimum interpolation method that takes into account latitude, longitude, and elevation using thin-plate splines (New et al., 1999; 2000). The accuracy of the obtained interpolations is assessed using cross validation as well as through objective comparisons with other climatologies. The higher resolution database was checked for inhomogeneities in the station records, by means of an automated procedure that refines previous methods using incomplete and partially overlapping records and through the detection of inhomogeneities with opposite signs in different seasons (Mitchell and Jones, 2005).

Monthly values of cloud cover, temperature and precipitation, were extracted from the CRU database for the window 35ºN-45ºN, 10ºW-0ºE. Under the scope of the Portuguese funded (FCT/ESA) project CARBERIAN (Terrestrial Vegetation Carbon Trends in the Iberian Peninsula), the CRU TS 1.2 10' climate datasets were interpolated to the GIMMS NDVI coordinates grid with a recently developed non-linear method (Zhao et al., 2005). The cloud cover time series were then converted to net solar radiation fields using the Soil and Water Assessment Tool, a method developed by

Neitsch et al. (2002). This procedure yielded monthly climate fields geographically compatible with GIMMS NDVI.

The Global Precipitation Climatology Project (GPCP) is an element of the Global Energy and Water Cycle Experiment (GEWEX) of the World Climate Research program (WCRP). It was established by the WCRP in 1986 with the major aim of providing monthly mean precipitation data on a 2.5°×2.5° latitude/longitude grid. Monthly mean precipitation estimates are being produced continuously since 1979. In this dataset infrared and microwave satellite estimates of precipitation were merged with rain gauge data from more than 6,000 stations. Infrared precipitation estimates are obtained from GOES (United States), GMS (Japan) and Meteosat (European Community) geostationary satellites as well as from the National Oceanic and Atmospheric Administration (NOAA) operational polar orbiting satellites. Microwave estimates are obtained from the U.S. Defense Meteorological Satellite Program (DMSP) satellites using the Special Sensor Microwave Imager (SSM/I). These data sets will be used to validate general circulation and climate models, to study the global hydrological cycle and to diagnose the variability of the global climate system.

In recent years the data sets have been updated and enlarged, to that besides the monthly mean product available, the GPCP has now a 2.5°×2.5° degree pentad data set since 1979, a 1°×1° daily data set since 1997 and (on request) the 0.5º×0.5º grid monthly data. Here we have used monthly precipitation data from the GPCC (Rudolf and Schneider, 2005) with the highest resolution (0.5º latitude by 0.5º longitude grid), covering the period 1982-2002 for the European window.

3.3.2 North Atlantic Oscillation

The North Atlantic Oscillation (NAO) has been recognized for more than 70 years as one of the major patterns of atmospheric variability in the Northern Hemisphere (Walker, 1924). The NAO refers to a meridional oscillation of the atmospheric mass with centers of action located near Iceland and over the subtropical Atlantic from the Azores across the Iberian Peninsula. When NAO is in its positive phase, low pressure anomalies over the Icelandic region and throughout the Arctic combine with high-pressure anomalies across the subtropical Atlantic to produce

stronger than average westerlies across the midlatitudes. Therefore, this phase of the oscillation is associated with cold conditions over the northwest Atlantic and warm weather over Europe, together with wet conditions from Iceland through Scandinavia and dry conditions over southern Europe.

However, only in recent years has this important atmospheric circulation mode become the subject of a wider interest (e.g. van Loon and Rogers, 1978; Rogers, 1984; Barnston and Livezey, 1987). More recently, the study by Hurrell (1995) had significant impact on the climatological community and has been followed by an increasing number of studies. It is within this context, that several studies have established links between the NAO index and winter season precipitation in Western Europe and, in particular, over the Mediterranean basin (Hurrell 1995; Qian et al., 2000; Trigo et al., 2004). This control exerted by NAO on the precipitation field over Europe is likely related to corresponding changes in the associated activity of North Atlantic storm tracks (Serreze et al., 1997; Osborn et al., 1999). In fact, this strong NAO-precipitation link has been used to develop rainfall forecast models that predict precipitation in Iberia several months in advance (e.g. Gámiz-Fortis et al, 2002; Rodriguez-Fonseca and Castro, 2002). The output of these models may provide useful seasonal forecasting tools for water resource managers and risk assessment teams (Trigo et al., 2004).

The NAO index used in this study is based on the one developed by the Climatic Research Unit (University of East Anglia, UK) which was originally defined, on a monthly basis, as the difference between the normalized surface pressure at Gibraltar, in the southern tip of the Iberian Peninsula and Stykkisholmur, in Iceland (Jones et al., 1997). For each year covering the 21-year long period from 1982 to 2002, we have derived a late winter NAO index, defined as the average of the monthly values of January, February and March of the corresponding year. In this work we will use the term NAO to refer to the three-monthly averaged as well as to any averaged quantity over January, February and March (e.g, P_{NAO} for averaged precipitation). It may be finally noted that the original time series of winter monthly values of the NAO index presents a positive trend over the last 30 years and therefore its distribution is dominated by positive values, leading to late winter averages above zero (Jones et al., 1997). As a representative example, Figure 3.14 shows the patterns of simple correlation computed over the period 1982-2002 the three monthly averages of winter

NAO (JFM) vs. winter precipitation (top panel) and surface air temperature (bottom panel).

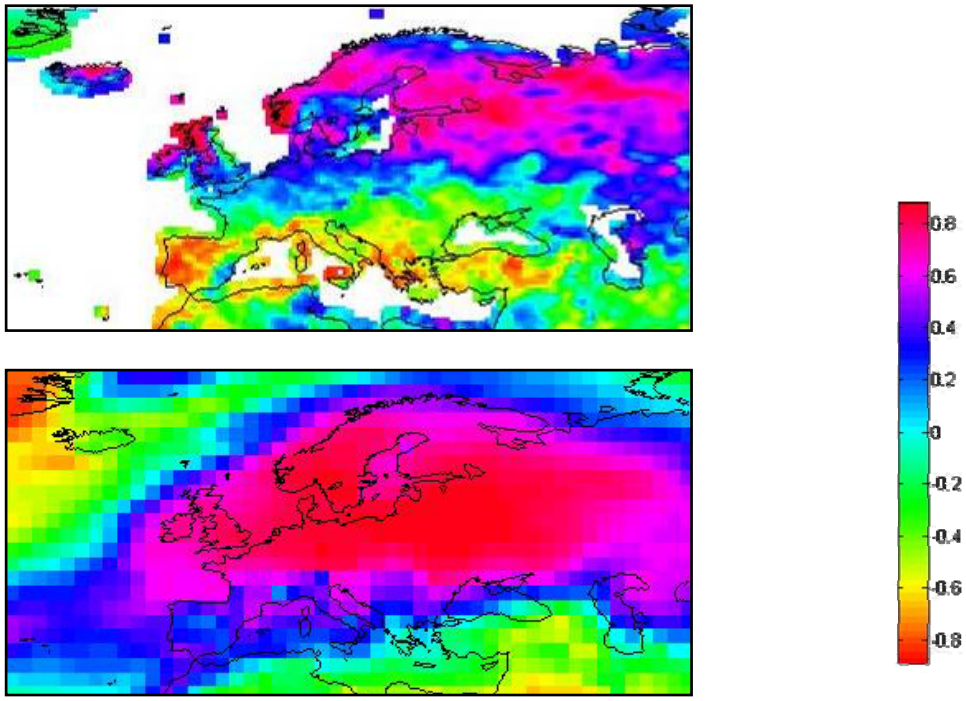

Figure 3.14 Patterns of simple correlation computed over the period 1982-2002 of three-monthly averages of winter NAO (JFM) vs. winter precipitation (top panel) and surface air temperature (bottom panel).

4. CLIMATE IMPACT ON VEGETATION DYNAMICS

4.1 Introduction

Over the last two decades, the continuous monitoring of vegetation from space has prompted new studies aiming to relate the observed major global changes in vegetation (e.g. trends, variability and extremes) with changes of surface climatic variables, such as temperature and precipitation (Myneni et al., 1997, Hansen et al., 1999, Zhou et al., 2001). In particular, several groups have shown that the recorded rise of temperature in the northern latitudes by 0.8ºC in the last 25 years has been accompanied by a significant reduction in annual snow cover as induced by an early melting of snow in spring (Groisman et al., 1994, Vinnikov et al., 1999). A longer active growing season has also been observed as a result of an early spring and delayed autumn (Bogaert et al., 2002, Shabanov et al., 2002). This change in the annual cycle is associated with an increase in photosynthetic activity of vegetation (Zhou et al., 2001), as detected from observed changes in the Normalised Difference Vegetation Index (NDVI).

Although no evidence has been given that such changes in NDVI are related to the positive trend in atmospheric concentration of CO2 (Kaufmann et al., 2002), the global carbon cycle has been certainly affected (Keeling et al., 1996) and there is a strong need for long-term and large-scale studies aiming to assess the impact of atmospheric circulation variability on surface climate and related vegetation activity. In this respect special attention has been devoted to investigating relationships between vegetation dynamics and the North Atlantic Oscillation (NAO), which (as shown in Chapter 3) is the major pattern of atmospheric variability in the Northern Hemisphere (Hurrell, 1995). A number of studies have naturally addressed the question of the relationship between NDVI and meteorological fields, namely temperature and precipitation. Vicente-Serrano and Heredia-Laclaustra (2004) have adopted the climatological viewpoint and focused their attention on the Iberian Peninsula where the influence of winter NAO on the

precipitation regime is especially prominent in the south-west region (Rodriguez-Puebla et al., 1998). They have shown the existence of a positive trend in annual vegetation productivity where the NAO influence is weaker, in strong contrast to the stable or negative trends that were detected in the areas located in the south of Iberia, where precipitation is mostly determined by NAO. However the authors pointed out the need for further studies, at finer temporal scales, namely at the monthly and seasonal ones.

Stöckli and Vidale (2004) have found that spring plant phenology over Europe is well correlated with the winter NAO index. Their study has focused on several geographical sub-domains of Europe that neither reflect any bio-geographical stratification nor any particular sensitivity to the NAO index. The Mediterranean and, in particular, the Iberian Peninsula was not included in the study because their analysis procedure required a large seasonal amplitude in the phenology. The aim of the present chapter is to fill the gap between the assessment made by land cover experts and by researchers that have looked at the problem from a climatological viewpoint. We will search for relationships between NAO and vegetation activity at the month and seasonal levels over Europe and look for regions where such activity presents a clear dependence on NAO both in spring and summer. We will then investigate how such dependence may be explained in terms of the impact of NAO on relevant surface climate variables, namely temperature and precipitation. We will pay special attention to the Iberian Peninsula and Northeastern Europe because of the distinctive vegetation response to precipitation and temperature. Finally, we will identify which of the variables have a determinant role on vegetation activity of different regions and make an assessment on the role played by the variables in the annual cycle of vegetation activity.

Accordingly, the main goals of this chapter are the following:

- To study the relation between vegetation phenology and NAO over Europe.
- To characterise the vegetation response to precipitation and temperature in two contrasting areas of Europe, respectively Northeastern Europe and the Iberian Peninsula.
- To assess the impact of NAO on the vegetative cycle in the two areas, and relate it to the different land cover types and their response to surface climate variability.

Relationships between NAO and diverse aspects of European vegetation dynamics have been addressed by various authors. D'Odorico et al. (2002) showed that spring phenology in the British Isles is influenced by NAO. Dates of leaf unfolding for a mean of nine plant species vary over a 40-day range, from approximately the spring equinox to the end of April. The Julian date of leaf unfolding is inversely correlated with the NAO phase, i.e. leaf unfolding occurs earlier under positive, and later under negative phases of NAO. Similar patterns are reported for Poland, Norway and Sardinia. D'Odorico et al. (2002) also found a strong NAO influence on the timing of the pollen season in Europe.

Cook et al. (2004) modelled the NAO-dependence of phenological variability in Europe, mediated by the NAO influence on synoptic scale winter temperature variability, and successfully reproduced observed patterns of growing degree-days over Europe. A projection of NAO trends 50 years into the future, based on climate change scenarios, indicated a sustained advance of the growing season start.

Stöckli and Vidale (2004) used AVHRR Pathfinder NDVI data, and found that spring phenology correlates well with anomalies in winter temperature and winter NAO index. They established the existence of trends towards an earlier onset and longer duration of the spring vegetation growing period, especially significant over Central Europe.

Vicente-Serrano and Heredia-Laclaustra (2004) analysed the relationship between the NAO index and vegetation productivity (represented by the annual integral of monthly AVHRR Pathfinder NDVI values) trends, for the Iberian Peninsula. Areas of stable or decreasing vegetation productivity were located in southern Iberia, where the NAO influence is stronger. Significant positive productivity trends occur in the north of the Peninsula, where the NAO influence on vegetation dynamics is weaker.

We will rely on AVHRR NDVI data from the Global Inventory Modelling and Mapping Studies – GIMMS group (see Chapter 3), which incorporate more thorough and accurate corrections of orbital drift, radiometric degradation, and volcanic aerosol effects than those previously applied to the Pathfinder AVHRR Land (PAL) product, used in earlier works.

4.2 Methodology

As pointed out in the introduction, we will look for relations involving large-scale atmospheric variability, vegetation greenness and surface climate. Accordingly the main sources of information consist of time-series of the NAO index, NDVI and, for surface climate, precipitation (P) and brightness temperature (T), which may be taken as a proxy of land surface temperature.

It may be noted that the time-series of NAO indices (see Chapter 3) was normalized over the 21-year period and therefore our three-monthly averages have zero mean and unit standard deviation between 1982 and 2002 (Figure 4.1). Accordingly, we have derived a late winter NAO index, defined as the average of the monthly values of January, February and March of the corresponding year. From now on we will use the term NAO to refer to the three-monthly averaged index and any averaged quantity over January, February and March will be also identified by the subscript NAO (e.g. P_{NAO} and T_{NAO}).

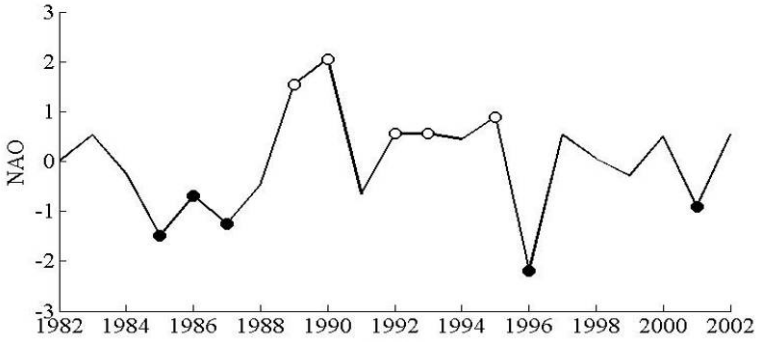

Figure 4.1 Interannual variability of late winter NAO index over the 21-year long period, from 1982 to 2002. Open (black) circles indicate years characterised by NAO indices above (below) the 3rd (1st) quartile.

We have also used monthly precipitation data from the Global Precipitation Climatology Centre (GPCC) (Rudolf and Schneider, 2005). Selected data are defined on a 0.5º latitude by 0.5º longitude grid and cover the same period and window as the satellite data (see Chapter 3).

Finally, we have used monthly values of NDVI and channel 4 brightness temperature, at 8-km resolution, from the Advanced Very High Resolution Radiometers (AVHRR), as provided by the Global Inventory Monitoring and Modelling System (GIMMS) group (see Chapter 3). Selected data are defined on a window covering the Eurasian and North Atlantic regions, from 30º W to 60º E and from 30º N to 75º (Figure 4.2). For each grid point we have computed spring and summer values of NDVI, T and P, respectively defined as the average of March, April and May and of June, July and August. Spring and summer values of a given quantity will be respectively denoted by the subscripts SPR and SUM. The results were then re-projected to Geographic Coordinates, based on the nearest neighbour scheme (Chapter 2). Figure 4.2 presents the spatial distribution of the temporal averages of $NDVI_{SPR}$ (left panel) and $NDVI_{SUM}$ (right panel) for the considered period (1982-2002). As expected, very low values of $NDVI_{SPR}$ may be observed over Iceland and the Scandinavian Peninsula along the borders of the areas covered by snow and ice. Low values of $NDVI_{SPR}$ cover south-western Iberian and south Scandinavia, whereas the highest values are located over central and western Europe. A strong increase in vegetation activity may be also observed during summer for the entire European window, with the exception of the Iberian Peninsula.

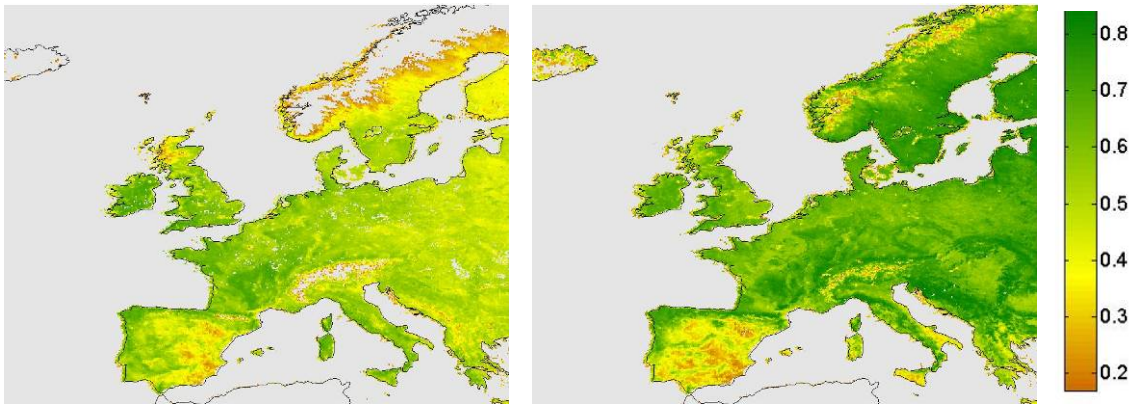

Figure 4.2 Temporal averages of $NDVI_{SPR}$ (left panel) and $NDVI_{SUM}$ (right panel) over the period from 1982 to 2002. Gray pixels over land correspond to areas covered by snow and ice.

Figure 4.3 shows the spatial distribution of the temporal averages of T_{NAO} and P_{NAO}. In the case of T_{NAO} the lower values may be found in Northern Sweden, Iceland and the Alps, and the lower values spread over the south of the Iberian Peninsula. On

the other hand, the highest values of P_{NAO} may be found for western Sweden and Britain and high values may be also found in North-western Iberia.

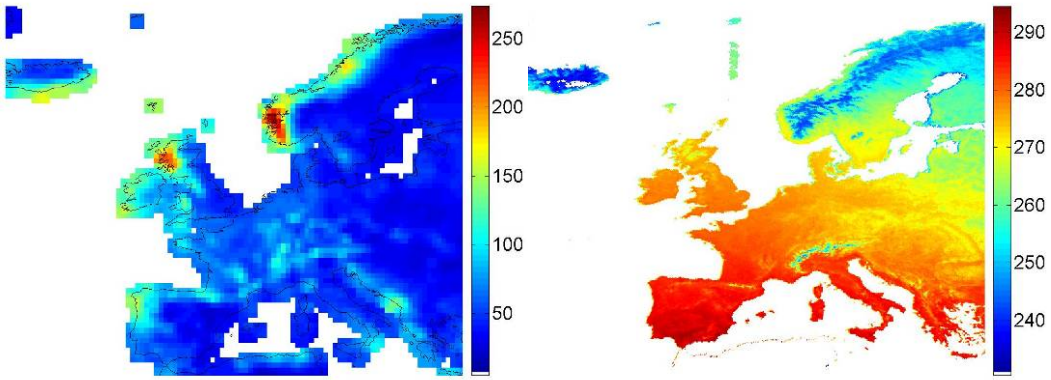

Figure 4.3 As in Figure 4.2 but for P_{NAO} (left panel) and T_{NAO} (right panel).

4.3 NAO and Vegetation Greenness

Figure 4.4 displays the spatial patterns, over the selected European window, of point correlation values of NAO vs. $NDVI_{SPR}$ and NAO vs. $NDVI_{SUM}$ for the considered 21-year period. Results show a positive correlation region over Central Europe for spring (left panel), the highest values (between 0.6 and 0.8) spreading around the north-eastern region. The largest negative correlation regions are located over the Iberian Peninsula and Iceland, some values reaching as low as -0.8. It may be noted that obtained patterns are consistent with the recent findings by other authors, at both the global (Buermann et al., 2003) and the regional (e.g. Vicente-Serrano and Heredia-Laclaustra, 2004) scales. However, it is worth stressing that we have based our analysis on a much finer spatial resolution than Buermann et al. (2003) and, despite the overall consistency, some differences do exist, namely the higher values of correlation that we obtained over the north-eastern sector.

In the case of summer (Figure 4.4, right panel) the correlation field presents negative values over almost all Central-Eastern Europe. This pattern is also consistent with the findings of Buermann et al (2003), but their maximum core is located towards the northern Black Sea area, whereas ours is confined to the upper Danube region.

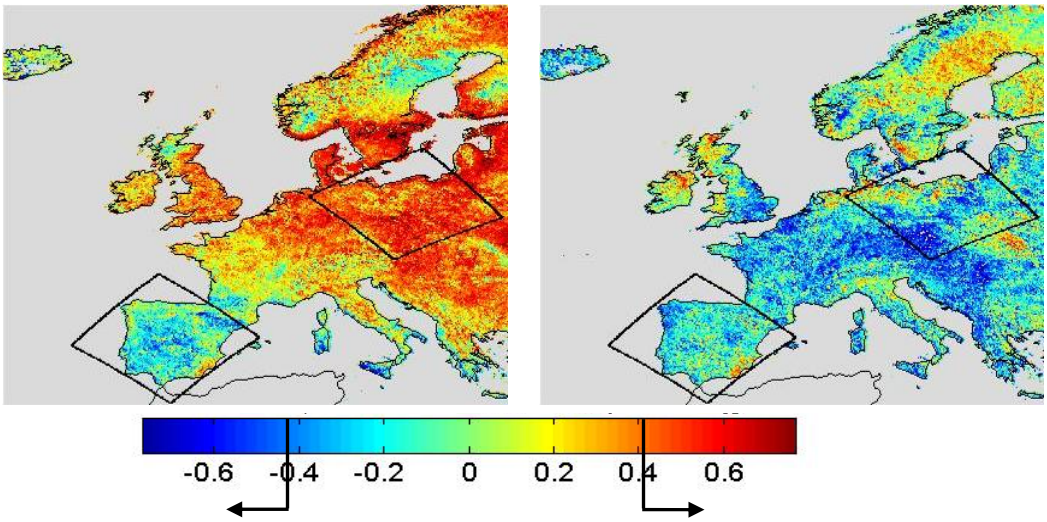

Figure 4.4 Point correlation fields of NAO vs. $NDVI_{SPR}$ (left panel) and NAO vs. $NDVI_{SUM}$ (right panel) over the period from 1982 to 2002. Black frames identify the Baltic region and the Iberian Peninsula. The colorbar identifies values of correlation and the two arrows indicate the ranges that are significant at 5% level.

The contrasting behaviour of north-eastern and south-western regions of Europe is worth being further investigated. For this purpose we have selected two regions, namely Northeastern Europe (hereafter NE) and the Iberian Peninsula (hereafter IB). These two regions are identified by black frames in Figure 4.4 and it may be noted that selection was made in such a way to obtain an amount of land pixels of the same order in the two regions, respectively 9639 over NE and 9080 over IB. Both NE and IB show fairly coherent values of correlation of NAO vs. NDVI for both spring and summer. It is also apparent that over IB, NAO is anti-correlated with vegetation greenness both in spring and summer, whereas over NE the correlation is positive in spring and predominantly negative in summer. During spring, the distribution of correlation values over NE presents a median value about 0.5, whereas the distribution over IB has a median of -0.2 and spans a wide range of negative values, reaching as low as -0.7 (Figure 4.5). During summer, both areas exhibit distributions with similar medians about -0.2, but the lower dispersion is now observed over IB.

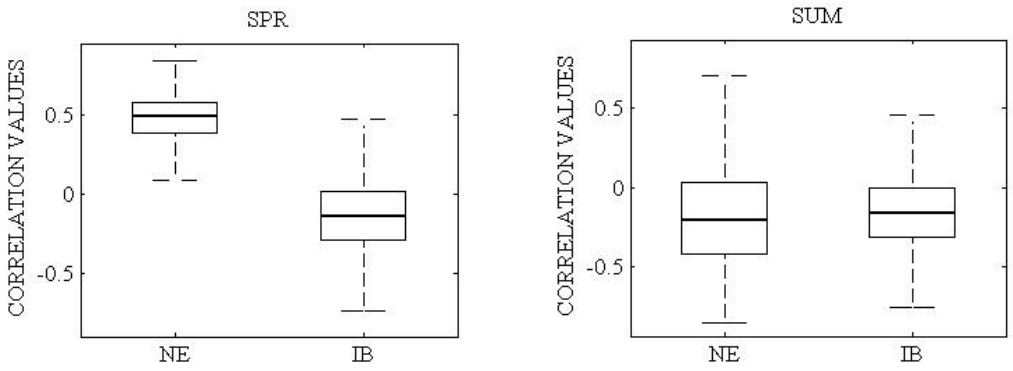

Figure 4.5 Box plots of simple correlation between three months composite of North Atlantic Oscillation (NAO) and NDVI for the 2 selected areas (NE and IB).

The observed distinctive behaviour between the Iberian Peninsula and Northeastern Europe is to be expected and reflects, on the one hand, the different response of the annual variability of meteorological parameters of the two areas to large-scale atmospheric variability associated to the NAO mode; on the other hand, it reflects the different responses of vegetation to atmospheric variability, in particular changes induced by temperature and precipitation in the annual cycle of heat and moisture. For instance in the case of wheat that is grown in both regions, water is the main limiting factor for growth in IB (Gouveia and Trigo 2008), whereas it is temperature that limits its growth in NE.

It may be noted at this point that climate conditions are not the only factor that acts on vegetation dynamics; the nature and quality of the plant substrate, the over-use of agriculture land and the employment of irrigation are important factors linked to the human influence that may disturb the relationship between atmospheric parameters and vegetation activity. With the aim of isolating the effect of natural atmospheric variability, as represented by the NAO, on vegetation dynamics from factors related to the human influence, we have compared the NDVI fields over IB and NE for two years associated to extreme NAO indices. Figure 4.6 shows a comparison of $NDVI_{SPR}$ for the two chosen years, i.e. 1986 (NAO^-) and 1995 (NAO^+). In the case of IB, anomalies of $NDVI_{SPR}$ present well defined quasi-meridional dipoles of opposite signs in 1986 (upper left panel) and 1995 (middle left panel). The southern anomaly centre is particularly intense, positive (negative) anomalies being observed in spring 1986 (1995). The dipolar structure is especially apparent when differences are computed between 1995 and 1986 (lower left panel). In the case of NE (right panels) large patterns of negative

(positive) anomalies of $NDVI_{SPR}$ may be observed in 1986 (1995). Observed anomalies are particularly intense in 1986 (NAO^-) and this feature is well apparent when analysing differences between 1995 and 1986 (lower right panel).

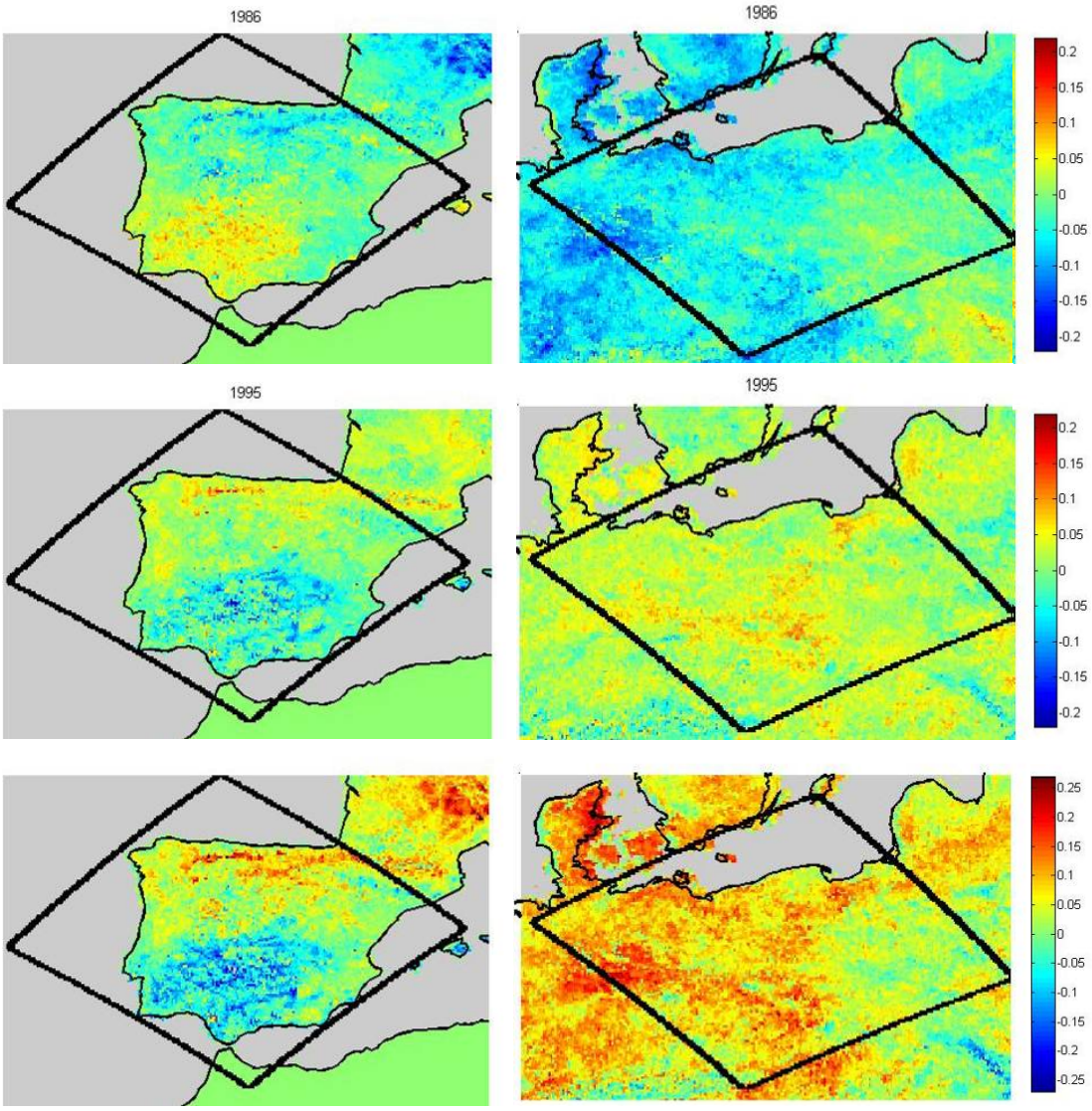

Figure 4.6 Seasonal anomalies of $NDVI_{SPR}$ for 1986 (NAO+), 1995 (NAO-) and for differences between 1995 and 1986 (upper, middle and lower panels, respectively) over IB and NE (left and right panels respectively).

4.4 NAO and Climatic Activity

Taking into account the results of the previous section, we will now pay attention to the influence of the NAO mode over two atmospheric parameters relevant to vegetation activity, namely surface temperature and precipitation. The analysis will

focus on the Iberian Peninsula and Northeastern Europe and the different roles played by temperature and precipitation in the two sub-areas will be emphasized.

Figure 4.7 shows spatial patterns over the selected European window of point correlation fields between the NAO index and the contemporaneous late winter means of surface temperature and precipitation, i.e. NAO vs. TNAO and NAO vs. PNAO. Obtained patterns display the well known response to the NAO signal, of temperature and precipitation over Europe (Hurrell, 1995; Trigo et al., 2002). In the case of temperature, a region of positive values over Central and Eastern Europe is well apparent (Trigo et al., 2002). Albeit less intense, negative values of correlation may also be identified over the Iberian Peninsula. For precipitation, a well developed meridional dipolar structure is conspicuous over Europe, delimiting two well defined zonal bands of positive and negative correlation values, which spread over Northern Europe and along the Mediterranean regions, respectively. These results are in good agreement with those obtained by several authors (e.g. Sáenz et al., 2001; Castro-Díez et al., 2002) who have pointed out that the connection between NAO and Iberian temperature is not as clear-cut as in the case of precipitation. Finally, the intense east-west precipitation gradients observed in southern Norway/Sweden as well as over Ireland and England is worth being point out. These strong precipitation gradients over such short distances are associated with the mountain ranges located in the western sector of these three regions and highlight the lee effect.

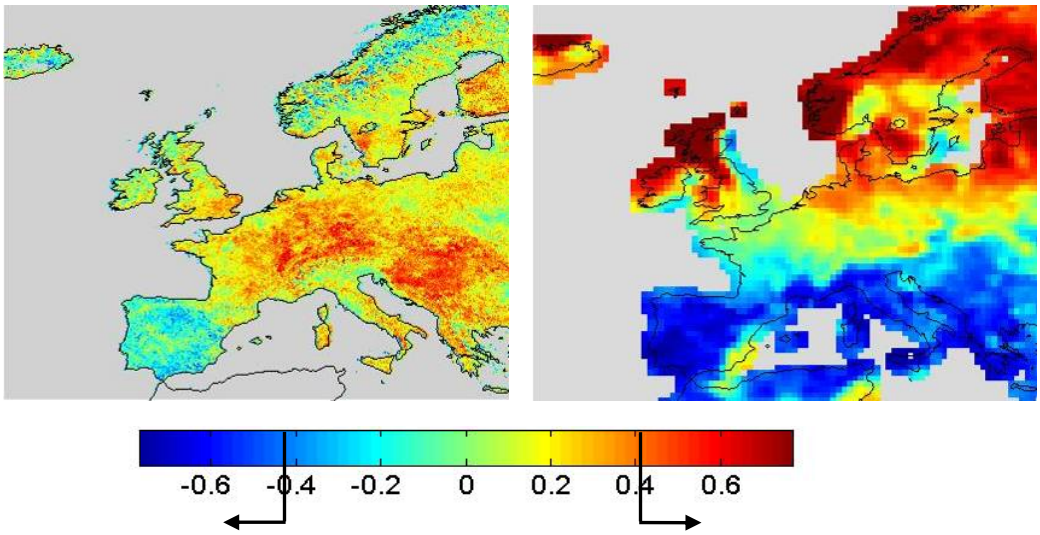

Figure 4.7 Point correlation fields of NAO vs. T_{NAO} (left panel) and NAO vs. P_{NAO} (right panel) over the period from 1982 to 2002. The colorbar shows values of correlation and the two arrows indicate the ranges that are significant at 5% level.

Although it is known that the impact of NAO on temperature and precipitation described above is especially prominent in winter (e.g. Vicente-Serrano and Heredia-Laclaustra, 2004, Trigo et al., 2004), such behaviour contrasts with that obtained for vegetation activity (Figure 4.4), where the impact of NAO is clearly apparent both in spring and summer (i.e. NAO vs. $NDVI_{SPR}$ and NAO vs. $NDVI_{SUM}$). This gives a strong indication that special attention must be devoted to the relationship between late winter temperature and late winter precipitation, with vegetation greenness in the following spring and summer seasons.

Since we are particularly interested in pixels characterised by the strong influence of NAO on vegetation activity, we will restrict our analysis to IB and NE (as identified in Figure 4.4), and will focus on those pixels that exhibit the highest (lowest) values of positive (negative) correlations of $NDVI_{SPR}$ and $NDVI_{SUM}$ with NAO. Henceforth, they will be called NAO High Correlation Pixels (NHCP).

As pointed out in the previous section, vegetation greenness over the IB is negatively correlated with NAO, both in spring and summer. Accordingly, we selected, for each one of the two seasons, the 500 highest NHCP. In the case of NE, NHCP were predominantly correlated with NDVI in spring and anti-correlated in summer. Therefore we selected the 500 pixels with the highest (lowest) values of positive (negative) correlation in spring (summer). Figures 4.8 and 4.9 show the geographical distribution of the NHCP for spring and summer, respectively over IB and NE. Information about the land cover type associated to each pixel is also provided, as obtained from the Global Land Cover 2000 (GLC2000) database (Chapter 3). Table 4.1 shows descriptive statistics of the NHCP associated with the two most common types of vegetation namely in what respects to the distribution of NDVI anomalies for two classes of years, characterised by extreme NAO indices, i.e. the NAO^+ and NAO^-, as described in section 3. NDVI anomalies in a given pixel are defined as differences from the respective 21-year mean (1982-2002) and the two considered classes of years. For each area and season the statistical distributions of NDVI anomaly values for the two classes of years (NAO^+ and NAO^-) and the two types of vegetation cover are characterised by means of the respective median (Q2), first and third quartiles (Q1 and Q3), and percentiles 1 and 99 (P1 and P99).

As expected, there are marked differences in the obtained distributions of NDVI anomalies for NAO^+ and NAO^- classes for a given type of vegetation, in a given season, over a given region. For instance, it is worth noting that there is no class overlap when restricting to median values between P1 and P99. This feature was taken into account in Figures 4.8 and 4.9, where a given year is characterised by its median value.

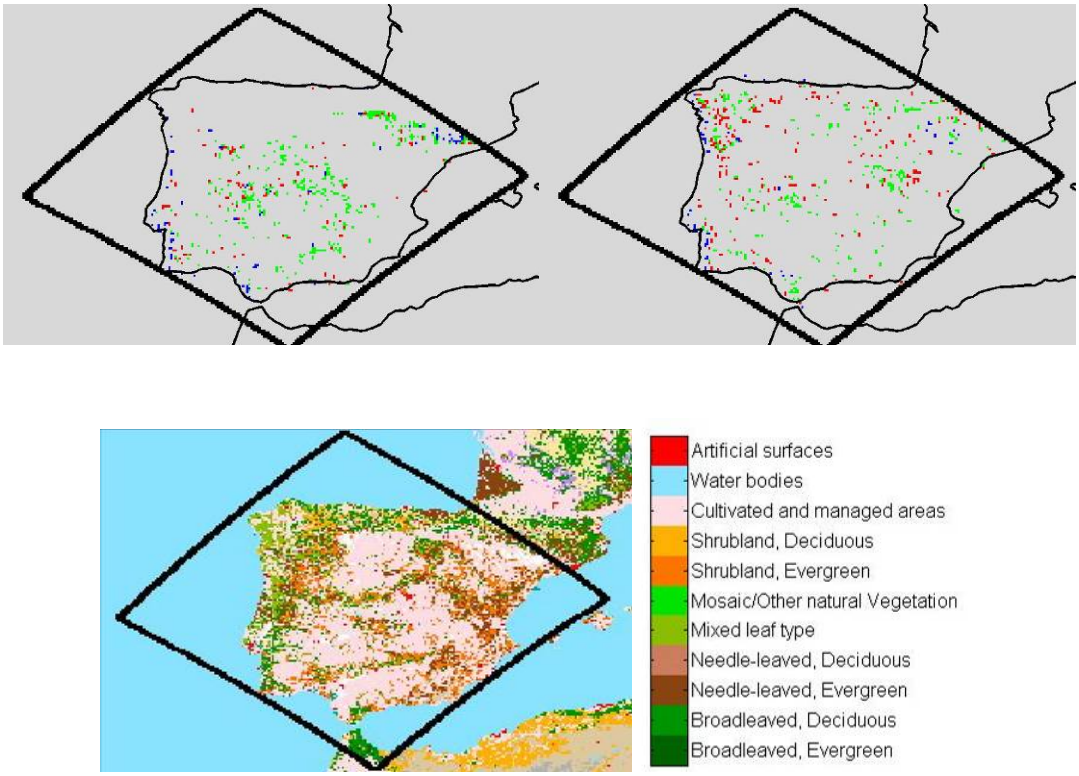

Figure 4.8 Geographical distribution of sets of selected pixels over the IB (upper panels), based on the strong values of correlation of $NDVI_{SPR}$ (upper left panel) and $NDVI_{SUM}$ (upper right panel) with NAO. Red, green and blue pixels are respectively associated to forest and shrub, cultivated areas and other types of vegetation cover. Land cover type (low panel) as obtained from GLC2000).

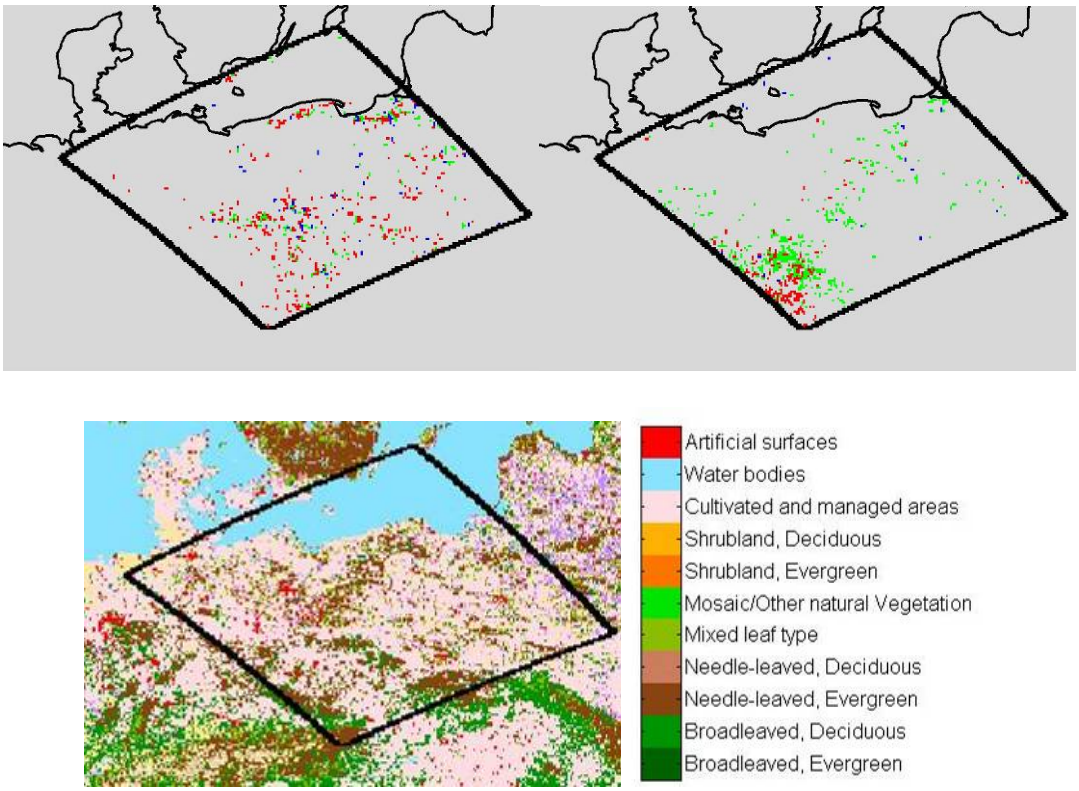

Figure 4.9 As in Figure 4.8 but respecting to NHCP over NE. Red, green and blue pixels are respectively associated to needle-leaved, evergreen, cultivated and other types of vegetation cover.

Differences in the distribution of types of vegetation are also conspicuous for the two regions and the two seasons. In the case of the Iberian Peninsula, almost two thirds (64%) of the NHCP correspond to areas of spring crops and about one sixth (17%) are forests and shrublands. The relative proportion of the two types undergoes a significant change in summer, when a strong decrease may be observed in the difference between the fraction of NHCP belonging to the two types (29% to forest and shrubland, and 47% to cultivated areas). In the case of NE, there is a dramatic change from spring to summer between the distributions of NHCP of the two types of vegetation; the predominance in spring of forest and shrubland (47%) over cultivated areas (25%) gives way, during the summer, to a predominance of NHCP representing agricultural crops (63%), over those representing forests and shrublands (27%).

Table 4.1 Descriptive statistics of the distributions of NDVI anomalies for NAO High Correlation Pixels (NHCP) associated to the two most important vegetation types as found in the cases of spring and summer over IB and NE. P1, Q1, Q2, Q3 and P99 respectively denote percentile one, the first quartile, the median, the third quartile and percentile 99. Percent figures in parenthesis below the types of vegetation indicate the fraction of pixels of the considered NHCP associated to that type.

IB

Spring

	Forest & shrubland (17%) *					Cultivated (64%)				
	P1	Q1	Q2	Q3	P99	P1	Q1	Q2	Q3	P99
NAO^+	-0,049	-0,030	-0,021	-0,013	0,002	-0,080	-0,041	-0,031	-0,022	-0,004
NAO^-	0,004	0,015	0,024	0,033	0,066	0,003	0,019	0,027	0,038	0,071

Summer

	Forest & shrubland (29%) **					Cultivated (47%)				
	P1	Q1	Q2	Q3	P99	P1	Q1	Q2	Q3	P99
NAO^+	-0,053	-0,031	-0,023	-0,017	0,005	-0,066	-0,036	-0,026	-0,014	0,000
NAO^-	-0,001	0,011	0,016	0,022	0,039	0,003	0,012	0,018	0,025	0,054

NE

Spring

	Needle-leaved Evergreen (47%)#					Cultivated (25%)				
	P1	Q1	Q2	Q3	P99	P1	Q1	Q2	Q3	P99
NAO^+	0,011	0,027	0,033	0,041	0,071	0,009	0,026	0,033	0,044	0,060
NAO^-	-0,084	-0,054	-0,043	-0,035	-0,014	-0,072	-0,055	-0,045	-0,037	-0,010

Summer

	Needle-leaved Evergreen (27%)##					Cultivated (63%)				
	P1	Q1	Q2	Q3	P99	P1	Q1	Q2	Q3	P99
NAO^+	-0,059	-0,037	-0,028	-0,021	-0,008	-0,068	-0,039	-0,030	-0,022	-0,005
NAO^-	0,006	0,020	0,025	0,032	0,056	0,009	0,022	0,027	0,034	0,052

* Includes 14% of Needle-leaved Evergreen, 26% of Broadleaved deciduous and 60% of Shrubland.
** Includes 31% of Needle-leaved Evergreen, 25% of Broadleaved deciduous and 44% of Shrubland

Includes 12% of Needle-leaved Evergreen and 88% de Broadleaved deciduous
Includes 35% of Needle-leaved Evergreen and 65% de Broadleaved deciduous

The above results may be viewed in terms of the distinct responses of the various vegetation types to moisture and heat conditions prevailing during the previous winter. These conditions, in turn, are determined by the nature of the relationships between the surface annual variability of atmospheric parameters, P_{NAO} and T_{NAO}, and the different phases (NAO^+ and NAO^-) of the NAO atmospheric mode. Figures 4.10 and 4.11 show scatterplots, for IB and NE, respectively, of spring and summer anomalies of vegetation

greenness against winter anomalies of temperature and precipitation. Each dot represents a pair of median values of a given set of selected 500 NHCP, for a given year of the considered period (1982-2002), of winter anomalies of P_{NAO} (left panels) and T_{NAO} (right panels) vs. anomalies of $NDVI_{SPR}$ (upper panels) and $NDVI_{SUM}$ (lower panels). Years belonging to the subset of NAO^+ (NAO^-) are marked in red (green) and the variability of the NHCP is characterised by means of horizontal and vertical bars indicating the respective interquartile ranges.

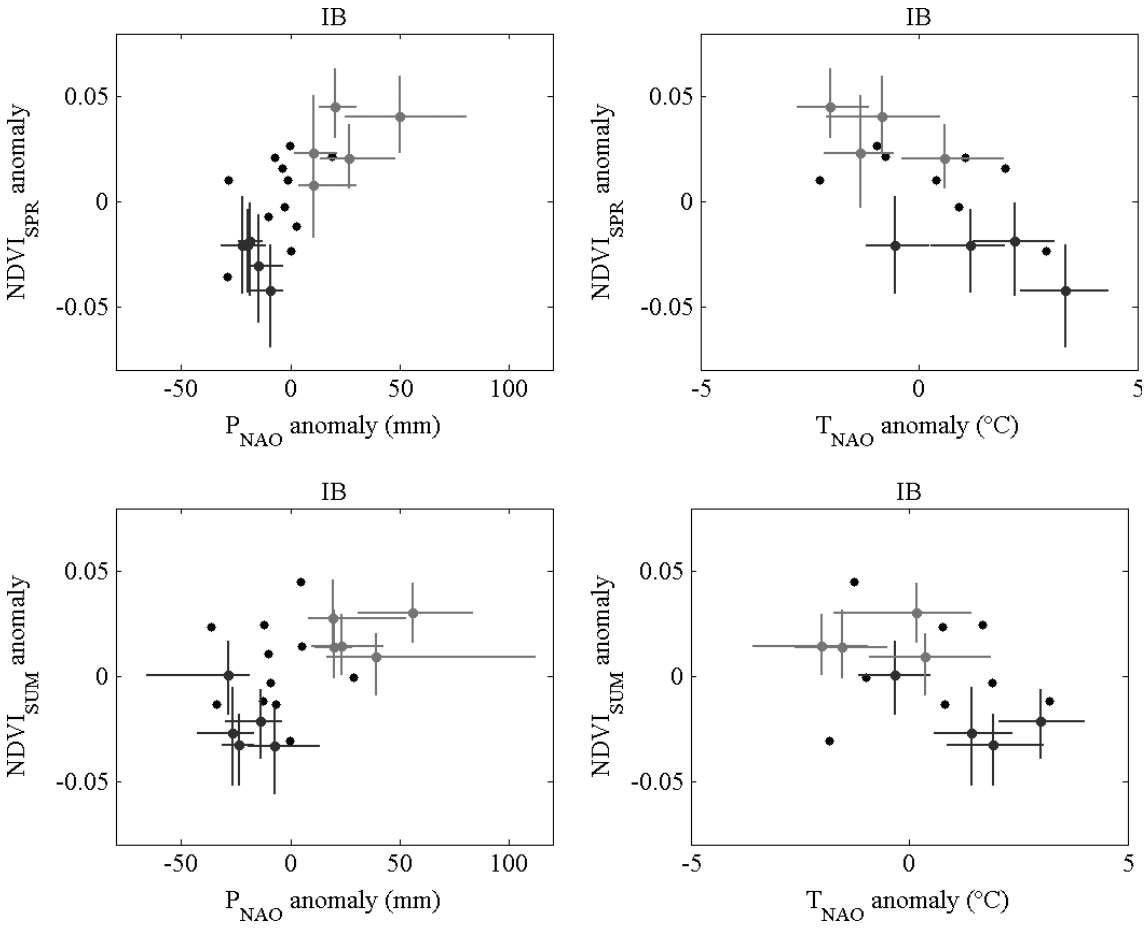

Figure 4.10 Dispersion diagrams of $NDVI_{SPR}$ (upper panels) and $NDVI_{SUM}$ (lower panels) vs. P_{NAO} (left panels) and T_{NAO} (right panels) for selected pixels over the IB. Each dot represents a pair of median values of a given set of selected 500 pixels, for a given year of the considered period (1982-2002). Years that belong to the subset of NAO^+ (NAO^-) are marked in red (green) and the respective variability is characterised by means of horizontal and vertical bars indicating the interquartile ranges.

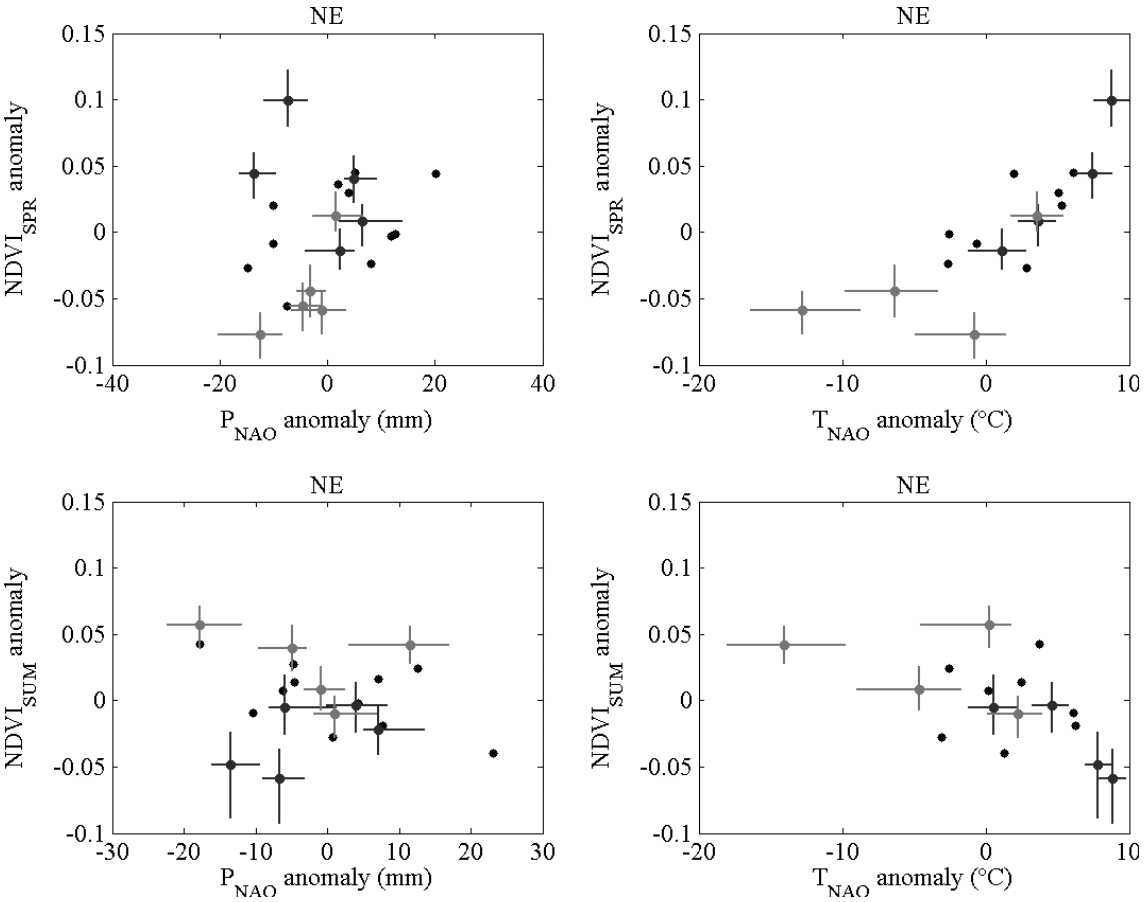

Figure 4.11 As in Figure 4.10, but respecting to NE.

As shown in Figure 4.10, IB region presents a similar spring and summer vegetation response to precipitation, i.e. an increase (decrease) of vegetation greenness for NAO^- (NAO^+) years. In both seasons there is less variability of precipitation in the set of NAO^+ NHCP, in comparison with NAO^-, especially in spring. A slight dependence of vegetation greenness on temperature is also apparent in the case of spring, with $NVDI_{SPR}$ median values showing a tendency to decrease from NAO^- to NAO^+. It may be noted that the obtained stronger dependence of vegetation on precipitation than on temperature is consistent with the already pointed out fact that over the Iberian Peninsula the influence of NAO is particularly strong on the precipitation regime whereas the relationship between NAO and temperature is less clear. In the case of NE (Figure 4.11) there is a marked dependence of vegetation greenness on winter temperature, but the nature of such dependence is reversed from spring to summer. In the first case, $NDVI_{SPR}$ shows a strong increase from NAO^- to NAO^+, whereas a sharp decrease is observed for summer. The lower variability of temperature in the set NHCP for NAO^+ is again evident, when compared with the

corresponding set for NAO^-. Concerning winter precipitation, no effects are apparent on vegetation greenness for both spring and summer. Finally, the differences in magnitude of the impacts of NAO on precipitation and temperature in IB and NE is worth being emphasised; the impact on precipitation (temperature) is three times larger over IB (NE) than the corresponding impact over NE (IB), a feature that is in good agreement with the found dependences of NDVI on precipitation (temperature) over IB (NE). This is to be expected, since vegetation growth is much more water-limited in IB than in NE.

4.5 The role NAO on the vegetative cycle

The striking differences that were obtained in the response of vegetation to moisture and heat conditions and to anomalies in P_{NAO} and T_{NAO} associated to the NAO atmospheric mode, warrant further analysis of the NDVI annual cycle for the NHCP over IB and NE. Figure 4.12 presents the annual cycles of NDVI monthly values for the NHCP, for spring (upper panels) and summer (lower panels), over IB (left panels) and NE (right panels). The annual cycles of mean NDVI for the entire period (1982-2002) are represented by thick solid black lines, whereas the annual cycles of averages for the NAO^- (NAO^+) subsets are identified by the thin solid (dashed) curves.

In the case of IB the most interesting feature for both spring and summer (Figure 4.12, left panels) is that the highest impact of NAO is observed to occur during the periods of the year characterised by more intense vegetation activity (Ji and Peters, 2003), i.e. around April (June) in the case of the NHCP for spring (summer). During spring, two thirds of the NHCP (Table 4.1) correspond to cultivated areas that mainly consist of crops adapted to the relatively dry Iberian conditions. Due to the generally observed high temperatures, vegetation has a short growth cycle that starts as soon as water is available, a situation that is especially favoured by NAO^-. This is especially apparent in Figure 4.13 (left panel) where the annual cycles of NDVI are compared for the years of 1986 (NAO^-) and 1995 (NAO^+) that were chosen because of being associated to extreme NAO indices. In the case of summer the vegetation that is most affected by NAO initiates its growing period late in the year and therefore the response to precipitation tends to extend late in the year.

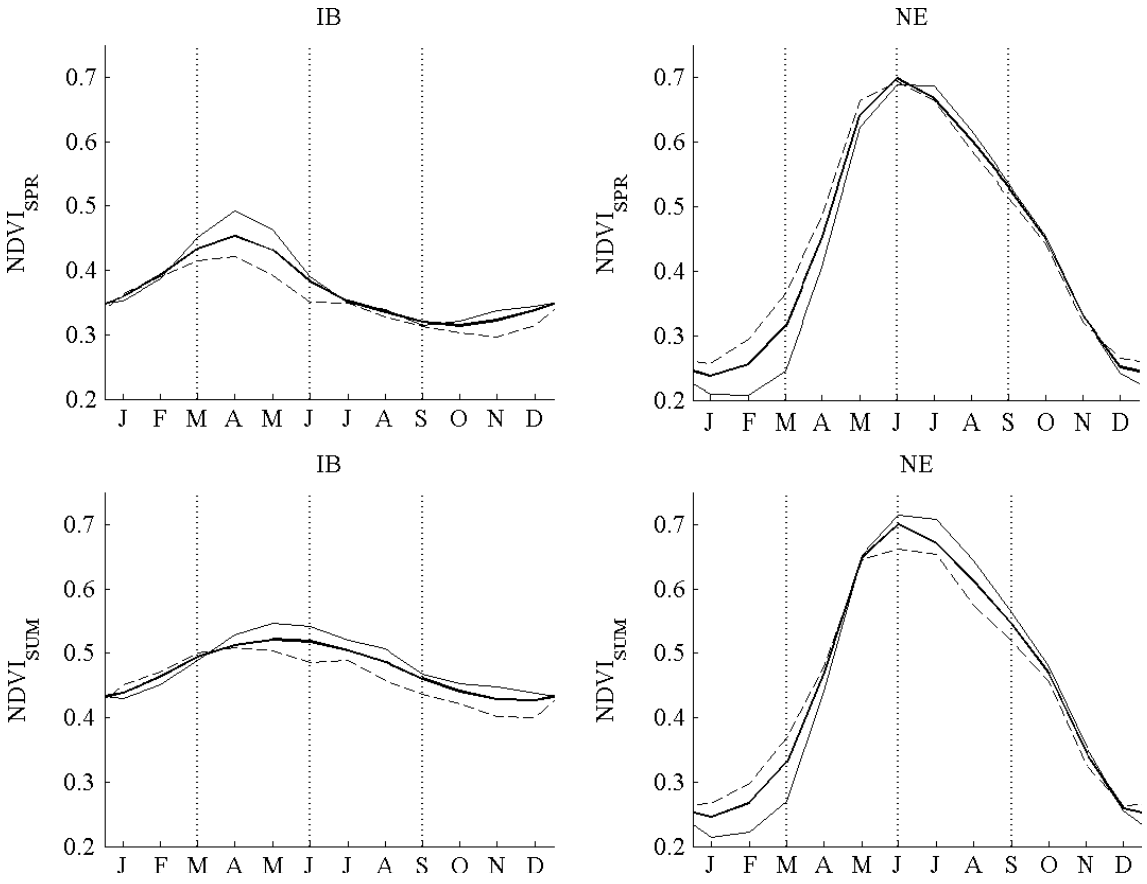

Figure 4.12 Annual cycles of monthly values of NDVI for NAO High Correlation Pixels (NHCP), for spring (upper panel) and summer (lower panel), over IB (left panel) and NE (right panel). The annual cycles of average NDVI values for the entire period (1982-2002) are represented by thick solid lines, whereas the annual cycles of averages for the NAO^- (NAO^+) subsets are identified by the thin solid (dashed) curves. Vertical dashed curves delimit the season of the year.

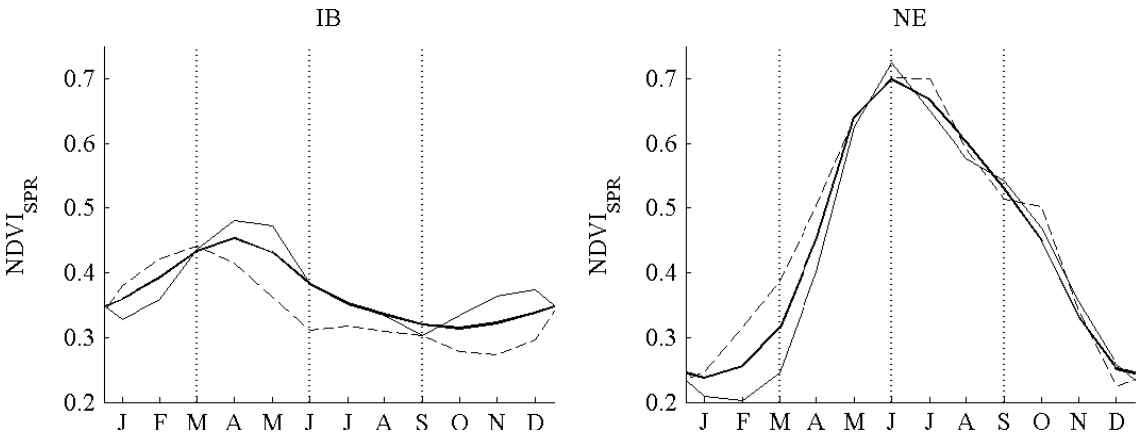

Figure 4.13As in Figure 4.12, but restricting to the annual cycles of NDVI for the individual years of 1986 (NAO^-) and 1995 (NAO^+), respectively represented by the dashed and the solid lines.

In the case of NE (Figure 4.13, right panels) the annual cycles present characteristics that are very different from those observed over IB. The impact of NAO is especially conspicuous during the first months of the year, suggesting that green vegetation growth tends to occur early and intensively, due to the combined effect of warm conditions, especially of the former, since water availability is seldom a problem in NE. This contrast in the response of vegetation during the early months is also well apparent in Figure 4.13 (right panel) where the years of 1986 (NAO^-) and 1995 (NAO^+) are compared. The distinct behaviour of vegetation in spring (Figure 4.12, upper panel) and summer (lower panel) is also worth pointing out. In the case of the spring, the NAO impact is almost negligible, whereas in the case of the summer the growth of vegetation is enhanced under NAO- conditions. This is to be expected, since snow melt is expected to occur later in the year, due to the lower winter temperature. Accordingly, vegetation growth will be reduced in spring, getting delayed until summer, when solar radiation availability increases (Blenckner and Hillebrand, 2002; Menzel 2003; Wang and You, 2004).

4.6 Conclusions

We analysed the relationship between the NAO atmospheric mode and vegetation activity (NDVI) over the two contrasting regions of Iberia and Northeastern Europe. As expected the behaviour of vegetation reflects the different response of surface climate to large-scale atmospheric variability associated to the NAO mode. A systematic analysis was performed over two contrasting regions of Europe, namely IB and NE. Over IB there is strong evidence that positive (negative) values of winter NAO induce low (high) vegetation activity in the following spring and summer seasons. This feature is mainly associated with the impact of NAO on winter precipitation, together with the strong dependence of spring and summer NDVI on contemporary water availability. NE shows a different behaviour, with positive (negative) values of winter NAO inducing high (low) values of NDVI in spring, but low (high) values of NDVI in summer. This behaviour mainly results from the strong impact of NAO on winter temperature associated with the critical dependence of vegetation growth on the combined effect of warm conditions and water availability during the winter season. (D'Odorico et al., 2002).

In both spring and summer NHCP over the Iberian Peninsula there is less precipitation variability under NAO^+ than under NAO^-, especially in the spring. This feature may be associated with the strong impact of climate variability in semi-arid areas, namely regarding effects of drought conditions on vegetation activity (Vicente-Serrano and Heredia-Laclaustra, 2004), in particular during the intense spring vegetation growth period. A weak dependence of vegetation greenness on temperature is also visible in spring, with median values of spring NVDI tending to decrease from NAO^- to NAO^+ conditions. In the case of NHCP over NE there is a marked dependence of vegetation greenness on winter temperature, but the nature of such dependence is reversed from spring to summer. In spring there is a strong increase of NDVI from NAO^- to NAO^+, whereas a sharp decrease is observed for summer. Again the lower variability of temperature in the set of NHCP for NAO^+, when compared with the corresponding one for NAO^-, is evident.

Finally, the NAO impact on vegetation dynamics over the two regions was evaluated by studying the corresponding annual cycles of NDVI and comparing their behaviour for years associated with opposite NAO phases. In Iberia the NAO impact is greater on non-forest vegetation which responds rapidly to spatio-temporal variations in precipitation and soil moisture. During the summer, forests and other dense vegetation areas display the highest sensitivity to NAO dynamics. This vegetation shows slower response to precipitation, and the NAO impacts are delayed until late in the year. Over NE, the NAO impact is especially apparent during the first months of the year, suggesting that green vegetation growth tends to occur early and intensely in NAO^+ years due to the relatively warmer conditions associated to the absence of ice cover and early melting. NAO has a strong effect on temperature which, in turn, impacts vegetation activity. The latter impact is well depicted when comparing monthly values of NDVI for the first months of the year, under NAO^+ and NAO^- (Figure 4.12).

The magnitude of the NAO-precipitation relationship in Iberia has been well documented in the literature over the last decade (e.g. Rodó et al., 1997; Trigo et al. 2002; 2004). However, only recently have such connections started to be taken into account when developing precipitation forecast models and predicting precipitation over the Iberian Peninsula with several months in advance (e.g. Gámiz-Fortis et al., 2002, Rodríguez-Fonseca and Castro, 2002). It is highly desirable that such models are implemented at the operational level because of their capacity of providing important

seasonal forecasting information to be used by water resources and agricultural managers. However, it should be stressed that our lagged relationships between winter NAO and NDVI values for spring and summer already represent an added value since they allow formulating, by the end of March, simple outlooks of vegetation greenness for certain land cover types over the European region that may provide useful information in a wide range of application encompassing; crop forecasts, long-lead wildfire risk assessment and early warning for public health issues, such as pollen-induced allergies.

5. INTERANNUAL VARIABILITY OF WHEAT YIELD IN PORTUGAL

5.1 Introduction

Crop assessment at the large or even the global scale fulfils at least two important roles. On the one hand, the identification of drought conditions and of associated shortages that are likely to follow is a major concern for government officials and to those that are responsible for international response programmes and relief efforts. On the other hand, subsidies that are becoming more and more available to agro-industries have prompted the development of sophisticated modelling techniques aiming to maximise the effectiveness of grants. It may be noted that whereas the first role is especially important in underdeveloped and developing countries, the second one is of particular value for developed ones.

In such a global context, usage of remote sensing techniques for data gathering, together with Geographic Information Systems (GIS) for data referencing provides powerful means of data processing and allows data to be combined with information collected using traditional field techniques. Remotely sensed data also allow a suitable preparation of base terrain evaluation, land use classification and land degradation maps. Finally, and taking into account that agriculture and associated vegetative phenomena are dynamic both in time and space, remote sensing techniques allow for a correct assessment of conditions at any time and place and are the only operational way for a continuous and global monitoring of trends and patterns in land cover as well as for assessing both processes and yields.

An example of the above-described procedures is the one provided by the Global Agriculture Monitoring (GLAM) Project that aims to enhance the capability of the USDA Foreign Agricultural Service (USDA/FAS) to both perform agricultural monitoring and to estimate crop production, using NASA's moderate resolution satellite data. The primary mission of GLAM is to supply agricultural information for global food security through regular assessments of global agricultural production and the

conditions affecting it (Justice, 2005). For such purpose both satellite data and post-processing tools are used to monitor agriculture and to locate and keep track of the climatic factors that impair agricultural productivity, e.g. short and long-term droughts, floods and persistent snow cover. Monitoring of crop conditions for target agricultural regions worldwide is based on multiple remotely sensed products as derived from moderate resolution sensors. Performed activities include providing USDA crop analysts with a sophisticated web interface for analyzing MODIS temporal composites of vegetation indices (VIs), at the 250-meter resolution. An evaluation is performed on the evolution of the growing season and annual comparisons are made of seasonal dynamics either between individual years or using as reference long-term mean conditions. Such inter-annual comparisons yield anomaly images and plots which emphasize regions that are less productive than previous years e.g. due to drought and heat stress conditions, as well as regions that are more productive having experienced favourable climatic conditions (Figure 5.1). For instance, the year of 2005 was characterised by a severe drought in eastern Africa, leaving millions in need of food aid. Using VI time series and web analysis tools, FAS specialists tracked this

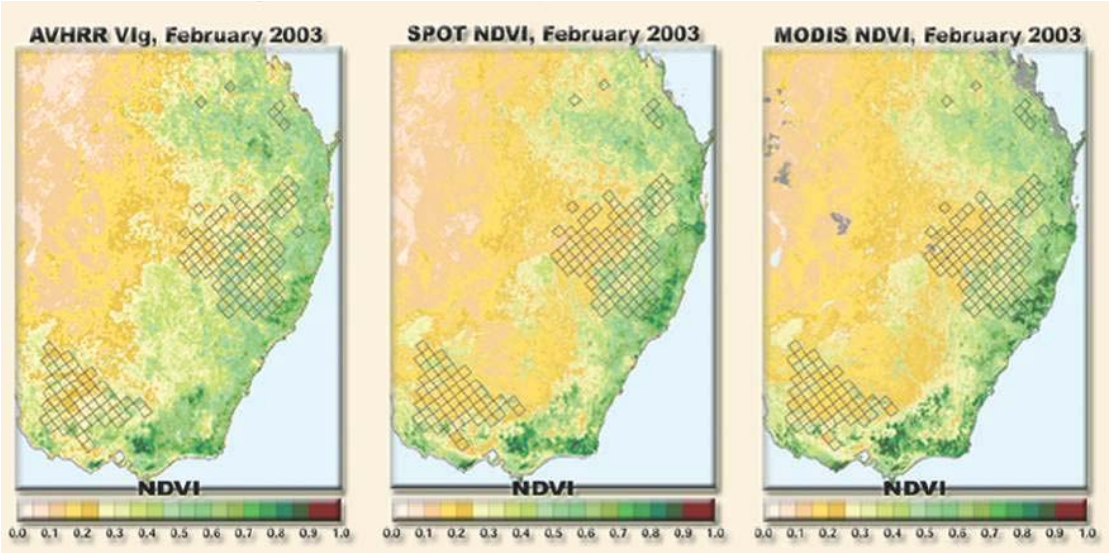

Figure 5.1 Comparison of AVHRR, SPOT and MODIS VIs over Southeastern, Australia, for February 2003 (Justice, 2005).

5.2 Wheat and Climate

During the last decades, the study of weather conditions and of their connection to plant growth and crop yield has been very important in agricultural research. At the same time, remote sensing technology has been developing steadily and its products may provide a large number of applications in agriculture, namely in the cases of crop identification, crop growth monitoring and yield prediction.

Wheat production and quality are associated with several factors that include seed variety, soil type and fertilization techniques with the latter being taken as virtually unvariable over the European Union due to the strict regulations imposed by the European Community. Nevertheless, climate is still one of the major factors which influence the spatio-temporal distribution of most agricultural systems, which are vulnerable to inter-annual climate variability and, in particular, to extreme events and trends in traditional patterns of regional climate (Hoogenboom, 2000).

Winter atmospheric circulation affects the regional distributions of temperature and precipitation in Europe and relations have been found between them and wheat yield for the European countries (Maytelaube et al, 2004); however sensitivity to winter variability seems to be at the local scale and there is the need to perform a regional analysis with the aim of clarifying the relationship between winter variability and crops. Other studies have shown that a high North Atlantic Oscillation (NAO) index in winter is associated with better quality of the UK wheat crop (Atkinson et al., 2005) and with better wheat, rye, oat and citrus yields in the Iberian Peninsula (Gimeno et al, 2002). Estimations of the effects of climate variability on the final crop yields has also been evaluated at five sites in Spain (Iglesias and Quiroga, 2007) and wheat and barley yields were predicted in the Ebro valley using drought indices and remote-sensed data (Vicente-Serrano et al., 2006).

Rodríguez-Puebla et al. (2007) have derived a model able to integrate effects of climate variables on winter cereals productivity in Spain. The model integrates the effects of abundant precipitation together with dynamic aspects of the air masses, during the maturation. The positive effects of warm winters at the beginning of the cereal growing season were also considered. Several authors have tried to integrate crop

simulation models with remotely sensed data through data-assimilation methods. This approach has the advantage of improving initialization of model parameters with remotely sensed observations to improve model performance (Fang et al., 2008; De Melo et al., 2008).

The most important meteorological variables associated with agriculture production are air temperature (daily maximum and minimum values), solar radiation and precipitation. In particular, solar radiation provides the energy for the processes that drive photosynthesis (Hoogenboom, 2000) and it has been shown that wheat yields in Canadian Prairies may be satisfactorily predicted by combining meteorological and remote sensing data (Boken and Shaykewich, 2002).

5.3 Wheat in Portugal

The majority of wheat in Portugal is sown in October and November and harvested in June and July of the following year, leading to a small production due to the existence of a very short vegetative cycle. A comprehensive assessment on the Portuguese wheat vegetative cycle and the corresponding relationship with climate variables is given by Sampaio (1990) and Feio (1991).

According to the Köppen's climate classification, continental Portugal belongs to the so-called Csa and Csb groups, which are characterized by a typical Mediterranean climate, with mild and relatively wet winters and dry summers. This situation may be further worsened by bad drainage of soils. The wheat yield in Portugal is therefore considerably smaller than the corresponding wheat yield in the North-western European countries, with cold (but not too wet) winters and relatively wet summers. During the grain filling until the complete grain ripening phase, the Mediterranean conditions may even get worse, due to the short period of time between frost episodes and relatively high temperatures at the end of spring (May/June). Another adverse situation, especially when compared with the same period for North-western European countries, consists in the low photoperiod (number of sun hours) and the high temperatures which may occur at the end of the maturation phase. During this phase large values of potential evapotranspiration may lead to weak photosynthetic activity, since the plant mostly spends this activity in the transpiration process in order to fight against the warm season

effects instead of producing dry matter. An excess of evapotranspiration may therefore lead to a decrease of wheat quality. On the other hand, and as already pointed out, there is also a strong dependence of wheat yield and quality on temperature, precipitation and radiation. We will shortly describe the impact of these three meteorological factors on the vegetative cycle of wheat.

Temperature. Wheat requires low temperature during winter (January/ February), while too high temperature at the end of the cycle may lead to bad productions. Low temperature and frosts during spring may also cause damages, as wheat spikes in this season are growing; they are especially sensitive to frost in this period.

Precipitation. Rainfall is the driving factor of soil moisture, a variable that is indispensable for the appropriate development of most cultures in Portugal. A good year for wheat production in Portugal is usually characterized by reasonable precipitation in late September and early October (in way to prepare the soil to catch-crop), followed by low precipitation in late autumn and early winter. Moderate precipitation in late winter and early spring is also beneficial, namely in April, and May. June should be dry, but not too dry in order to allow for a slow and complete maturation that promotes the emergence of filled and well formed grains. However intense rain in late June could favor the development of pests and consequently a decrease on wheat quality. It may be noted that, in the case of precipitation, the most important issue is the seasonal distribution throughout the year, not the total annual amount of rainfall. In Portugal this aspect is generally problematic, due to the irregularity and unpredictability of precipitation distribution that is typical in Mediterranean climates (Trigo et al., 2004).

Photoperiod (number of sun hours). Radiation has a distinct impact from temperature in wheat growing. Since solar radiation provides the energy needed to promote photosynthesis, the number of sunny hours is very important to induce flowering.

5.3.1 Production and Yield

Wheat yield data for Portugal were extracted from the Food and Agriculture Organization (FAO) database for the period 1961-2005. Annual averages of wheat yield in Portugal for the considered period may be observed in Figure 5.2. It may be noticed

that the yield time series has two components: a trend, due essentially to improvements in farm management practices and a weather-related yield interannual variability (Maytelaube et al., 2004). Since our aim is to assess the effects of climate related variability on crop yield, the "technologically driven" trend was removed from the raw time series, i.e. we will restrict to annual yield anomalies.

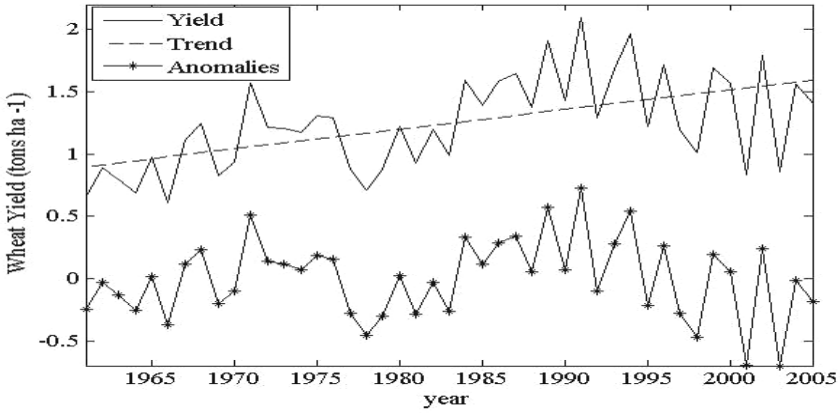

Figure 5.2 Time series of annual wheat yield in Portugal for the period from 1961 to 2005: yield (solid line), general trend (dashed line) and anomalies for detrended time series (line with asterisks).

Data of wheat yield for different regions in Portugal was provided by the Portuguese Instituto Nacional de Estatísitica (INE) and covers a shorter period from 1996 to 2003; however these data are available for both hard and soft yield wheat. The main wheat growing area is Alentejo, a region that is located in the southern sector of Portugal (Figure 5.3). Alentejo contributes with more than 80% of the total wheat production, and concentrates more than 95% of the total of hard wheat production (Figure 5.4). It worth stressing that this type of wheat is less sensitive to technological improvements

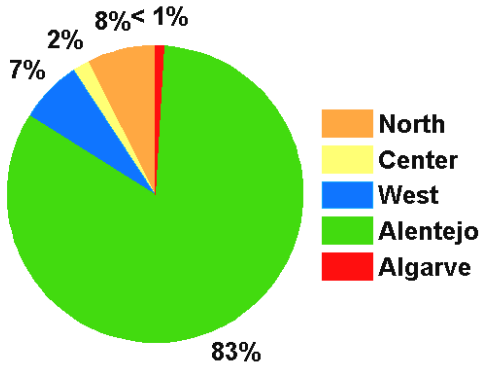

Figure 5.3 Contribution of different growing regions of Portugal to total wheat yield for the period from 1996 to 2003.

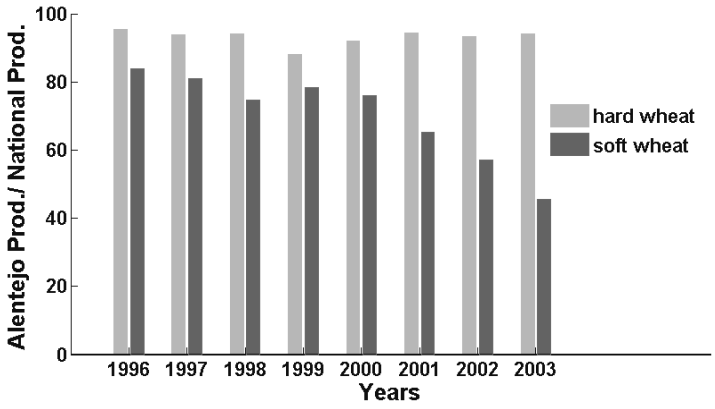

Figure 5.4 Percentage of Alentejo's wheat yield for hard and soft wheat for the period from 1996 to 2003.

5.3.2 Vegetative cycle

We have used the monthly NDVI dataset, at 8-km resolution, as obtained from the Advanced Very High Resolution Radiometers (AVHRR), provided by the Global Inventory Monitoring and Modeling System (GIMMS) group (Kaufmann et al., 2000). The data for the Iberian Peninsula covers the area between 10º W to 0º E and 35º N to 45º N and respects to the 18-year long period that spans between 1982 and 1999 (see Chapter 3).

Monthly and seasonal composites of NDVI were computed for spring (March, April and May, hereafter MAM). Figure 5.5 (left panel) shows obtained grid point correlations between spring NDVI composites and wheat yield considering the 18 year period between 1982 and 1999. Pixels over the Atlantic Ocean and Spain were naturally masked and, therefore, the figure is restricted to the correlation pattern over Portugal. It is worth noting that the highest positive and significant correlations (at the 99% level) are found over the southern region of Alentejo (Figure 5.5, right panel).

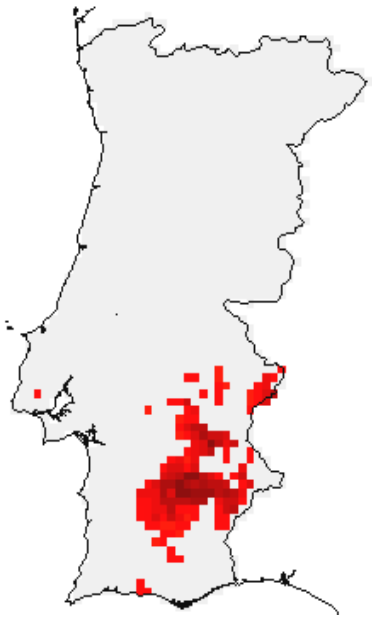

Figure 5.5 Patterns of simple correlation between spring NDVI composites and wheat yield in Portugal, for the period of 1982-1999 (left panel); patterns of simple correlation that are significant at the 99% level (right panel).

5.3.3 Spatial distribution

The Corine Land Cover Map (CLC2000), originally on a 250m by 250m grid, was re-projected to the scale of 8 km by 8km (i.e. the same as in the NDVI database), using the methodology described in Chapter 3. We have restricted the analysis to the set of pixels that were coded as non irrigated arable land (Figure 5.6, left panel) and have then characterized the statistical distribution of correlation coefficient values between wheat yield and spring NDVI (Figure 5.6, right panel). It is worth noting that the three higher correlation classes (i.e. those centered at 0.5, 0.7 and 0.9) represent more than 90% of pixels coded as non-irrigated arable land. We have then selected for further analysis the subset of pixels where correlation values are statistically significant at the 1% level. The subset of selected pixels is shown in Figure 5.7 and it may be noted that they present a rather homogenous distribution over the south of Alentejo that corresponds to areas of extensive cultivation of wheat. The considered subset of pixels will hereafter be referred to as "wheat-like" pixels. We will therefore assess the statistical significance of the relationship between spring NDVI and wheat yield by evaluating the correlation between detrended anomalies of wheat yield and averaged spring NDVI over the selected subset of "wheat-like" pixels.

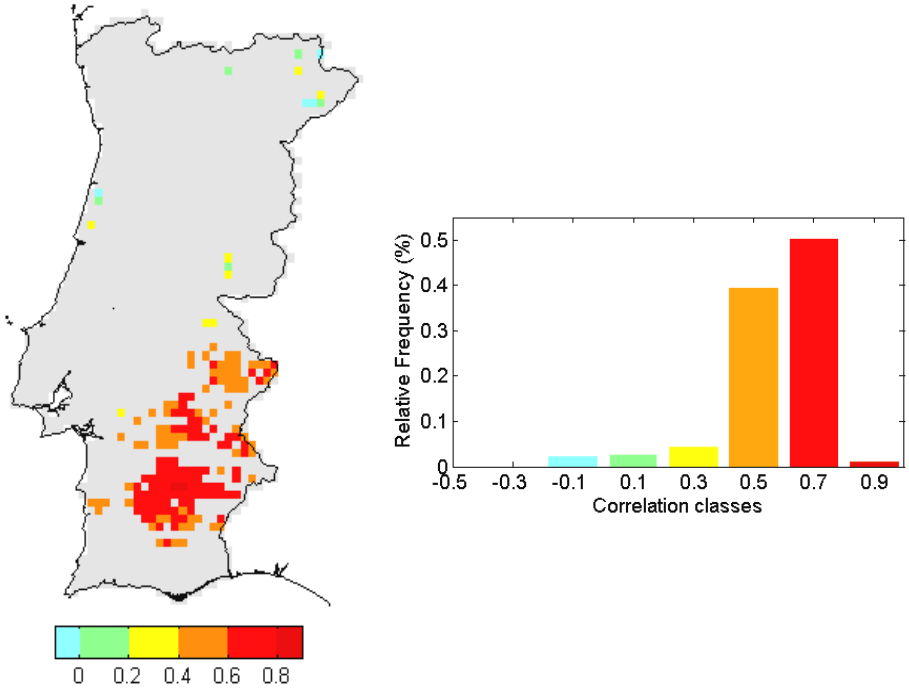

Figure 5.6 Pixels coded as "arable land not irrigated" according to Corine2000 for Portugal. (left panel). Relative frequency of correlation coefficient values between spring composite of NDVI and wheat yield in Portugal, for pixels coded as arable land (right panel).

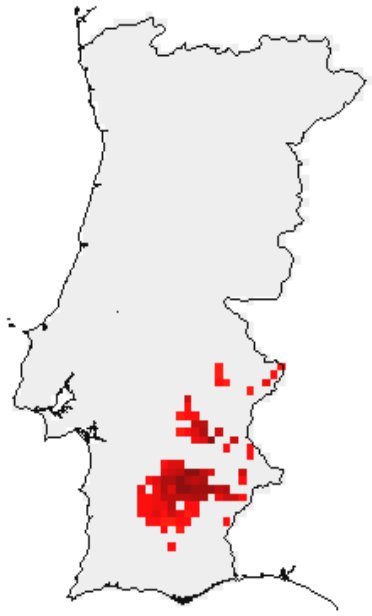

Figure 5.7 As in Figure 5.5 (left panel), but for the pixels with correlations that are significant at the 99% level.

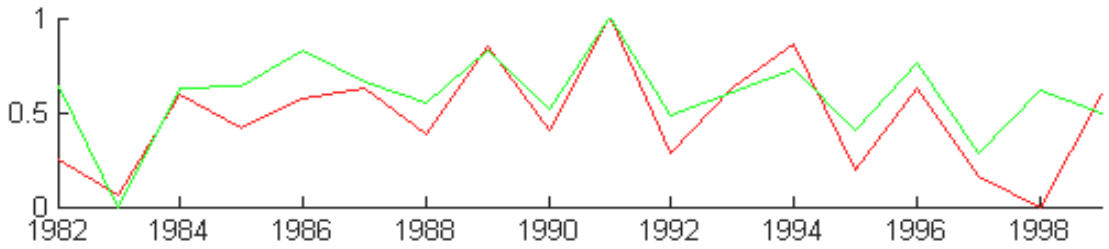

Figure 5.8 Time series for the period 1982-1999 of detrended anomalies of wheat yield in Portugal (green curve) and of spring NDVI averaged over the "wheat-like" pixels (red curve). Values of wheat yield were normalized by subtracting the mean and dividing by the standard deviation.

Table 5.1 Correlation values between spring NDVI and wheat yield and respective 95% confidence intervals and level of significance as obtained for 10,000 bootstrap samples.

	NDVI (MAM)
Correlation	0.75
[P5 P95]	[0.59 0.92]
Significance level	0.002

5.3.4 Meteorological variables

As previously pointed out, net short-wave radiation, temperature and precipitation are especially relevant meteorological parameters for the vegetative cycle of wheat. On the other hand, as already discussed in Chapter 4, the NAO phase has a strong impact on vegetation dynamics over the Iberian Peninsula. We have therefore focused our study on NAO as well as on the above mentioned meteorological variables.

Net short-wave radiation, temperature and precipitation were based on gridded data from the Climate Research Unit (CRU) datasets, covering the period 1982-1999. The NAO index is also the one derived at CRU and already adopted in Chapter 4. Details about all these datasets may be found in Chapter 3. The three meteorological parameters were detrended by means of a linear regression and the NAO index was normalized, having zero mean and unit standard deviation. It may be noted that the

study was restricted to the first six months of the year because the vegetative cycle of wheat ends in late June (or early July).

The impact of meteorological factors on wheat yield was assessed by computing monthly correlations between the detrended anomalies of yield and averaged values (over the "wheat-like" pixels) of net short-wave radiation, temperature and precipitation as well as with NAO. Obtained results are summarized in Table 5.2 and it is worth pointing out that they are in good agreement with the empirical findings about the roles (and timings) of the different meteorological factors along the different stages of the wheat vegetative cycle.

Table 5.2 Correlation coefficient values between annual wheat yield and monthly net long wave radiation, air surface temperature and precipitation (from January to June) for the pixels coded as arable land not irrigated. Bold values are representing correlations values that are significant at 95% level and red value is presented the correlation value significant at 99% level.

	JAN	FEB	MAR	APR	MAY	JUN
Radiation	0.13	-0.09	**-0.73**	-0.12	0.31	0.12
Temperature	-0.37	**-0.50**	**-0.49**	-0.25	-0.07	0.16
Precipitation	0.06	0.35	**0.54**	-0.17	-0.06	-0.27
NAO	0.09	-0.28	-0.21	**0.48**	0.07	**0.53**

For instance, the positive impact on wheat yield of cold temperature during winter and early spring is well illustrated by the persistent negative values of correlation, the ones obtained for February and March being statistically significant at the 5% level, for both months. The positive impact of precipitation in February and March is in turn supported by the respective positive values of correlation, the one for March, being statistically significant at the 5% level. The crucial role of solar radiation of March in the photosynthetic process is reflected by the conspicuously high negative correlation that is significant at the 1% level. Another interesting feature relates to the different roles played by the meteorological variables during the vegetative cycle and in this respect, the contrasts between late winter/early spring and late spring/early summer is worth being noted. Correlations involving temperature are persistently negative from January to April and become weak in May and Jun. Correlations involving precipitation are positive from January till March and become negative from April till June.

Correlations involving radiation are negative from February until April and become positive in May and June. Finally, it is worth noting that obtained results are in good agreement with the recent findings by Rodríguez-Puebla et al. (2007) for Spain.

The described impact of meteorological variables along the vegetative cycle of wheat is well apparent in Figure 5.9 that presents the monthly patterns of simple correlations, from January to June, between detrended anomalies of wheat yield and the three considered meteorological variables.

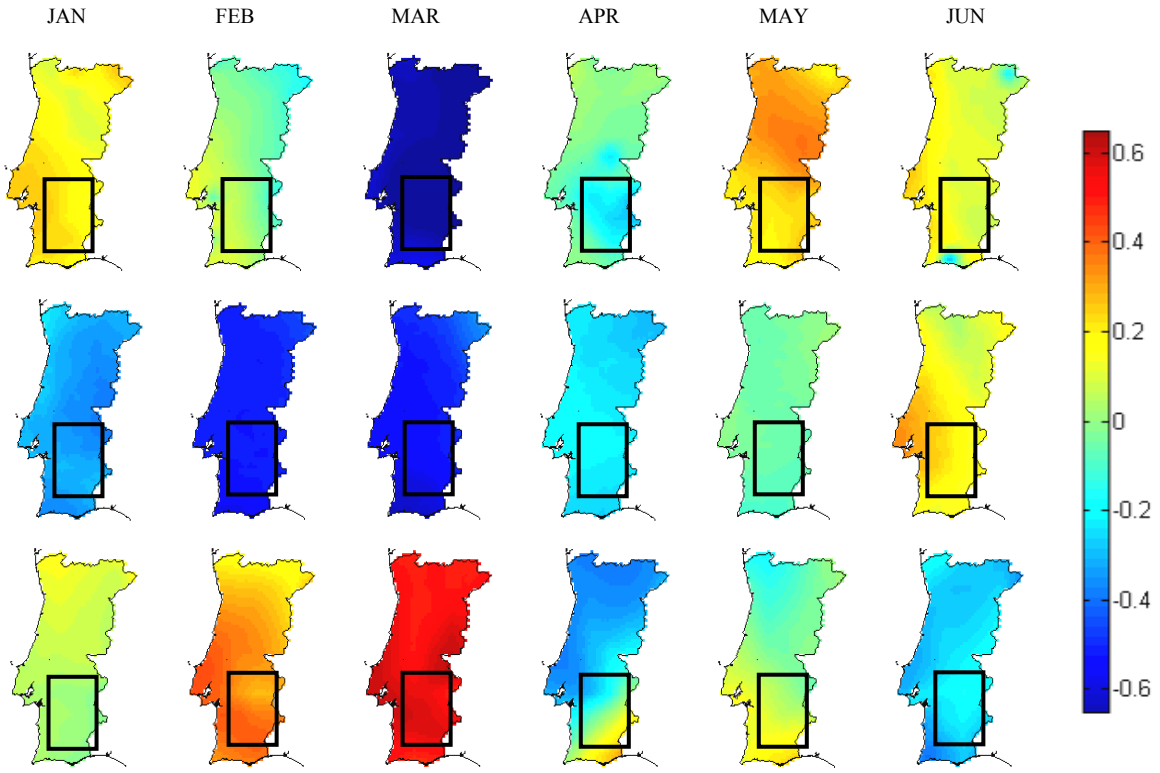

Figure 5.9 Patterns of simple correlation between wheat yield in Portugal and the three most relevant meteorological fields for the period of 1982-1999; top panel: net short wave radiation; middle panel: surface air temperature; bottom panel: precipitation. Boxes in the Southern sector delimit the area containing "wheat-like" pixels.

Obtained values of correlation between NAO and wheat yield also reflect the different role played by NAO along the vegetative cycle of wheat. In fact, the contrast between late winter/early spring and late spring/early summer is well apparent, with negative correlations between NAO and yield in February and March and positive correlations in April and June, both statically significant at the 5% level. This behavior may be viewed as reflecting the integrated impact on radiation, temperature and

precipitation fields of the large scale atmospheric circulation patterns associated to the different phases of NAO (see Chapter 4). The impact of NAO averaged for April, May and June on contemporaneous fields of radiation, temperature and precipitation is illustrated in Figure 5.10.

The key role played in March by meteorological is worth being stressed, taking into account that correlations of radiation, temperature and precipitation are all statistically significant at least at the 5% level. The role of NAO in June is also worth being mentioned, taking into account the need of warm temperatures during the maturation phase of wheat.

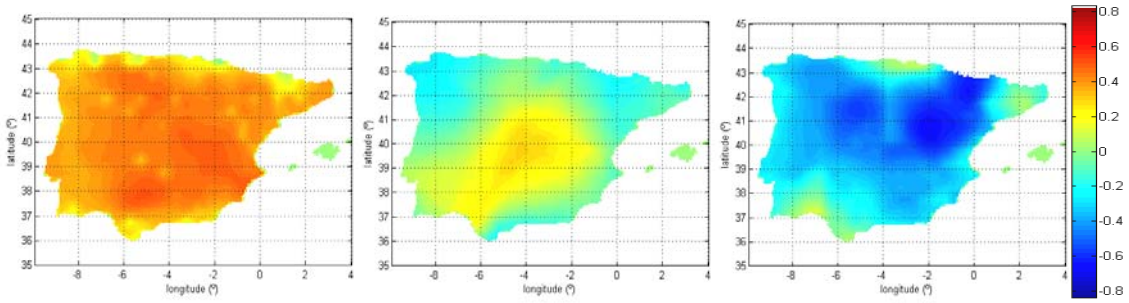

Figure 5.10 Patterns of simple correlation, over the Iberian Peninsula, between NAO averaged for April, May and June and contemporaneous fields of radiation (left panel), temperature (central panel) and precipitation (right panel) for the considered period 1982-1999.

Figure 5.11 presents, for the considered period 1982-1999, time series of detrended anomalies of wheat yield together with four selected meteorological factors, i.e., March monthly anomalies of net short-wave radiation, temperature and precipitation averaged over "wheat like" pixels and NAO in June. Table 5.3 presents the obtained values of correlation, together with the respective 95% confidence intervals and significance levels as estimated based on 10,000 bootstraps samples.

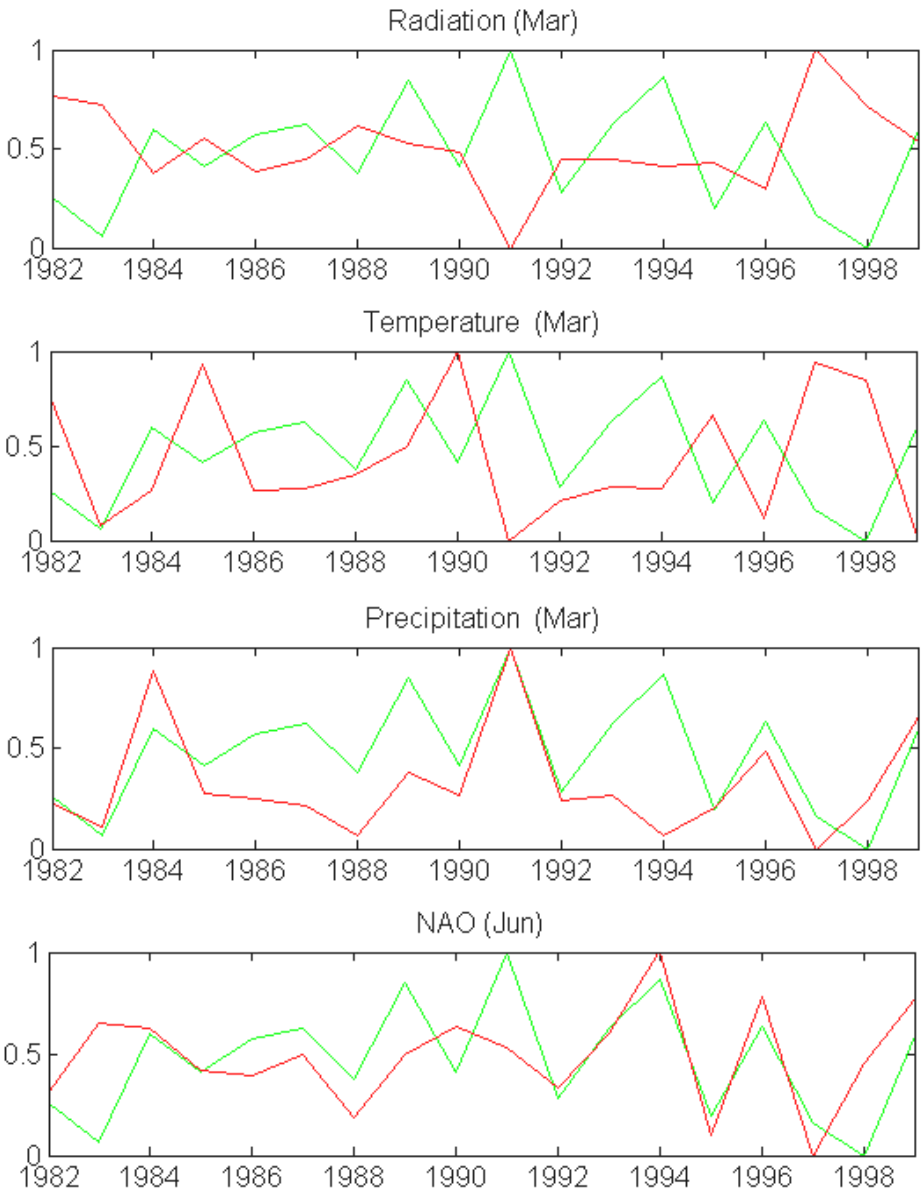

Figure 5.11 Patterns of simple correlation between wheat yield in Portugal and the three most relevant meteorological fields for the period of 1982-1999; top panel: net long wave radiation; middle panel: surface air temperature; bottom panel: precipitation.

Table 5.3 As in Table 5.1, but respecting to net short-wave radiation, temperature, precipitation in March and to NAO in June.

	Radiation (MAR)	**Temperature (MAR)**	**Precipitation (MAR)**	**NAO (JUN)**
Correlation	-0.73	-0.49	0.54	0.53
[P5 P95]	[-0.88 -0.52]	[-0.78 -0.13]	[0.18 0.80]	[0.23 0.78]
Significance level	0.0006	0.04	0.02	0.03

5.4 A simple regression model for wheat yield

Results obtained in the previous section suggest using spring NDVI together with meteorological variables to build up a simple model of wheat yield in Portugal for the period 1982-1999. We have accordingly tried several regression models that used as predictors spring NDVI combined with the meteorological factors shown in Table 5.3. Statistical models developed with relatively short time series are particularly prone to overfitting problems (Wilks, 1995), to solve this caveat it is advisable to apply cross validation techniques, i.e to split the available time series in a calibration and validation periods. Evaluation of model performance and prevention of overfitting was done by means of leave-one-out cross validation technique i.e., by using a single observation from the original sample as the validation data, and the remaining observations as the training data

Best results were obtained when using as predictors spring NDVI together with the NAO for June. The best performance of this model may be viewed as reflecting the fact that chosen predictors grasp the relevant information during two crucial stages for wheat; the growing and the mature stages. Spring NDVI is an indicator of the healthiness of wheat during the growing stage which in turn reflects the meteorological conditions in terms of radiation, temperature and precipitation regimes. On the other hand NAO for June is an indicator of the large-scale circulation affecting Portugal which in turn is related to regional conditions in terms of radiation, temperature and precipitation that have an important role in the process of maturation of wheat.

Figure 5.12 (upper panel) presents, for the considered period 1982-1999, the time series of observed and modeled wheat yield. The overall agreement is worth being noted, the two time-series presenting a correlation of 0.83.

Figure 5.12 (central panel) shows the time series of residuals, defined as departures of observed values from modeled ones. The 95% confidence intervals relative to these residuals (Chatterjee and Hadi, 1986) are plotted as error bars and it may be noted that 1998 represents the single outlier since its error bar does not cross the zero reference line.

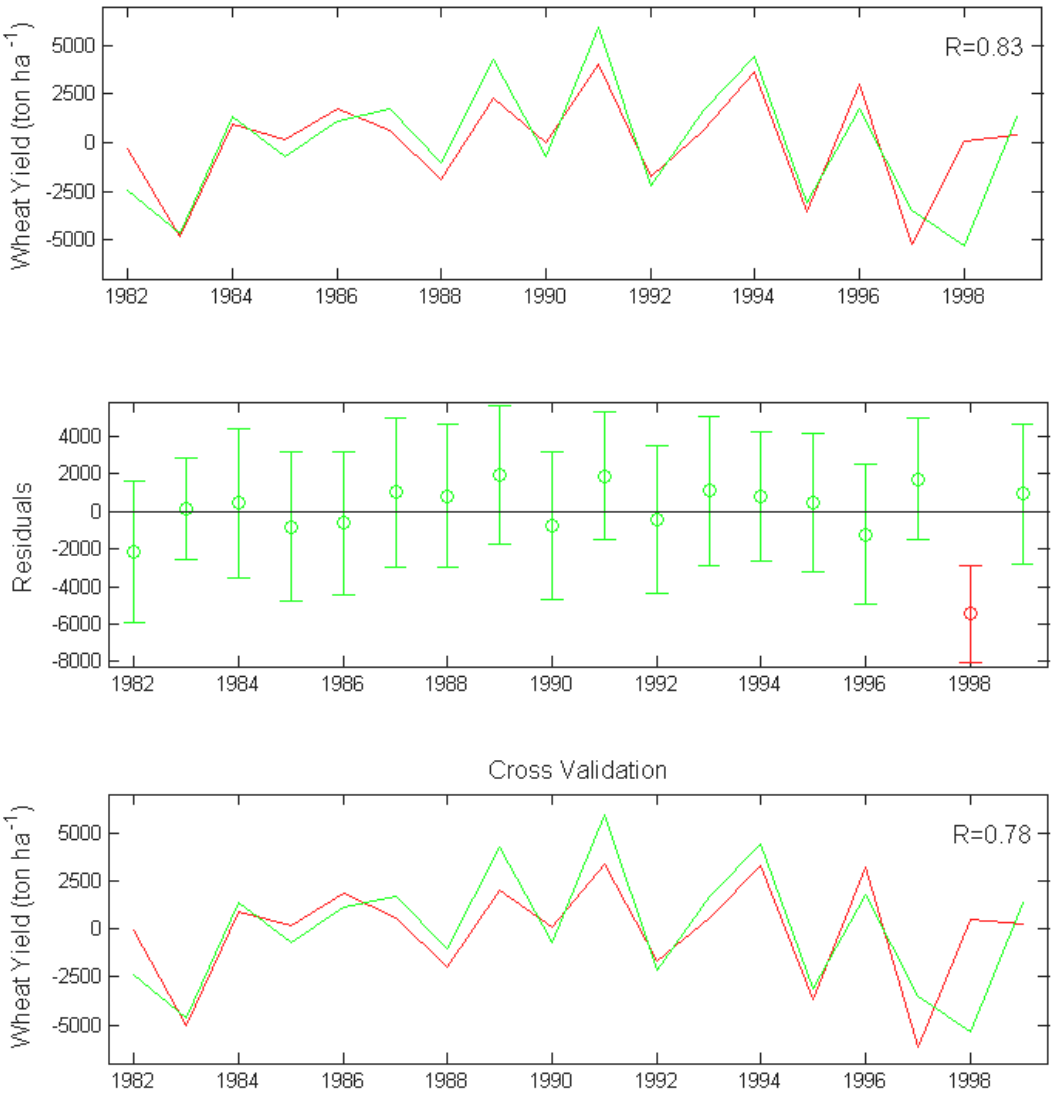

Figure 5.12 Time series (1982-1999) of observed (green curve) wheat yield in Portugal and of corresponding modelled values (red curve) when using a linear regression model based on spring NDVI and NAO in June (upper panel). Time series (1982-1999) of residuals and respective 95% level confidence intervals (central panel); the single outlier (in 1998) is highlighted in red. Time series (1982-1999) of observed (green curve) wheat yield in Portugal and of corresponding modelled values (red curve) as obtained from the leave-one-out cross-validation procedure.

Figure 5.12 (lower panel) presents the results obtained from the leave-one-out cross validation. The good agreement between the modelled time series by the regression model (upper panel) and the one obtained by the cross validation indicate that the developed model seems to be robust. This fact is further supported by the slight decrease (from 0.83 to 0.78) of the correlation between original and modelled time

series. However results of the model should be regarded with some caution, given the short length of the analyzed time series (18 years).

5.5 Final Remarks

We have computed point correlations between spring NDVI over Portugal and wheat yield during the period 1982-1999. We have found strongly negative correlations (statistically significant at the 1% level) over Southern Portugal (Alentejo), a region where more than 80% of wheat is produced and more than 95% of the total of hard wheat production is concentrated. We have then selected the so-called subset of "wheat-like" pixels, i.e. pixels coded as non-irrigated arable land associated to correlation values that are statistically significant at the 1% level.

The impact of meteorological factors on wheat yield was assessed by computing monthly correlations of the detrended anomalies of yield with averaged values (over the "wheat-like" pixels) of net short-wave radiation, temperature and precipitation as well as with NAO. Obtained results are in good agreement with the empirical findings about the roles (and timings) of the different meteorological factors along the different stages of the wheat vegetative cycle. In particular, cold temperatures during winter and early spring, precipitation in February and March and solar radiation in March have a positive impact during the growing stage, whereas a larger NAO index in July is beneficial for the maturation stage.

A regression model was finally built up using as predictors spring NDVI and NAO in June. Performance of the model was quite satisfactory, with a generally good agreement between observed and modelled wheat yield. Although results may still be considered as preliminary, given the short length of the analyzed series (18 years), the model is expected to be useful to for wheat yield monitoring. The model is also expected to be improved when extending it to an enlarged GIMMS dataset (1982-2006).

6. DROUGHT AND VEGETATION STRESS MONITORING

6.1 Introduction

The Iberian Peninsula is recurrently affected by drought episodes and by the adverse effects associated that range from severe water shortages to economic losses and related social impacts. For instance, during the hydrological year of 2004/2005, the Iberian Peninsula was hit by one of the two worst drought episodes that were recorded in the last six decades (Garcia-Herrera et al., 2007), reinforcing the need for a continuous monitoring of vegetation stress and for reliable estimates of the drought impacts. In this respect it is worth mentioning that more than 280 M€ were spent in order to compensate for the damage associated with the 2005 drought in continental Portugal (MADRP, 2005).

The strong dependence of vegetation dynamics on water availability has been for long recognized in the Mediterranean and other semi-arid regions (Eagleson, 2002, Rodríguez-Iturbe and Porporato, 2004, Vicente-Serrano and Heredia-Laclaustra, 2004, Vicente-Serrano, 2007). A combined effect of lack of precipitation over a certain period with other climatic anomalies, such as high temperature, high wind and low relative humidity over a particular area may result in reduced green vegetation cover. When drought conditions end, recover of vegetation may follow (Nicholson et al., 1998) but the process may last for longer periods of time (Diouf and Lambin, 2001).

Traditional methods of drought assessment and monitoring depend heavily on rainfall data as recorded in meteorological and hydrological networks. However the availability of reliable satellite imagery covering wide regions over long periods of time has progressively strengthen the role of remote sensing in environmental studies, in particular in those related to drought episodes (Kogan, 1995, 1997, 2000, Kogan et al., 2004, McVicar and Jupp, 1998, 1999, 2002). Drought early warning and monitoring are

crucial components of drought awareness and mitigation plans (Wilhite, 1993) and it is worth stressing, that with the help from environmental satellites, drought can be detected 4-6 weeks earlier than before and delineated more accurately (Kogan, 2000).

In recent years there has been a considerable amount of drought studies dealing with different regions of Europe as well as covering the entire European continent (Briffa et al., 1994; Gibb et al., 1978; Marsh and Lees, 1985; Phillips and McGregor, 1998; Bussay et al., 1999; Estrela et al., 2000; Lana et al., 2001; Lloyd-Hughes and Saunders, 2002). Summer droughts are the most important in terms of human perception, but water shortages during the other seasons may also have significant socio-economic impacts (EEA, 2001). Several authors have examined the special case of the Iberian Peninsula (Garcia-Herrera et al., 2007, Vicente-Serrano, 2006) and it may be noted that, even though the recent 2005 drought has been ranked among the strongest ones of the last century in Portugal, the episodes of 1945, 1981, 1983, 1992 and 1999 were also major events (Feio and Henriques, 1986; Godinho et al., 1992). In addition, a slight downward trend has been found in the annual precipitation recorded over Portugal (Zhang et al., 1997, Miranda et al., 2006) that is particularly noticeable in early spring (Trigo and DaCamara, 2000, Garcia-Herrera et al., 2007). However, less attention has been paid to the impacts of drought in vegetation activity as well as to the sensitivity of the photosynthetic mechanisms to water stress.

The aim of the present chapter is therefore to make use of remote-sensed information in order to monitor the spatial and temporal distribution of heat and water stress of vegetation in Continental Portugal. The severity of a given drought episode will then be assessed by evaluating the cumulative impact over time of heat and water stress conditions on vegetation in a certain region. Special attention will be devoted to the above mentioned extreme drought episode of 2005, as well as to those of 1999 and 2002. It may be noted that the latter episode has mainly affected Northeastern Portugal in strong contrast with the other two episodes that have struck hardest Southern Portugal.

6.2 Vegetation stress

The response of vegetation to heat and water stress was assessed based on fields of NDVI as derived from the VEGETATION instrument on-board SPOT5. As discussed in Chapter 3, any vegetation monitoring based on NDVI requires a previous correction of the time-series, in order to distinguish real changes in the annual cycles of vegetation greenness from those due other factors, e.g. contamination by clouds, shadows and snow and sun/view directional dependence of spectral response. Figure 6.1 presents monthly values of NDVI that were spatially averaged over Continental Portugal. The years of 1999, 2002 and 2005 are conspicuous because of the occurrence of low values of vegetation greenness, especially during the growing season, i.e., during the period of high photosynthetic activity. In the case of the droughts of 1999 and 2005, this is especially apparent when the spatial averages are performed over non-irrigated arable land, a feature that is in contrast with the case of 2002 where the lower values are well visible over broad-leaved forest. The delay of the growing season of arable land together with the observed relative insensitivity in the case of broad-leaved forest is another interesting feature that suggests drought conditions to be responsible for both delaying and shortening the growing season.

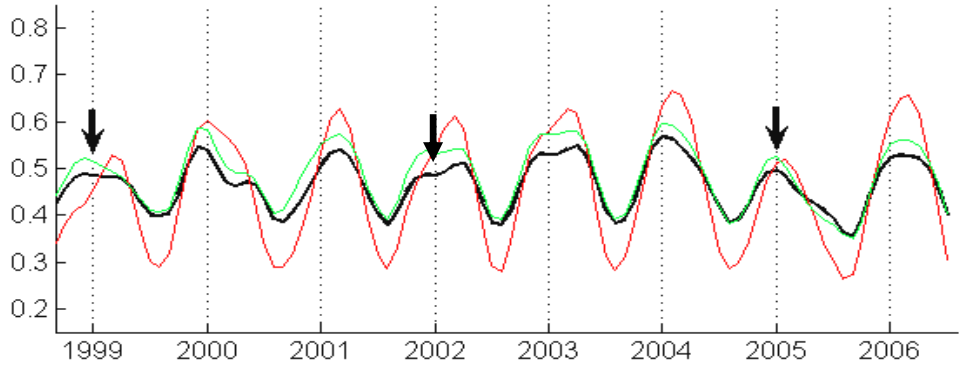

Figure 6.1 Monthly time-series (1999–2006) of NDVI averaged over Continental Portugal for all pixels (black line), for pixels of non-irrigated arable land (red line) and of pixels of broad-leaved forest (green line). Black arrows indicate the drought episodes of 1999, 2002 and 2005.

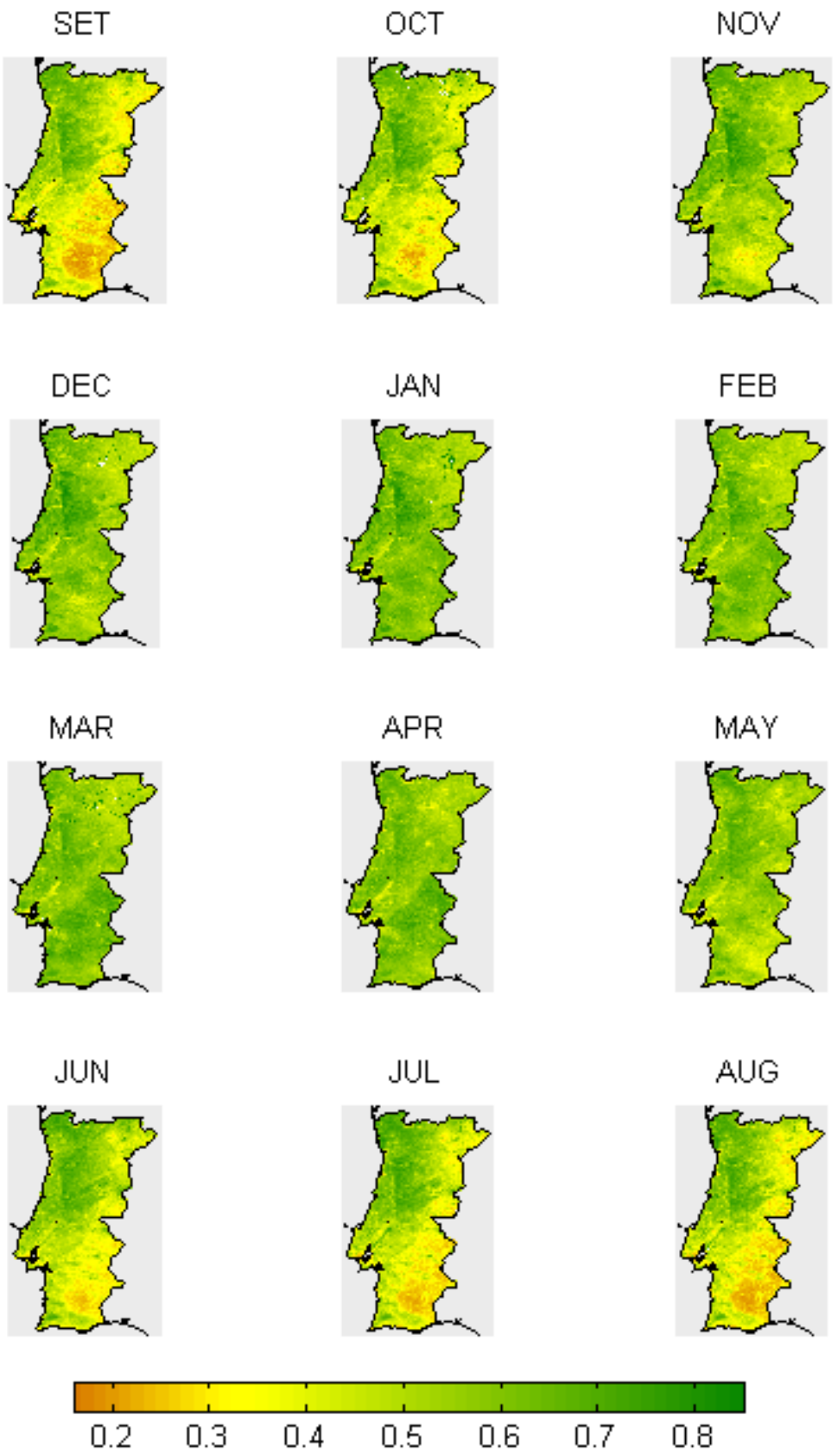

Figure 6.2 Monthly means of NDVI (1999-2006) over Continental Portugal, covering the period from September to August.

Figure 6.2 presents the monthly mean fields of NDVI from September to August, over Continental Portugal and covering the period 1999-2006. As expected, larger values of NDVI associated with an increase in photosynthetic activity, and therefore in vegetation greenness, may be found in winter and spring over Southern Portugal. During summer and autumn this region presents low values, a feature that is coherent with the vegetation types of a semi-arid environment. In contrast, Northwestern Portugal presents high values of vegetation greenness as expected from the presence of forest, the predominant vegetation cover.

6.3 Drought assessment

6.3.1 Annual cycle of NDVI

Figures 6.3 to 6.5 show monthly anomaly fields of NDVI from September to August, respectively for the years 1998/1999, 2001/2002 and 2004/2005. It may be noted that monthly anomalies of a given month are defined as departures from the median of that month (computed over the considered period 1999-2006). Usage of the median (instead of the mean) was made in order to avoid the lever effect by the extremely low NDVI values that were attained in the droughts years, taking into account the small length of the sample (8 years).

As already discussed, the three chosen drought years are characterised by low vegetation greenness activity associated to low values of NDVI (Figure 6.1). In the case of 1999 (Figure 6.3) the highest negative anomalies (around -0.30) present an early start in November and persistently remain until April. The most affected regions are located in Southern Portugal and it may be noted that the impact of the drought is apparent until May. A strong contrast in the spatial distribution may be observed in the case of 2002 (Figure 6.4) the highest negative anomalies being mainly located over Northeastern Portugal where negative values (around -0.10) may be found extending from November to February. During 2005 (Figure 6.5), the highest negative anomalies (around -0.30) may be observed, over Southern Portugal, between February and June.

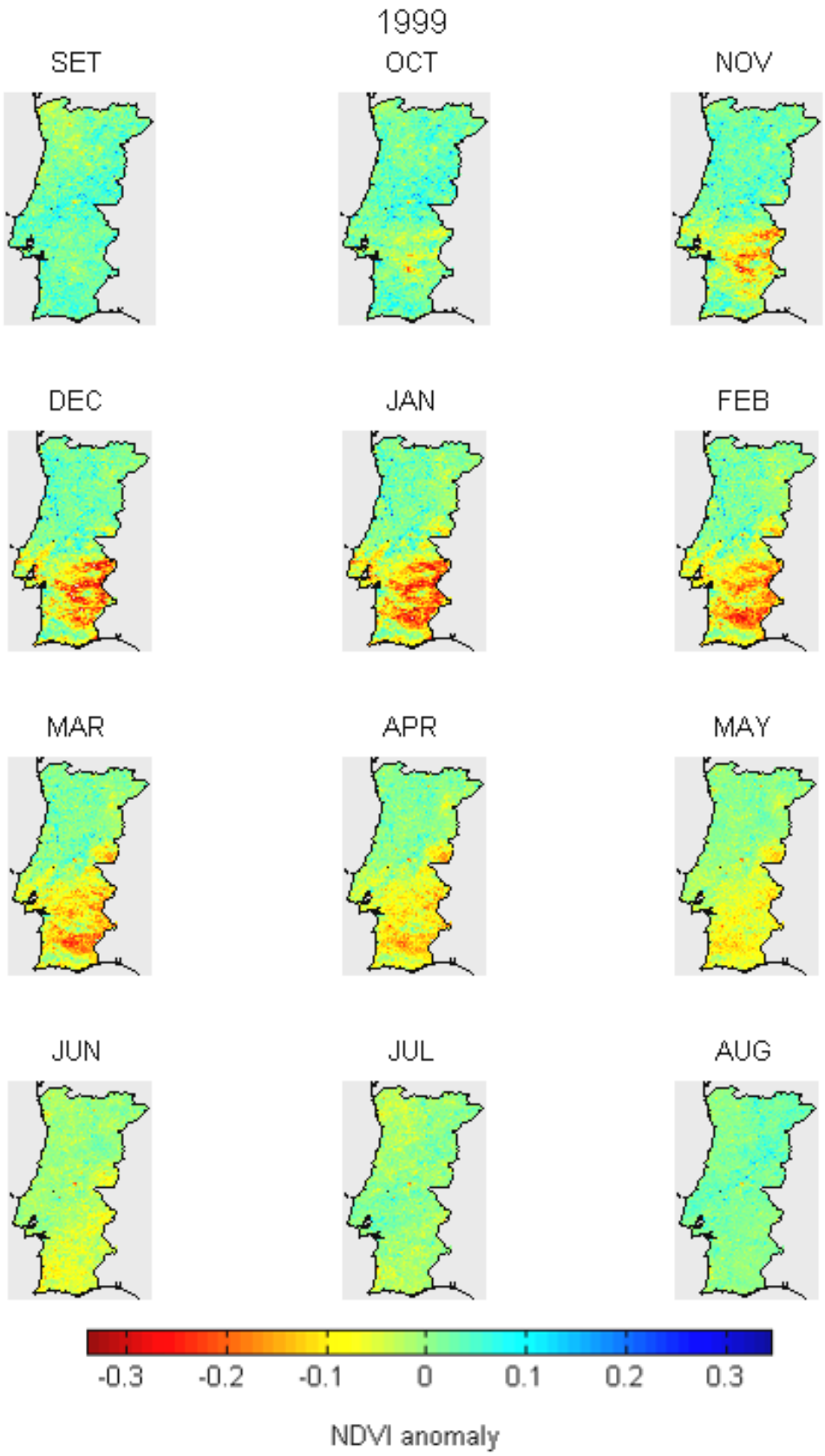

Figure 6.3 NDVI anomalies from September to August respecting to the year of 1998/1999.

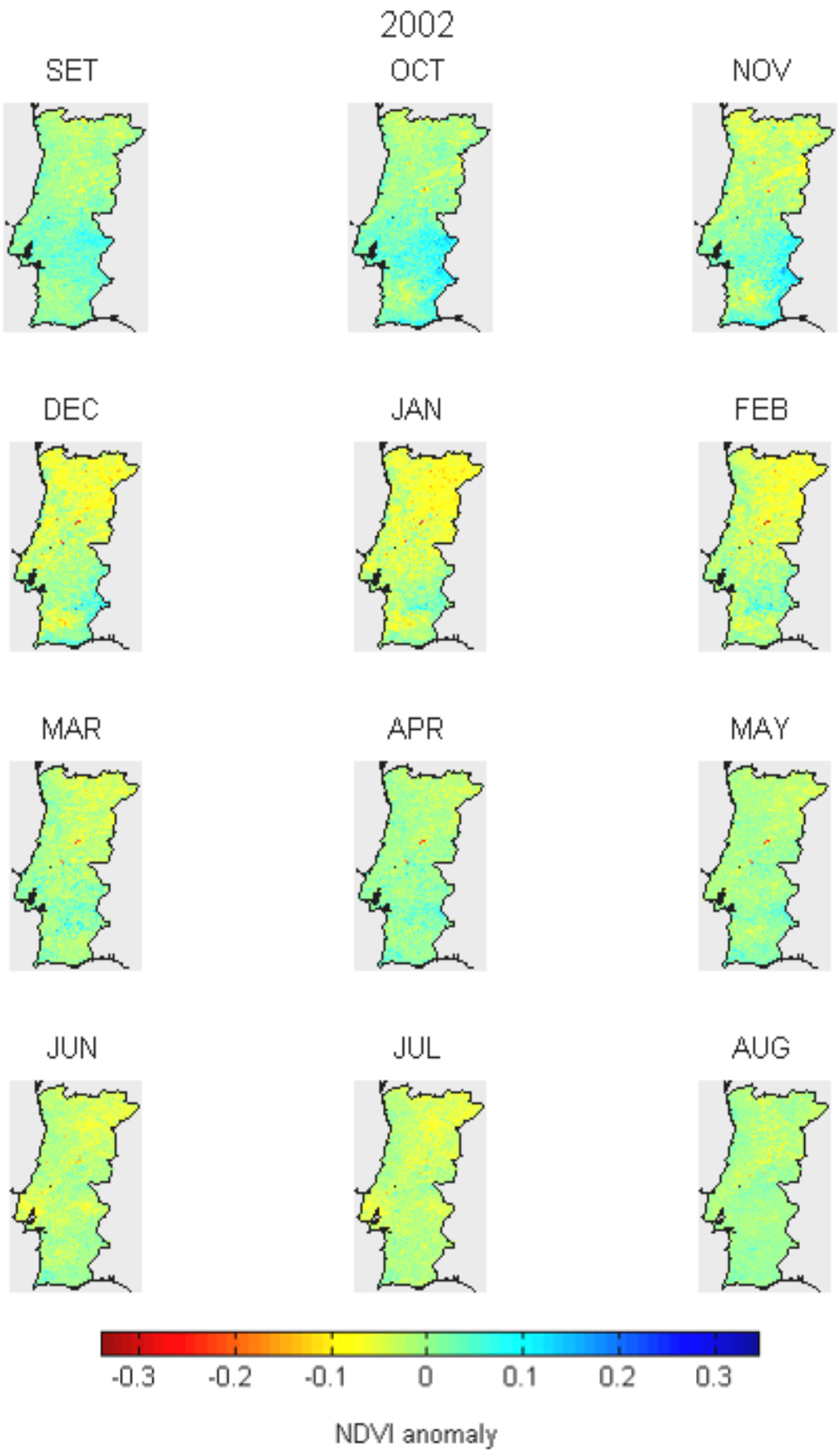

Figure 6.4 As in Figure 6.3 but respecting to the year of 2001/2002.

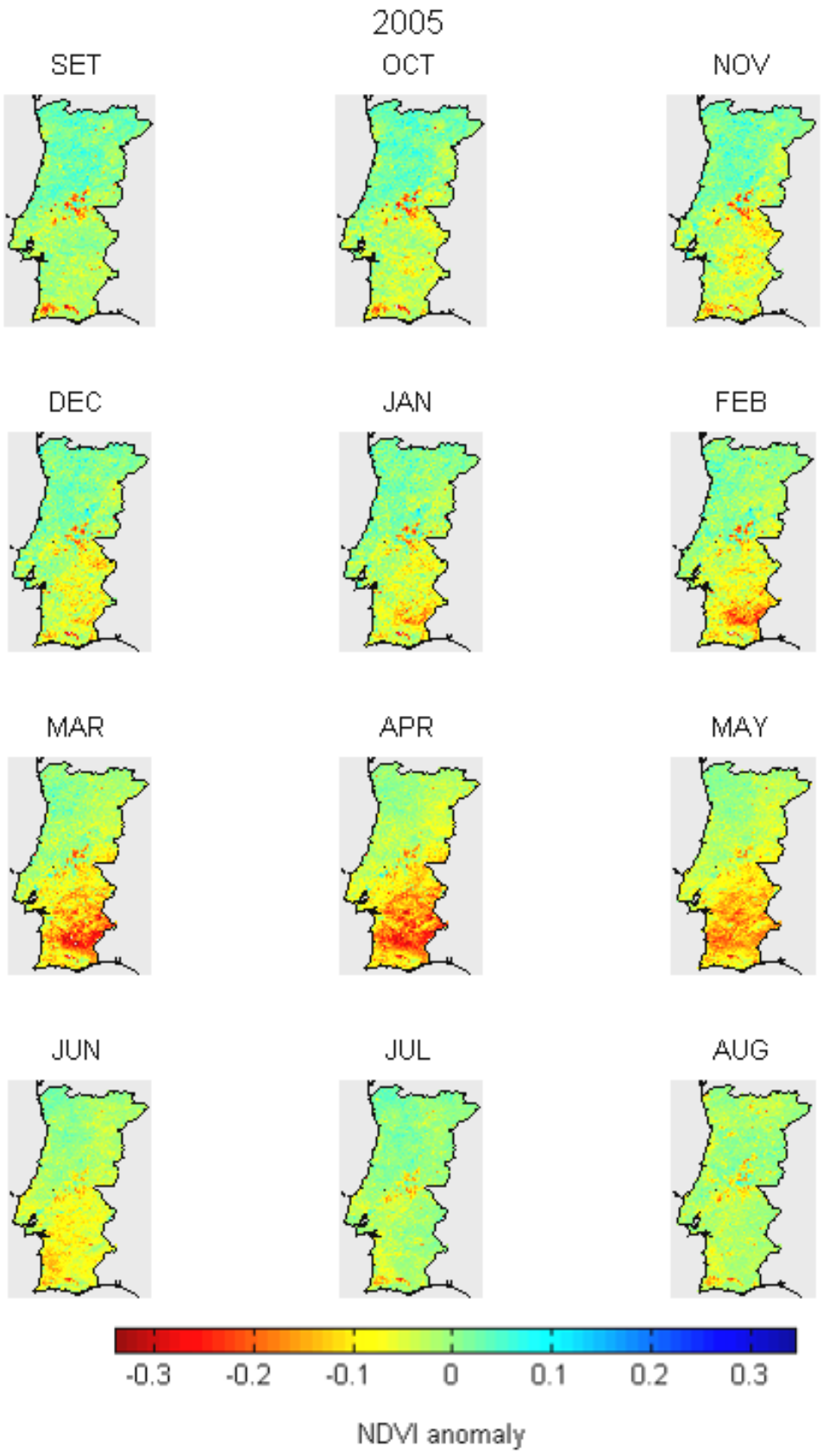

Figure 6.5 As in Figure 6.3 but respecting to the year of 2004/2005.

It is worth emphasising that, in the cases of the 1999 and 2005 drought episodes, the area of stressed vegetation is located in the south of Portugal, a region that is generally covered by non-irrigated arable land (Figure 3.9) with semi-arid characteristics and presenting a strong desertification risk. It may be further noted that the location of stressed pixels is also in good agreement with the results of Vicente-Serrano (2006) who has shown that the impact of climate variability and associated extreme events (such as drought) on vegetation activity is most pronounced over most arid areas. Finally, in the case of the 2005 drought episode, it is worth stressing that the observed negative anomalies are contemporaneous with the period of high photosynthetic activity (i.e., high NDVI values in Figure 6.2), leading to a further amplification of the negative impact on vegetation dynamics and therefore to an even larger drought impact.

6.3.2 Annual cycle of soil moisture

Since a quick response of vegetation to spatio-temporal variations in soil moisture is generally observed in semi-arid regions (Bonifacio et al., 1993; Sannier and Taylor, 1998), the impact of soil moisture on vegetation dynamics is worth being analysed. We have relied on the Global Soil Moisture Archive (http://www.ipf.tuwien.ac.at/radar/ers-scat/home.htm) for the period 1992-2005 (Scipal, 2002) and have extracted the so-called Soil Water Index (SWI) which is based on the method developed by Wagner et al. (1999a, b). The archive is based on information from the European Remote Sensing (ERS) Scatterometer instrument on-board ERS-1 and ERS-2 satellites, operated by the European Space Agency (ESA), which achieve global coverage within 3 to 4 days with a 25 km grid spacing. SWI fields were interpolated to a 0.25º latitude-longitude grid covering the same window that was defined for NDVI (see Chapter 3).

Figure 6.6 presents spatially averaged values over Portugal of SWI and it is well apparent that the drought episodes of 1999 and 2005 are characterised by an annual cycle reaching values well below the remaining years. Figure 6.7 presents the monthly mean fields of SWI from September to August, over Continental Portugal and covering the same period. The annual cycle of soil moisture is well apparent and the contrast

between the regions North and South of the Tagus valley is worth being noted in the transition seasons.

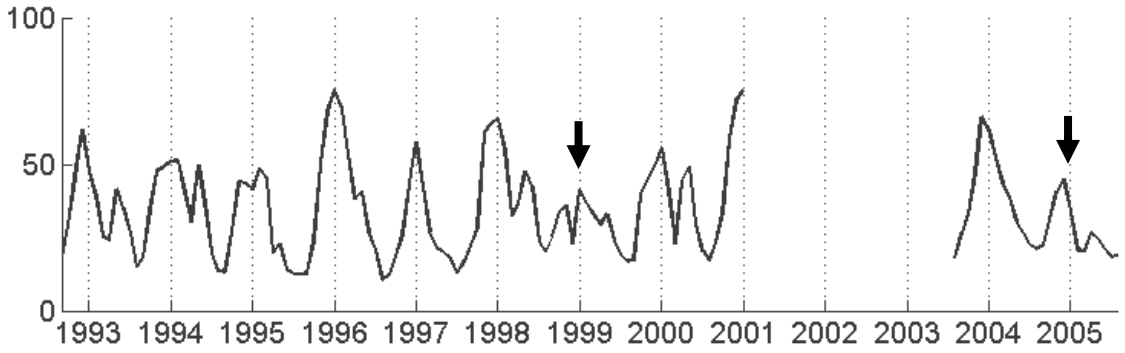

Figure 6.6 Monthly time-series (1992–2005) of SWI averaged over Continental Portugal. Values from January 2001 until August 2003 are missing. Black arrows indicate the drought episodes of 1999 and 2005.

The response of vegetation to soil moisture is well illustrated in Figure 6.8 that presents the annual cycle of SWI vs. NDVI as obtained from averaging the periods of study. The initial linear relationship between NDVI and SWI from August to December translates the contemporaneous response of vegetation to soil moisture that leads to a maximum of greenness in January. However, the following period presents a non linear behaviour. The strong decrease in SWI between January and April corresponds to a slight decrease of NDVI, suggesting that vegetation greenness is sustained by the cumulated soil water during winter time. A contemporaneous response of NDVI to SWI is again observed from April to August, closing the vegetation cycle.

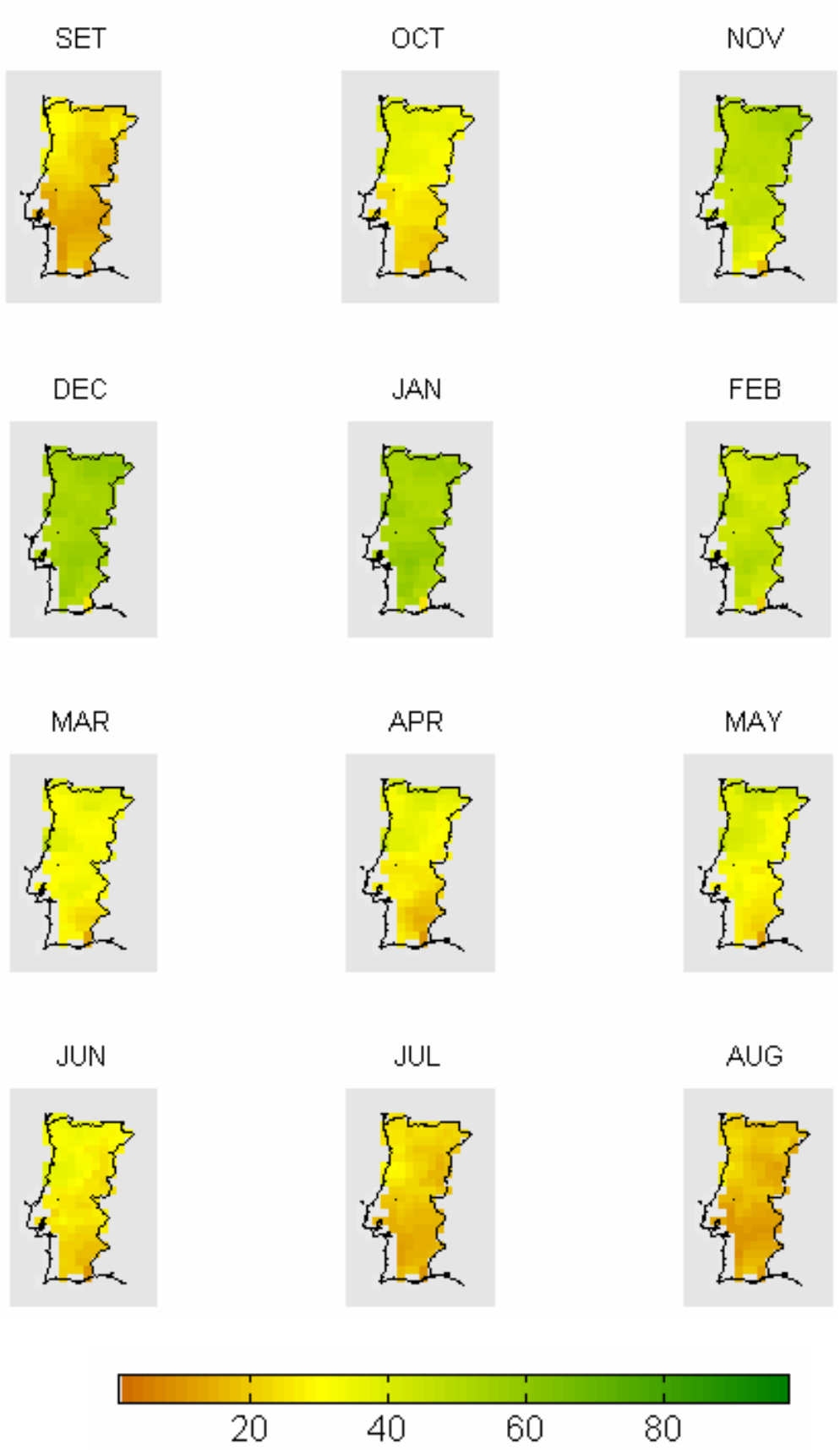

Figure 6.7 Monthly means of SWI (1992-2005) over Continental Portugal, covering the period from September to August.

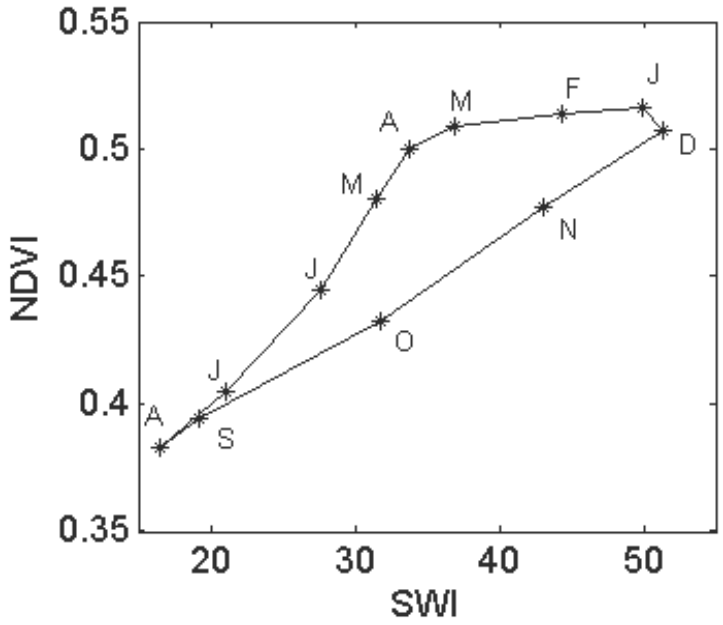

Figure 6.8 Climatological cycle of SWI vs. NDVI. Letters indicate months of the year.

Figures 6.9 and 6.10 present the spatial distribution over Continental Portugal of monthly anomalies of SWI for the drought episodes of 1999 and 2005. The drought episode of 2002 was not considered because of the unavailability of SWI data for the year 2001/2002. SWI anomalies are defined as departures from the mean of the respective month over the considered 14-year period (1992-2005) and as opposed to the drought episode of 2005, where the occurrence of negative anomaly values of SWI only begin in spring, drought conditions start to occur in the beginning of winter 1998/1999.

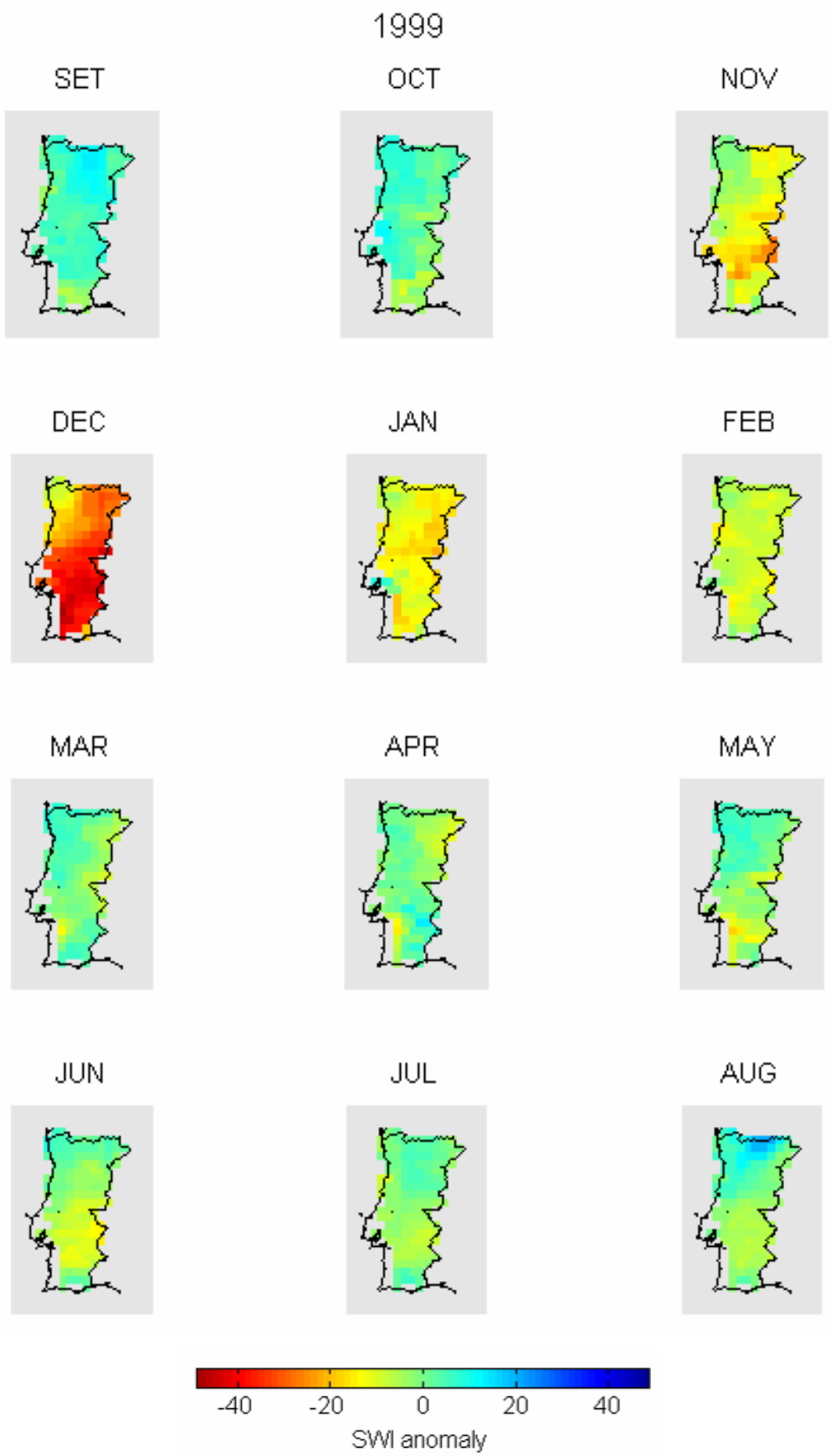

Figure 6.9 SWI anomalies for January to August respecting to the year 1998/1999.

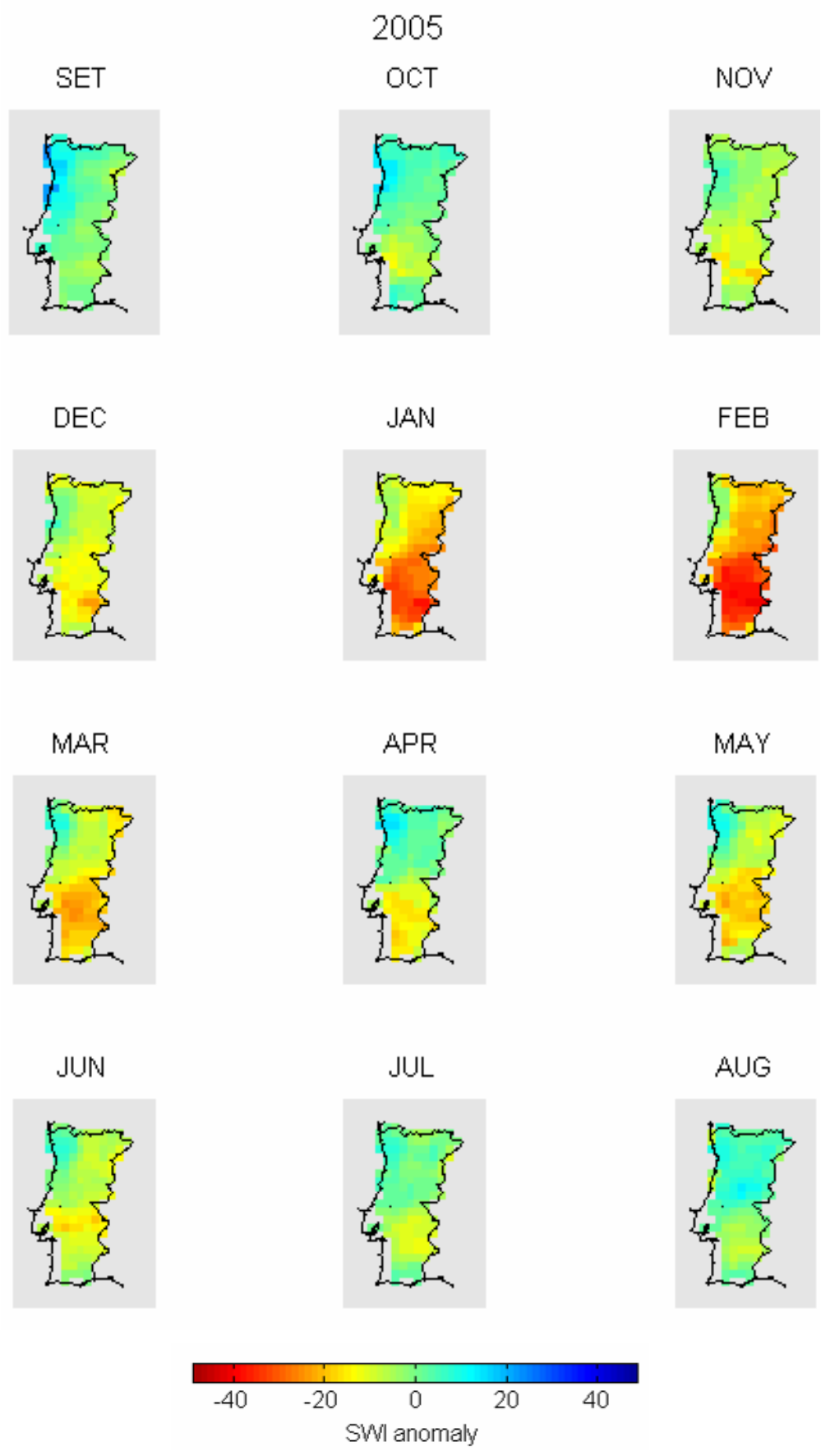

Figure 6.10 As in Figure 6.9 but respecting to the year 2004/2005.

The different impact of the soil moisture cycle on vegetation greenness in the cases of the 1999 and 2005 episodes is well apparent in Figure 6.11 that presents the respective annual cycles of SWI vs. NDVI. Results point out the role of soil moisture in winter and early spring in the green-up of vegetation over semi-arid regions, where there is a high level dependence of the vegetation cover on water availability (Nicholson et al., 1990, 1998; Nicholson and Farrar, 1994; Vicente Serrano, 2006). In the case of 1999 (Figure 6.11, left panel) there is a persistent shortage of soil moisture from November until May, with dramatics effects on vegetation greenness that are well apparent in the SWI vs. NDVI cycle that is contained within the respective climatological cycle. A different behaviour may be observed in the case of the drought episode of 2005 where a deficit in greenness is already apparent at the beginning of September. The superavit of SWI is reflected on a slight recovery of vegetation greenness but the severe shortage of soil water from December up to May has devastating effects on vegetation activity.

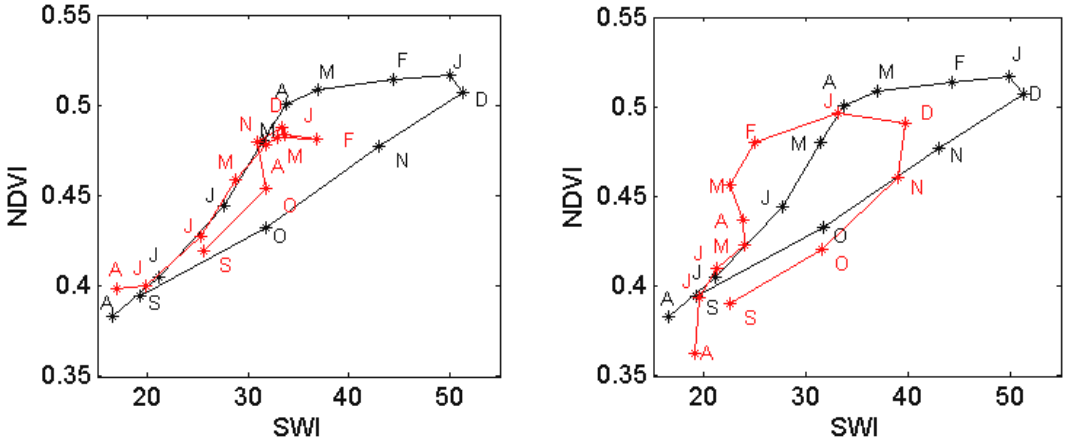

Figure 6.11 Annual cycles (red curves) of SWI vs. NDVI for the drought episodes of 1999 (left panel) and 2005 (right panel). The climatological cycle (black curves) is also presented for reference purposes.

The sensitivity of the different land cover types to the available soil moisture is illustrated in Figure 6.12 that presents annual cycles of spatially averaged NDVI for each year of the considered period (1999-2006) over non-irrigated arable land (top panel) and coniferous forest (bottom panel). The two drought episodes of 1999 and 2005 are enhanced and the impact of dry periods is clearly observed in the case of arable land, with minimum values occurring in winter for the case of 1999 and in spring

for the case of 2005. However, over coniferous forests, lower than average values of NDVI may still be observed during the beginning of winter in the case of 1999 and during spring in the case of 2005.

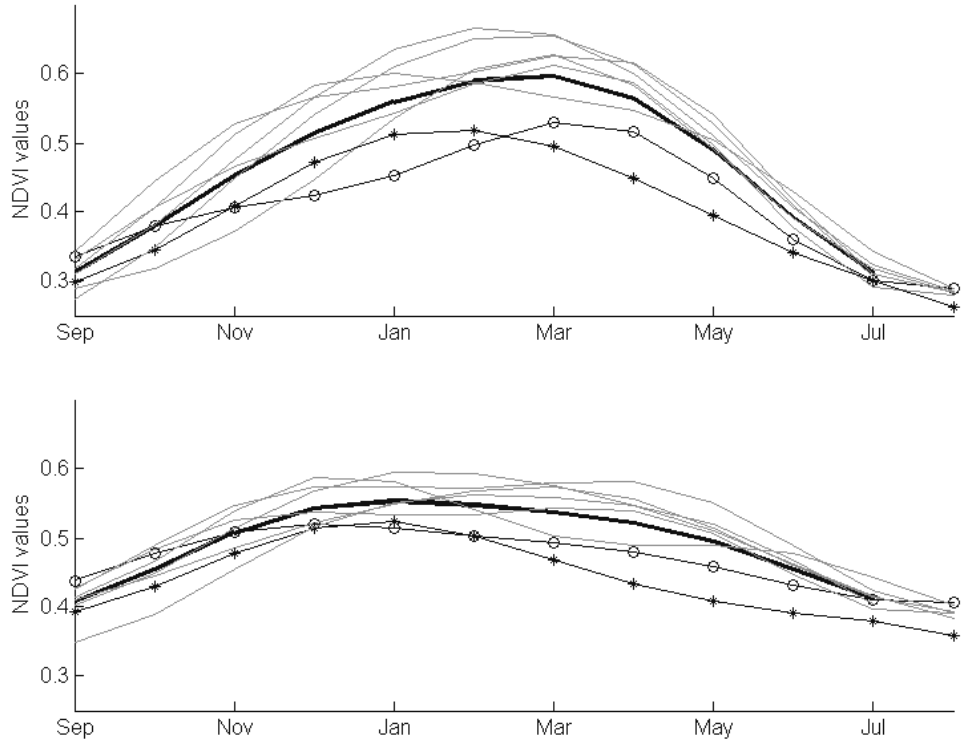

Figure 6.12 Annual cycles of spatially averaged NDVI for each year of the considered period (1999-2006) over non-irrigated arable land (top panel) and coniferous forest (bottom panel). The drought episodes of 1999 and 2005 are represented, respectively, by the curves with circles and asterisks. The line in bold refers to monthly means over the entire period.

6.4 Drought persistence

The severity of a given drought episode is often assessed by means of the so called Palmer Drought Severity Index (PDSI) that is based on a supply-and-demand model of soil moisture (Palmer, 1965). The aim of PDSI is to provide standardized measurements of moisture conditions so that comparisons can be made between locations and between months.

Based on the concept of water balance, PDSI is mainly a meteorological index which responds to weather conditions that have been unusually dry or unusually wet.

Details on the evaluation of PDSI, as well as about its usefulness and limitations, may be found e.g., in Alley (1984). The index is usually computed on a monthly basis and has proven as especially adequate to characterise long-term droughts. Values of PDSI, which roughly vary between -6.0 and +6.0 are derived from the following relationship

$$X_i = 0.897 X_{i-1} + \frac{Z_i}{3} \qquad (6.1)$$

where X_i and Z_i respectively denote the monthly values for month i of PDSI and the so-called moisture anomaly index which takes into account the difference between the actual precipitation in month i and the amount of precipitation that is "climatologically appropriate" for the existing conditions, weighted by a "climate characteristic", K (Palmer, 1965). Since the first term of the equation (6.1) introduces an autoregressive process, PDSI has a certain length of memory (Karl, 1986).

Drought episodes are associated to negative values of PDSI and are usually grouped into the so-called drought severity classes which are defined as follows; moderate drought (PDSI $\approx$ -2), severe drought (PDSI $\approx$ -3) and extreme drought (PDSI $\approx$ -4).

Figure 6.13 presents, for the year of 2004/2005, the evolution on a monthly basis (black curve) of the percentage of continental Portugal that is under extreme drought conditions according to WMO (2006). The respective evolution of the percentage of the territory with stressed (red bars) and very stressed (green bars) vegetation is also shown in the figure. It may be noted that the area of stressed (very stressed) vegetation was estimated based on the fraction of pixels with anomalies lower than 0 (lower than -0.025). The severity of the drought episode of 2005 is well apparent taking for instance into account that, in May, almost 90% of continental Portugal is covered by pixels with NDVI anomalies lower than 0.

Figure 6.13 also shows the existence of a delay of about three months of PDSI relatively to NDVI. This delay, that is especially visible for very stressed vegetation, translates the above mentioned memory of PDSI. Moreover, the observed good agreement, for the 2005 drought episode, between the percentage of territory affected by extreme drought and associated to very stressed vegetation suggests adopting a threshold of -0.025 to identify pixels affected by drought conditions in the remaining years of the study period.

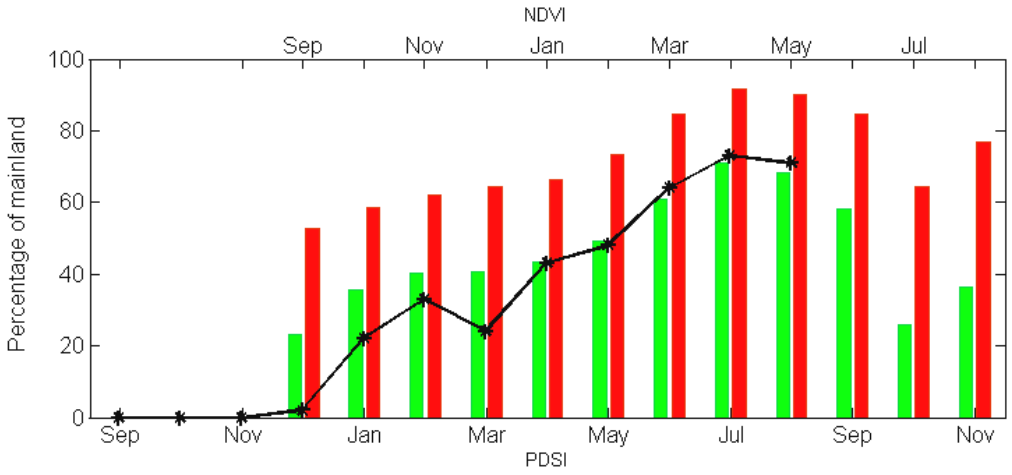

Figure 6.13 Percentage of continental Portugal with monthly NDVI anomalies lower than 0 (red bars) and lower than -0.025 (green bars), from September to August of 2005. The black line represents the percentage of mainland affected by extreme drought, i.e., with PDSI ≈ -4. The 3-month delay of PDSI relatively to NDVI (as indicated by the two different horizontal time axes) is worth being noted.

As mentioned above, an important aspect to be considered when assessing drought severity respects to the persistence of dry conditions for a given location. Accordingly, we have evaluated drought persistence by simply counting, for each pixel, the number of months with NDVI anomalies lower than -0.025. Results are shown in Figure 6.14 and the years of 1999, 2002 and 2005 are particularly striking due to the large areas affected by persistent drought. In the cases of the drought episodes of 1999 and 2005, pixels located over the south of Portugal reveal up to nine months (out of eleven) of persistently stressed vegetation. In the case of the drought episode of 2002 a considerable vast area over Noutheastern Portugal presents more than eight months (out of eleven) of stressed vegetation.

Table 6.1 presents the percentage of mainland Portugal stricken by serious drought, i.e., with monthly NDVI anomalies below -0.025 in more than 9 months (out of 11). The exceptionality of 2005 is again conspicuous, with more than one third of Portugal with more than 9 months in vegetation stress, an area that is twice the one observed in 1999. The amount of 11% of mainland affected in the case of 2002 is still contrasting with the remaining years of the considered period.

Table 6.1 Percentage of mainland Portugal stricken by serious drought, i.e., with monthly NDVI anomalies below -0.025 in more than 9 months (out of 11).

Years	*1999*	*2000*	*2001*	*2002*	*2003*	*2004*	*2005*	*2006*
% mainland severe drought	**18**	1	3	**11**	1	4	**36**	9

In the cases of the drought episodes of 1999 and 2005, it is worth reinforcing that the region affected is located in southern Portugal, more precisely in the province of Alentejo, an area that is responsible for more than 80% of the total of wheat production in Portugal (Gouveia and Trigo, 2007). Drought analysis in this area is especially important not only because droughts may cause significant economic losses (Morales et al., 2000; Iglesias et al., 2003) but also due to the fact that there is a strong dependence of the economy and society on agriculture yields (Vicente-Serrano, 2006).

We have also compared the vegetation response to water stress of different land cover types, for the three drought episodes of 1999, 2002 and 2005. As shown in Table 6.2, in all three episodes, non-irrigated arable land, forest and shrubland represent more than 55% of pixels characterised by at least six months (out of eleven) of monthly NDVI below -0.025.

Table 6.2 Total amounts and relative proportions of pixels affected by drought for different land cover types during the drought episodes of 1999, 2002 and 2005.

Year	Non-irrigated Arable land	Forest	Shrubland	Other	Total
1999	10498 (25%)	9375 (23%)	4310 (10%)	17206 (42%)	41389 (100%)
2002	2542 (9%)	5125 (19%)	8035 (30%)	11094 (42%)	26796 (100%)
2005	11722 (25%)	11841 (23%)	5974 (10%)	23032 (44%)	52569 (100%)

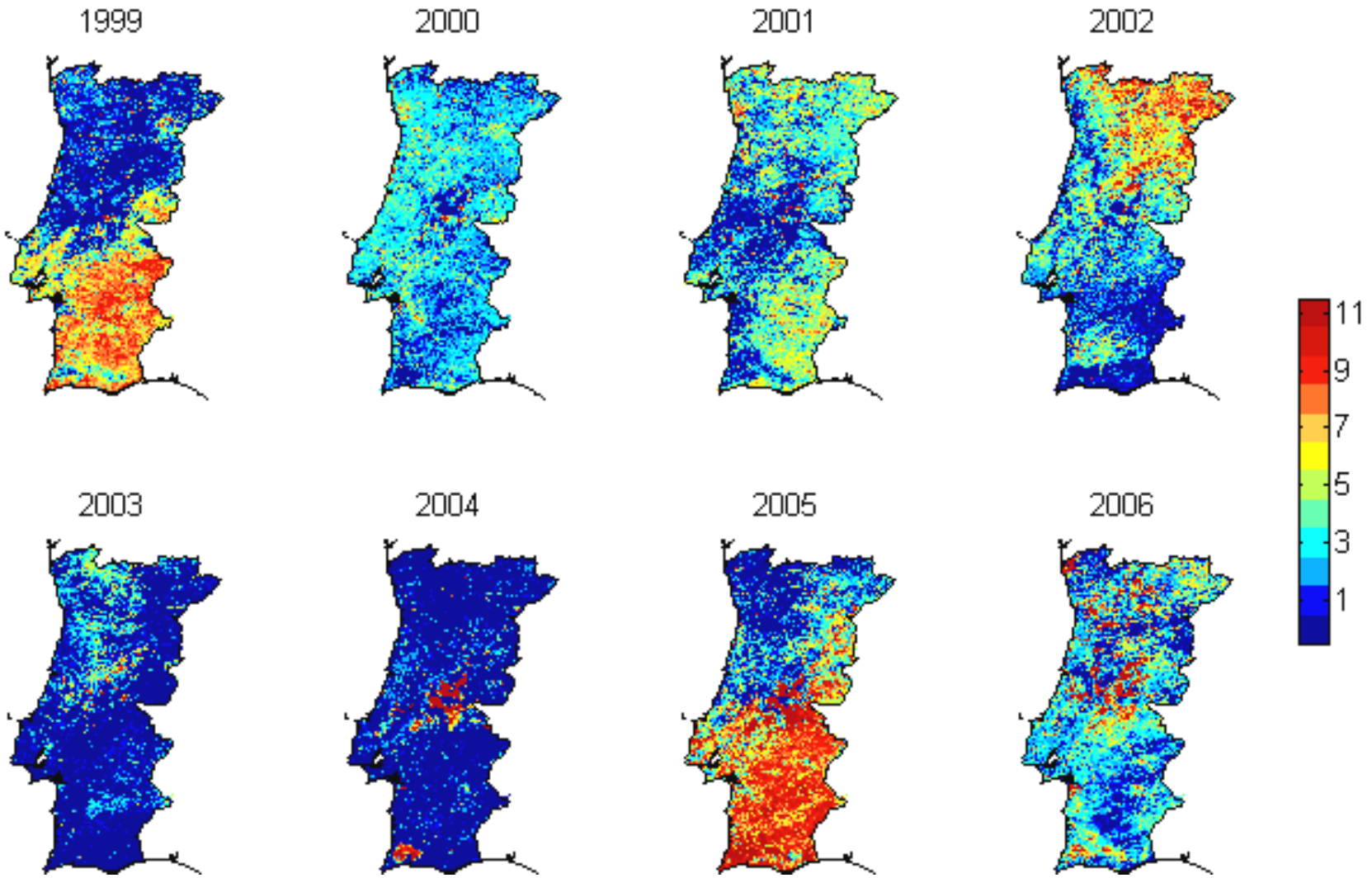

Figure 6.14 Number of months between September and August that are characterised by NDVI anomaly values below -0.025, for each year of the considered period (1999-2006).

As expected the episode of 2005 ranks first in what respects to the total amount of affected pixels (52569), followed by 1999 (41389) and 2002 (26796). However there are interesting differences when comparing the drought episodes of 1999 and 2005 versus the episode of 2002 in what respects to the proportion of affected vegetation types. Arable land was especially affected during the 1999 and 2005 episodes, whereas shrubland was the most affected land cover type during the 2002 episode. Forest was affected in similar proportions during the three drought episodes and the remaining types of vegetation do not show as well noticeable differences among episodes.

The cumulative effect of drought conditions on the three considered types of vegetation was further investigated by analysing the relative proportions of pixels that remained with monthly anomalies of NDVI below -0.025 for 7, 8 and 9 months. Results are presented in Table 6.3 and conspicuous differences may be found among the three drought episodes. The exceptional strength of the drought episode of 2005 is well illustrated by the percentage of affected pixels of all vegetation types (including forest), with more than half of the pixels being affected for more than 9 months. In the case of the drought episode of 1999 non-irrigated arable land was the main vegetation type affected, with a total amount of almost one third of the pixels being affected for more than 9 months. Finally, in the case of the episode of 2002, shrubland was the most affected vegetation type with slightly more than one third being affected for at least 9 months.

Table 6.3 Cumulative effect of drought conditions for specific land cover types during the drought episodes of 1999, 2002 and 2005.

Nº Months	Non-irrigated Arable land	Forest	Shrubland
	1999		
≥ 6	100	100	100
≥ 7	87	76	74
≥ 8	64	47	43
≥ 9	**31**	17	18
	2002		
≥ 6	100	100	100
≥ 7	72	66	74
≥ 8	48	43	53
≥ 9	29	26	**34**
	2005		
≥ 6	100	100	100
≥ 7	93	85	83
≥ 8	83	71	66
≥ 9	**65**	54	50

6.5 Final remarks

An assessment was made on the potential usage of environmental satellites for the detection and monitoring of drought events in Continental Portugal. For this purpose, annual cycles of vegetation greenness were analysed by examining, for each year, the monthly anomalies of NDVI. Special attention was devoted to the years of 1999, 2002 and 2005 because of the occurrence of low values of vegetation greenness during the growing season. In the case of the drought episodes of 1999 and 2005, southern Portugal was mostly affected, whereas in the case of 2002 the highest negative anomalies were mostly located in Northern Portugal.

The impact of soil moisture on vegetation dynamics was also assessed by studying the annual cycle of SWI *vs*. NDVI and by analysing monthly anomalies of SWI. Obtained results pointed out the different impact of the soil moisture cycle on vegetation greenness; while in 1999 shortage of water in the soil persisted from November until May, in the episode of 2005 the deficit in greenness was already apparent at the beginning of September. The sensitivity of the different land cover types to the available soil moisture was also studied. The impact of dry periods was clearly observed in both cases of arable land and forest, the former vegetation type presenting a higher sensitivity than the latter.

The relationship between PDSI and NDVI was also studied for the year of 2005. In the case of NDVI anomalies below -0.025, the existence of a delay of about three months of PDSI relatively to NDVI suggested using this threshold to identify pixels associated to stress vegetation. Drought persistence was therefore assessed by counting, for each pixel, the number of months with NDVI anomalies lower than -0.025. As expected, the years of 1999, 2002 and 2005 were particularly striking because of the large areas affected by persistent drought. The exceptionality of 2005 was again conspicuous not only because more than one third of Portugal was covered by pixels with more than 9 months in vegetation stress, but also because the most relevant vegetation types (non irrigated arable land, forest and shrubland) were all affected. In the cases of the episodes of 1999 and 2005, persistent drought especially affected arable land, in particular over the province of Alentejo, an area that is responsible for more than 80% of the total of wheat production in Portugal. In the case of 2002, pixels under persistent stress are mainly located in Northern Portugal and shrubland was the mostly affected vegetation type.

The main results obtained in the present chapter are summarised in Figure 6.14 that gives, for each year of the considered period 1999-2006, the location of pixels affected by persistent drought conditions. In this respect, the drought episodes of 1999, 2002 and 2005 are prominent and the specific characteristics of each episode, both in terms of spatial distribution and time persistence, may be readily identified. The years of 2000, 2003 and 2004 present opposite characteristics, the whole territory being characterised by unstressed vegetation.

However a closer look to the year of 2004 reveals an unexpected behaviour. In fact two well defined regions, respectively, located in Central Portugal and in the Southwest, show a deep contrast with the background, the pixels presenting monthly anomalies below -0.025 for 9 to up 11 months. Such a behaviour is not compatible with the one associated to drought conditions. In fact, a comparison with a map of fire scars respecting to the summer season of 2003 could immediately lead to the identification of the two areas as representing the signature of wildfires that occurred in the previous year.

This feature is especially interesting because it raises the possibility of adapting the developed technique to identify burned areas and to assess the recovery of vegetation over areas stricken by fire. Figure 6.15 is an updated version of Figure 6.14, where we have masked all pixels that were identifying as burned areas using the procedure described in Chapter 7, that is dedicated to the problem of burned area monitoring and vegetation recovery.

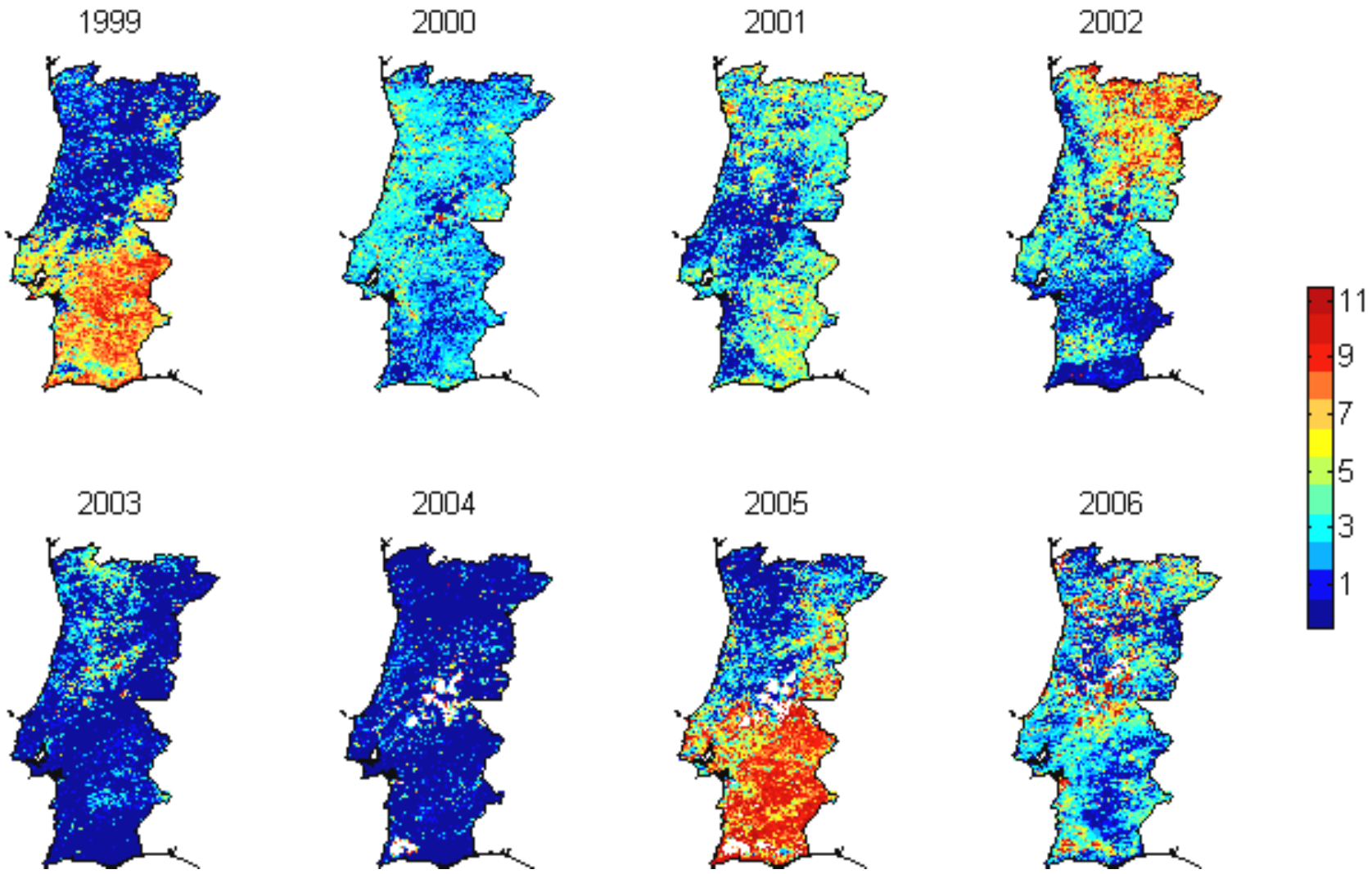

Figure 6.15 As in Figure 6.14, but all pixels that are identify as burned areas are masked

7. MONITORING BURNED AREAS AND VEGETATION RECOVERY

7.1 Introduction

The number of fires and the extent of the burned surface in Mediterranean Europe have strongly increased during the last decades. This may be due either to land-use changes (e.g. land abandonment and fuel accumulation) or to climatic changes (e.g. reduction of fuel humidity) that increase fire risk and fire spread (Pausas and Vallejo, 1999). As in the Mediterranean ecosystems, fires in Portugal have an intricate effect on vegetation regeneration due to the complexity of landscape structures as well as to the different responses of vegetation to the variety of fire regimes (Wittenberg et al., 2006). Vegetation cover has, in turn, a key role on soil erosion and land degradation processes (Shakesby et al., 1993). For instance, the destruction of vegetation by wildfires generally leads to an intensification of runoff and erosive processes (Inbar et al., 1997; 1998). Thornes (1990) has suggested that a minimum of 30% in vegetation cover is required to protect the soils against water erosion. Studies performed at various spatial scales and under different ecological conditions indicate that the majority of loss of sediments occurs during the first year after fire occurrence (DeBano et al., 1998, Inbar et al., 1998 and Cerda and Doerr, 2005) and that the risk of post-fire soil erosion increases with the time required for vegetation to reach the minimal threshold cover (Shakesby et al., 1993; Inbar et al., 1998; Cerda, 1998a; Cerda, 1998b). A thorough evaluation of vegetation recovery after fire events becomes therefore crucial in land management (Wittenberg et al., 2006).

In the above mentioned context remote sensing plays an important role because it has revealed to be particularly useful to estimate post-fire vegetation dynamics. A

considerable number of fire recovery studies based on remote sensing have been conducted in regions characterised by Mediterranean climates (Jakubauskas et al., 1990; Marchetti et al., 1995; Viedma et al., 1997; Díaz-Delgado et al., 1998; Henry and Hope, 1998; Ricotta et al., 1998). Several authors have also tested the use of NDVI to monitor plant regeneration after fire (Malingreau et al., 1985; Paltridge and Barber, 1988; Viedma et al., 1997; Illera et al., 1996). It may be noted, however, that satellite data are not adequate to accurately detect high resolution changes in the structure of vegetation.

Several studies have shown that rapid regeneration occurs within the first 2 years after the fire occurrences (Trabaud, 1981; Kutiel, 1994; Inbar et al., 1998), with distinct recovery rates at the north and the south facing slopes (Cerda and Doerr, 2005). Pausas and Vallejo (1999) have shown that, in the Iberian Peninsula, one year after a single fire event vegetation cover reached 52% on the north facing slope and 32% on the south facing slope. Similar trends were found at the Mt. Carmel region, Israel, after the 1988 fire event (Kutiel, 1994; Inbar et al., 1998). Díaz-Delgado et al. (2002) have observed lower NDVI values after the second of two successive fires occurring within an 11-year interval, i.e. the green biomass diminishes significantly when disturbances occur within short time intervals. They concluded that increased fire frequency might reduce ecosystem resilience, i.e. the ability of the system to recover to a pre-disturbance state.

We will present a methodology that allows identifying large fire scars in Portugal using monthly values of NDVI at the 1km×1km spatial scale. We will then show how the developed procedure may be applied to assess vegetation recovery after a fire event.

7.2 Rationale

As pointed out at the end of Chapter 6, the year of 2004 presents several areas characterized by persistent negative anomalies of NDVI which are associated to burned scars resulting from wildfire events that occurred in the summer of the previous year. A close inspection of burned scars revealed that, besides their persistence, pixels belonging to scars were characterized by extremely low negative anomalies of NDVI. This behaviour suggests identifying pixels belonging to burned areas resulting from fires of year Y-1 as those associated to NDVI anomalies in year Y that are below a

sufficiently low threshold T and last for at least M months of a specified long enough period.

As shown in Figure 7.1, choice of T = -0.075 and M = 5 during the period from September to May leads to the identification of burned areas with shape and spatial distribution that closely resemble those that were identified by Direcção Geral dos Recursos Florestais (DGRF) based on information (with 30 m resolution) from Landsat imagery.

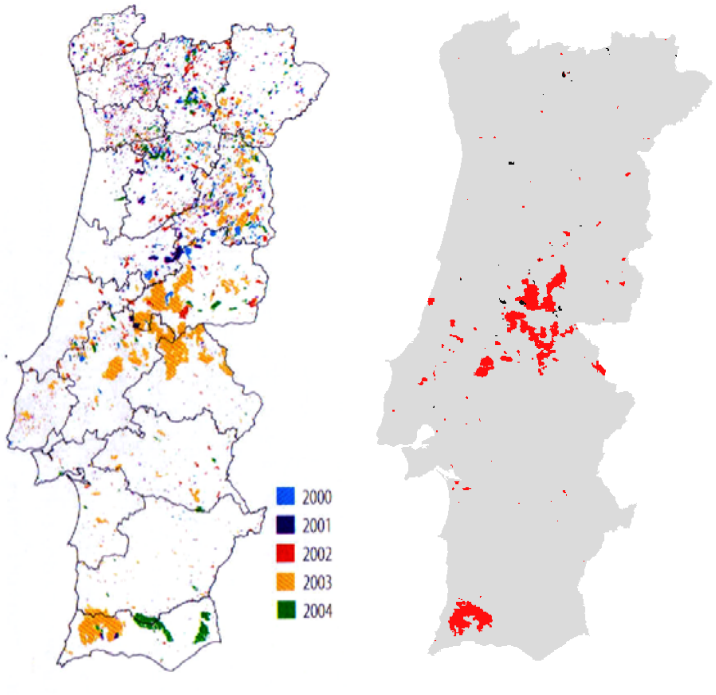

Figure 7.1 Annual burned areas in Continental Portugal (right panel) for the fire season of 2003 (red pixels) using the criterion of at least 5 months of NDVI anomalies below -0.075 during the period from September to May of 2004; black pixels refer to burned scars for the previous fire season of 2002. Annual burned areas in Continental Portugal (central panel) for the period 2000-2004 as identified from Landsat imagery. The central panel was adapted from Pereira et al. (2006).

Figure 7.2 (left panel) shows results that are obtained when applying the above described criterion to the year of 2005 in order to identify burned areas associated to wildfire events of 2004. When comparing obtained results from those of DGRF (Figure 5.2, central panel), a large number of erroneously identified burned pixels is well apparent in Southern Portugal leading to an overestimation of the burned area by almost a factor of 9.5This behaviour is due to the fact that, as discussed in Chapter 6, the year of 2005 was affected by severe drought. Accordingly, pixels associated to drought were

mistakenly identified as burned areas. In order to circumvent this problem the criterion was modified by introducing a larger number of months (M =7) during an enlarged period (from January to August). Figure 7.2 (right panel) shows the obtained results with the new criterion and it may be observed that a large number of false alarms have indeed been eliminated.

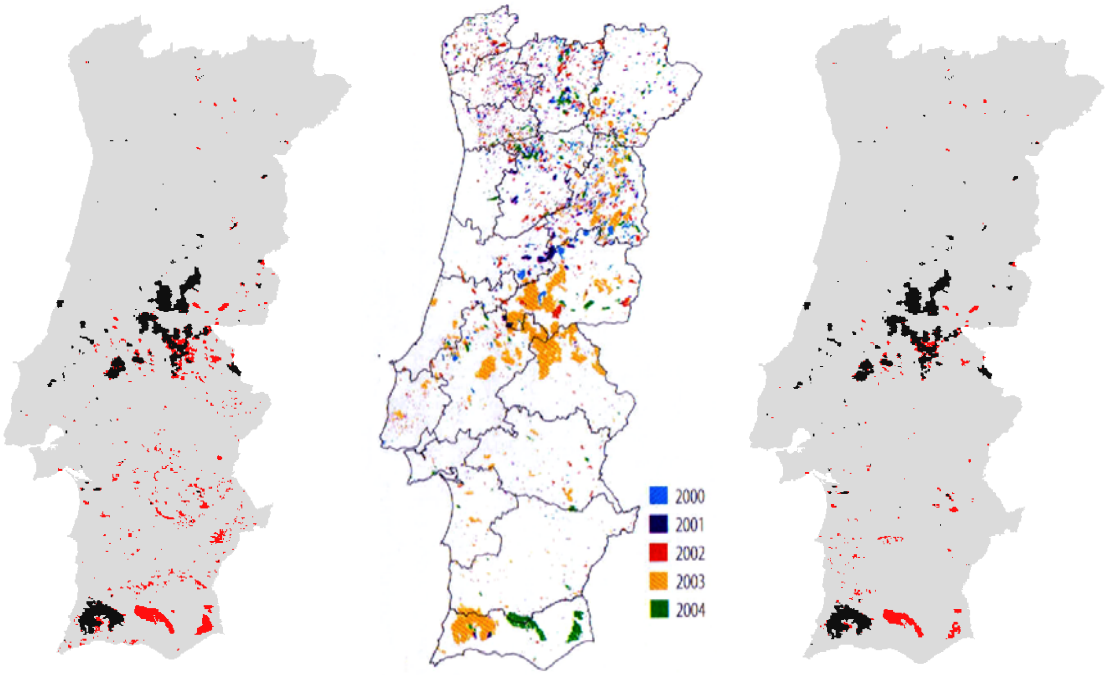

Figure 7.2 Annual burned areas in Continental Portugal (left panel) for the fire season of 2004 (red pixels) using the criterion of at least 5 months of NDVI anomalies below -0.075 during the period from September to May of 2005; black pixels refer to burned scars for the previous fire season of 2003. Annual burned areas in Continental Portugal (central panel) for the period 2000-2004 as identified from Landsat imagery. Annual burned areas in Continental Portugal (right panel) for the fire season of 2004 (red pixels) using the criterion of at least 7 months of NDVI anomalies below -0.075 during the period from January to August of 2005; black pixels refer to burned scars for the previous fire season of 2003. The central panel was adapted from Pereira et al. (2006).

Figure 7.3 (left panel) shows a third example, namely results obtained when applying the first criterion to the year of 2006 in order to identify burned areas associated to wildfire events of 2005. Again there is the problem of false alarms that spread all over the country, leading to an overestimation of burned area by a factor of 1.9. The problem is related to the fact that the year of 2006 had a late starting of the vegetative cycle because of the effects of the previous drought episode of 2005. The criterion was again adapted by delaying the five month period, now defined from

January to August. The improvement in identification of burned areas using the new criterion (Figure 7.3, right panel) is well apparent when results are compared with those obtained by DGRF (central panel).

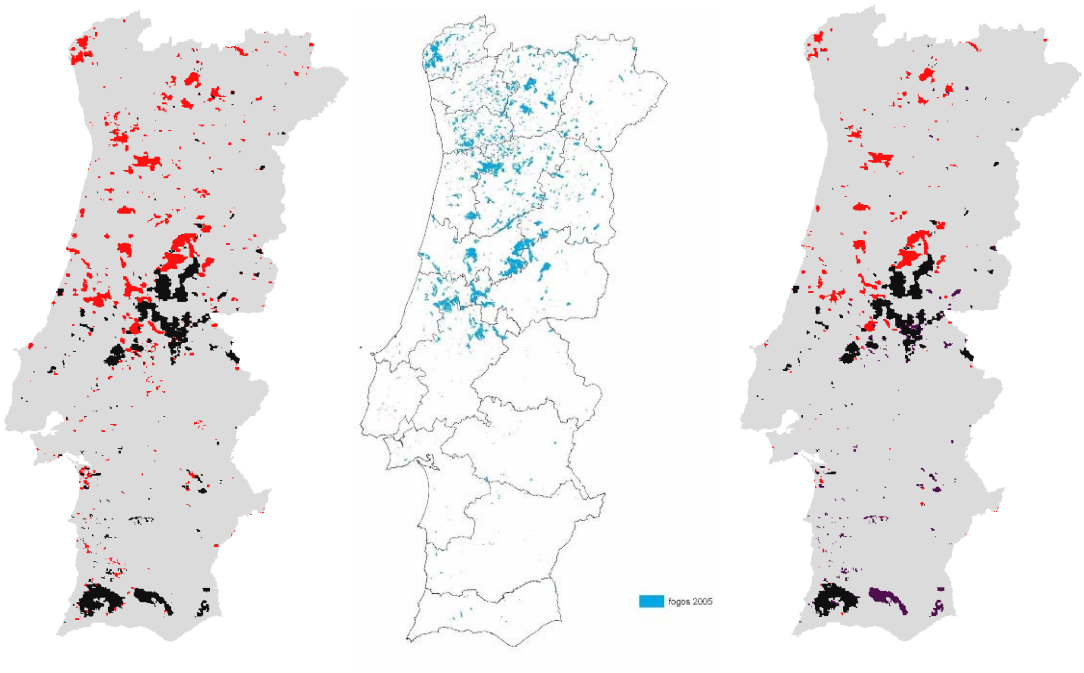

Figure 7.3 Annual burned areas in Continental Portugal (left panel) for the fire season of 2005 (red pixels) using the criterion of at least 5 months of NDVI anomalies below -0.075 during the period from September to May of 2006; black pixels refer to burned scars for the previous fire season of 2004. Annual burned areas in Continental Portugal (central panel) for the year of 2005 as identified from Landsat imagery. Annual burned areas in Continental Portugal (right panel) for the fire season of 2005 (red pixels) using the criterion of at least 5 months of NDVI anomalies below -0.075 during the period from January to June of 2006; black pixels refer to burned scars for the previous fire season of 2004. The central panel is courtesy from J.M.C. Pereira.

Obtained results suggest adopting the following criteria to identify burned areas in Portugal during the period 1998-2004:

- for extreme drought years (1999, 2002 and 2005) burned pixels (by fires of the previous year) are those characterised by more than 7 months with monthly NDVI anomalies below -0.075 in the period from January to August;
- for years that follow extreme drought years (2000, 2003 and 2006) burned pixels (by fires of the previous year) are those characterised by 5 months with monthly NDVI anomalies below -0.075 in the period from January to August;

- for years not affected by drought (2001 and 2004) burned pixels (by fires of the previous year) are those characterised by 5 months with monthly NDVI anomalies below -0.075 in the period from September to May.

7.3 Vegetation recovery in burned areas

Figure 7.4 presents on a yearly basis the burned scars that were identified, during the period 1998-2004, by applying the methodology described in the previous section. A visual comparison of obtained results with the ones based on Landsat imagery for the years 2000-2004 (Figure 7.2, central panel) and 2005 (Figure 7.3, central panel) reveals that a good agreement may be found for years affected by severe wildfires that caused large burned scars. This is the case of 2003 in Central Portugal, of 2004 in South Portugal and in the Southeast, and 2005 in Central Portugal and in the Northwest. Results for 2000, 2001 and 2002 are quite poor because burned areas in these years are of a much smaller extent. This is not surprising taking into account that NDVI data have a resolution of 1km×1km whereas Landsat data have a 30m×30m resolution and are represented on a map with a scale of 1:100,000.

The total amount of burned area for each year as obtained with the developed methodology was also compared with the corresponding total amounts as obtained by accumulating burned areas (of more than 100 ha) for all recorded events in the DGRF database. Results are shown in Figure 7.5 and despite the high correlation value (that reaches 0.97) between the two time series, which reflects the overall agreement in inter-annual variability, there is a systematic underestimation by the method based on NDVI (2004 being the unique exception). As expected, the underestimation is particularly severe in the years of low fire activity (1998, 1999, 2001 and 2002).

Table 7.1 shows on a yearly basis the distribution among different CLC2000 land cover types of pixels that were classified as burned using the developed methodology. The deep contrast in vulnerability to fire conditions between forest and shrubland vs. arable land and crops is well apparent. The prevalence in 1998 and 1999 of the transitional woodland-shrub class over the forest and the non-irrigated arable land classes is also conspicuous, especially when comparing with the opposite behaviour that

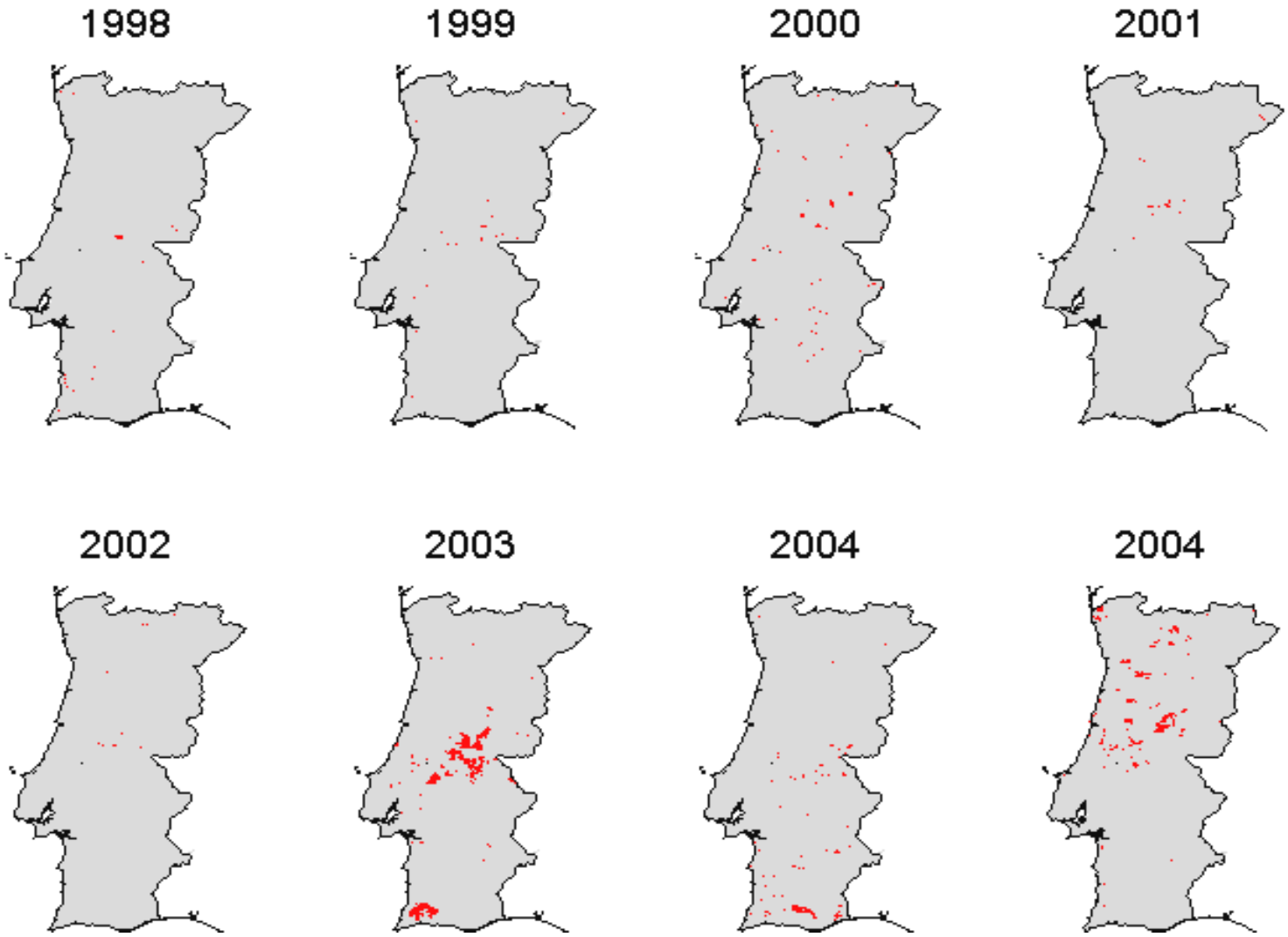

Figure 7.4 Burned scars for each year of the period 1998-2005 as identified based on NDVI anomalies

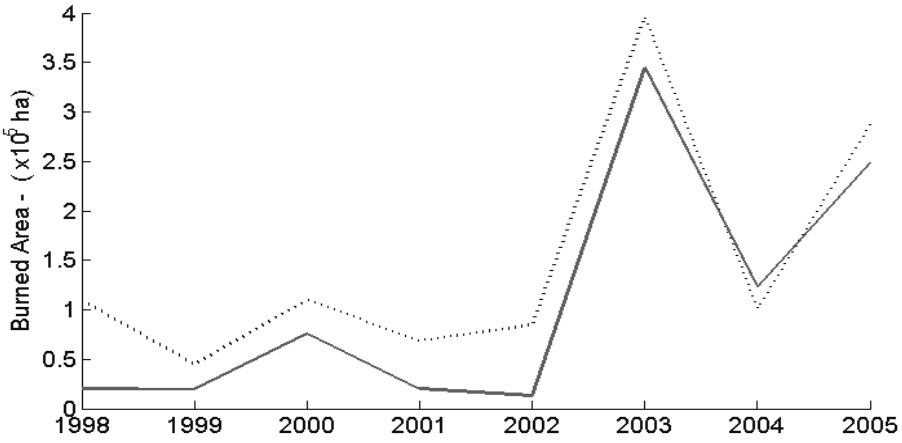

Figure 7.5 Time series of annual burned areas in Continental Portugal for the period 1998-2005 as obtained from the developed methodology (solid line) and based on DGRF information (dotted curve).

Table 7.1 Percentage of burned pixels for pixels classified as non irrigated Arable Land, Forest, Transitional woodland-shrub and Shrubland (using Corine Land Cover Map 2000, CLC2000) for the fire seasons from the years 1998 to 2005.

Years	Non irrigated arable land	Annual crops/ permanent crops	Forest	Transitional woodland--shrub	Shrubland	Others
1998	11	1	21	38	4	19
1999	2	1	22	58	3	14
2000	16	4	23	18	9	30
2001	2	1	44	17	29	7
2002	0	0	76	16	3	5
2003	1	1	69	14	7	8
2004	4	1	55	8	9	23
2005	1	2	51	28	9	9

may be observed from 2000 onwards. However, this may be explained by the fact that burned areas in 1998 and 1999 (i.e. in years immediately prior to 2000) were naturally classified as transitional woodland-shrub according to CLC2000, meaning that vegetation was still in the process of recovering from fire events. In the same context, the sudden increase in 2005 of the percentage of burned pixels associated to transitional woodland-shrub is also worth being noted. Such increase is due to the recurrence in 2005 of fires in regions that had burned prior to 2000.

Figure 7.6 shows, for selected pixels in a set of eight large fire scars, the respective time series of NDVI, each one corresponding to an event that has occurred in a given year of the considered 8-year period (1998-2005). The behaviour of the annual cycles of NDVI, that display always a sharp decrease in the year of the fire event and a steady increase in the following years, is a strong indication about the adequacy of the adopted methodology. Results obtained further suggest using the procedure to assess vegetation recovery after a large scale fire event.

An example of how vegetation recover assessment may be performed based on the developed methodology is given in Figure 7.7. The figure presents the time series of NDVI averaged over three large scars, two of them located in Central Portugal and respecting to events in 2001 and 2003, and the third one located in Algarve and respecting to an event in 2003. Differences in vegetation recovery are well apparent between the two years and the two locations. In the case of the fire scars located in Central Portugal it may be observed that the recovery is much faster in 2001 than in 2003, a feature that is explained by the fact that 2003 was followed by an extreme drought event that started in 2004 and reached a peak in 2005. In the case of the event of Algarve, the recovery is much slower than in the case of the event of the same year that took place in Central Portugal. Again this may be partly explained by the fact that drought conditions of 2004/2005 were particularly severe in the southern part of Portugal (see Chapter 6).

Final remarks

We present a methodology aiming to identify large fire scars using monthly values of NDVI at the 1km×1km spatial scale. The procedure is based on the analysis of

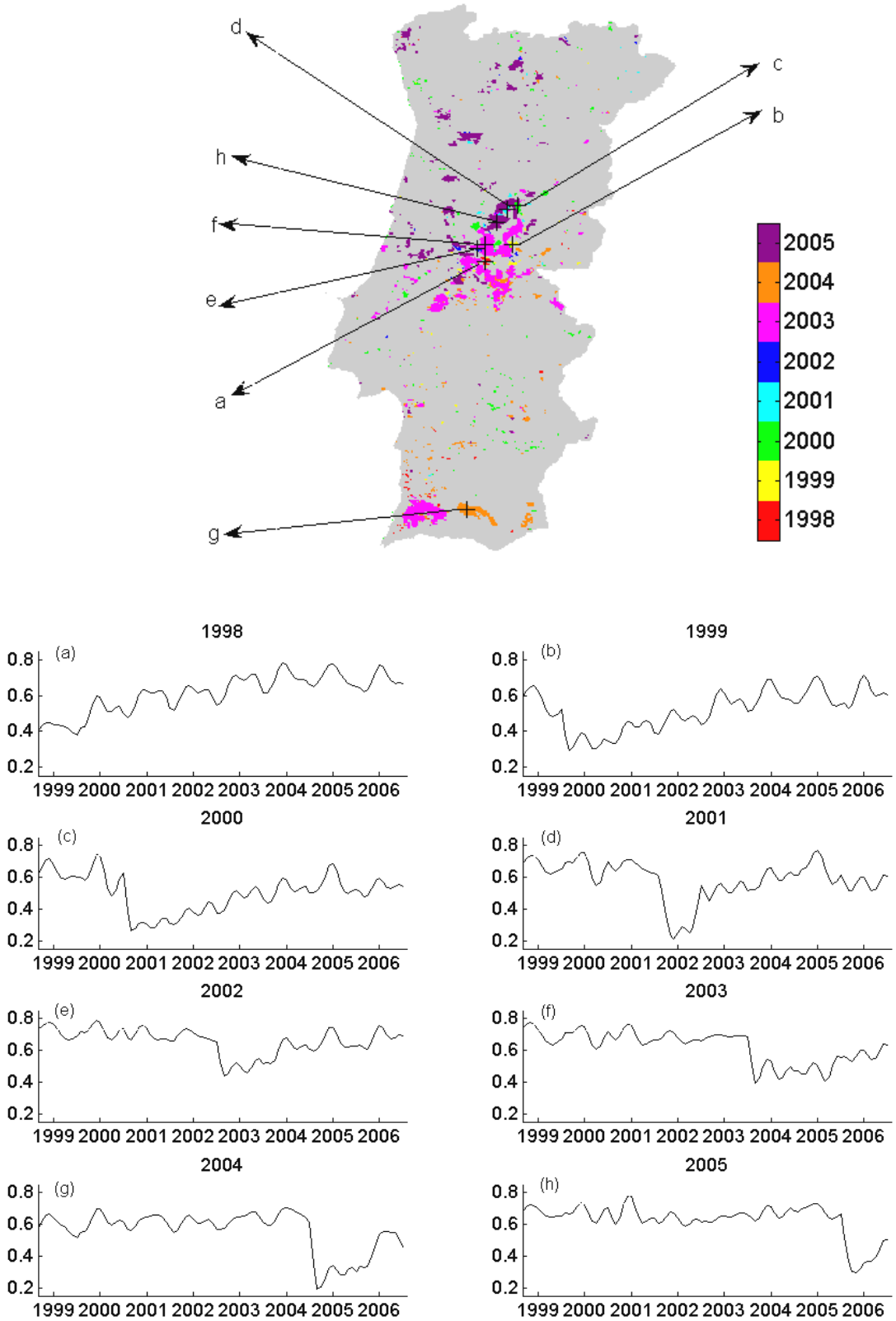

Figure 7.6 Time series of NDVI for selected pixels in a set of eight large fire scars, each one corresponding to an event that has occurred in a given year of the 1998-2005. The location of the selected fire scars is given in the upper panel.

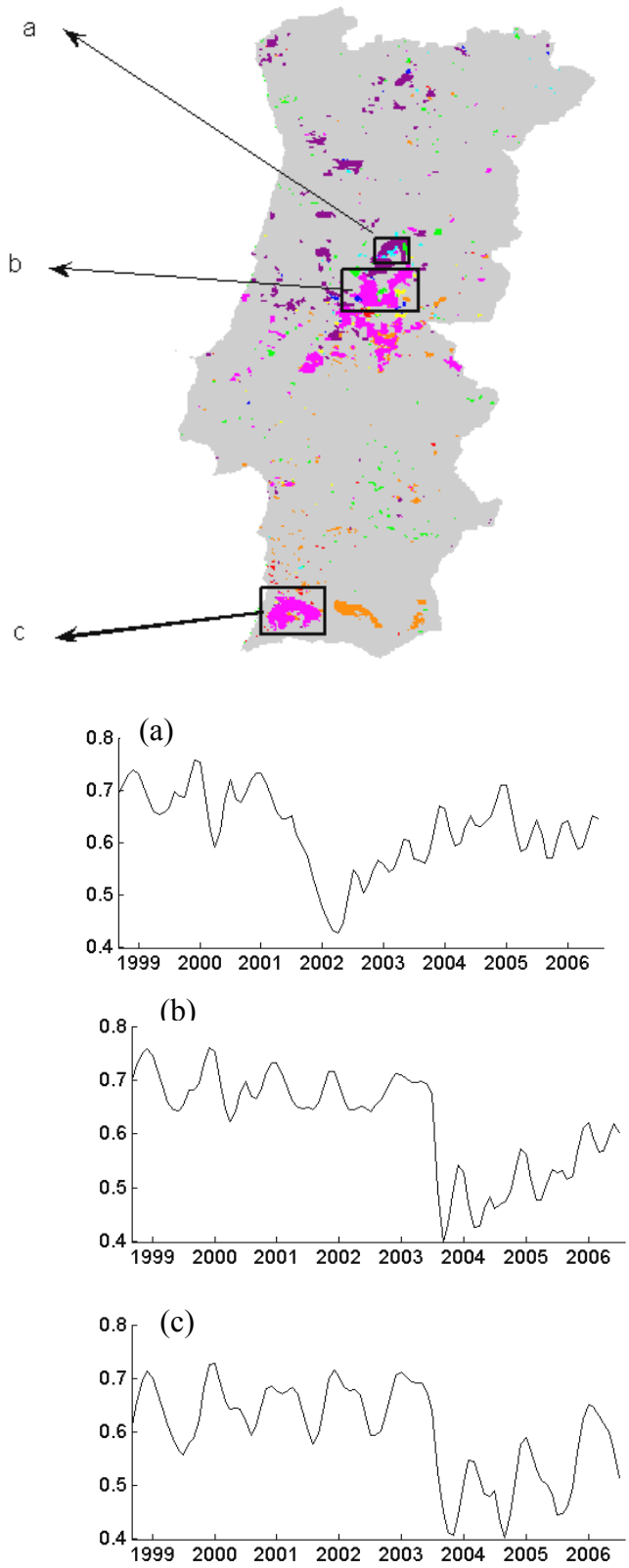

Figure 7.7 Time series of averaged NDVI over three large fire scars, one of them associated to an event in 2001 and the remaining associated to two events in 2003. The location of the selected fire scars is given in the upper panel.

strongly negative anomalies of NDVI that persist during the vegetative cycle of the year that follows the fire event.

Obtained results respecting to burned scars from fire events that have occurred in the period 1998-2005 reveal that the developed methodology leads to an adequate identification of burned areas for years affected by severe wildfires that caused large burned scars. When comparing yearly amounts of burned area by the proposed method with the corresponding ones from the official DGRF database, a systematic underestimation is found, in particular in the case of years of low fire activity. However the methodology based on NDVI anomalies allows monitoring the vegetation recovery in areas affected by large fires.

A case study was performed involving two large burned areas in Central Portugal associated to fire events that took place in 2001 and 2003 and a third one in Algarve associated to a wildfire in 2003. Differences in vegetation recovery are well apparent between the two years and the two locations, which were found to be mainly associated to the meteorological conditions of the following year. In particular it was found that vegetation recovery was slower for the two 2003 burned areas because of the prolonged following drought of 2004/2005, especially in the case of Algarve where the effects of drought were more severe.

8 CONCLUSIONS

Vegetation plays a crucial role in the global carbon balance because of the large amounts of carbon stored in green vegetation. Over the last two decades, continuous monitoring of vegetation from space has prompted new studies aiming to relate observed major global changes in vegetation (e.g. trends, variability and extremes) with changes in surface climatic variables, such as temperature and precipitation. Despite the global nature of the problem, studies at the regional and local scales are especially relevant in these contexts due to the socio-economical impacts in land management.

The primary motivation of our work was to contribute to a better understanding of the impact of climate variability on vegetation status and dynamics at the European scale, but in particular at the scale of Continental Portugal. We began by assessing the relationship between vegetation greenness and the NAO index. The study covered the 21-year period of available homogeneous datasets from 1982 to 2002, and was based on monthly composites of NDVI and Brightness Temperature from GIMMS dataset as well as on monthly precipitation from GPCC. A systematic analysis was initially performed of point correlation fields over the 21-year period between the winter NAO index and the spring and summer NDVI. An assessment was then performed on the vegetation response to precipitation and temperature conditions in winter, over two contrasting regions, namely the Iberian Peninsula and Northeastern Europe. The impact of NAO on vegetation dynamics over the two considered regions was finally evaluated by studying the corresponding annual cycles of NDVI and then comparing their behaviour for years associated with opposite NAO phases.

There is strong evidence that positive (negative) values of winter NAO induce low (high) vegetation activity, over the Iberian Peninsula, in the following spring and summer seasons. This feature is mainly associated with the impact of NAO on winter precipitation, together with the strong dependence of spring and summer vegetation on water availability during the previous winter. In Iberia, the NAO impact is larger on non-forested vegetation, which responds quickly to spatio-temporal variations in precipitation and soil moisture. During summer, forests and other dense vegetation areas

display the highest sensitivity to NAO dynamics, as well as a slower response to precipitation, the NAO impacts being delayed until late in the year. Obtained results, in particular those related to the relationships found between winter NAO and NDVI for spring and summer represent an added value since they allow formulating simple outlooks of vegetation greenness that may provide useful information for a wide range of application, such as crop forecasting and long-lead wild fire assessment.

In this context, we have further investigated how variations in vegetation greenness over Continental Portugal might be related with NDVI as derived from the GIMMS database. We have focused on wheat yield for the period 1982-1999 and strongly negative correlations were found between wheat yield and spring NDVI over the wheat production area located in Southern Portugal (Alentejo). The impact of meteorological factors on wheat yield over this region was also assessed by computing monthly correlations of detrended anomalies of yield with net short-wave radiation, temperature and precipitation as well as with NAO. Results obtained indicate that cold temperatures during winter and early spring, precipitation in February and March and solar radiation in March have a positive impact during the growing stage, whereas a larger NAO index in June is beneficial for the maturation stage. Therefore, a simple multi-linear regression model was built up using, as predictors, the values of spring NDVI and NAO in June. Simple and cross-validation have confirmed that the performance of such a straightforward model can be quite satisfactory, with a general agreement between observed and modelled wheat yield.

NDVI fields as derived from the VEGETATION instrument were also used to monitor drought episodes. The severity of a given drought episode was assessed by evaluating the cumulative impact over time of drought conditions on vegetation. Special attention was given to the drought episode of 2005, as well as to those that took place in 1999 and 2002. The impact of soil moisture on vegetation dynamics was also evaluated by studying the annual cycle of SWI *vs*. NDVI and by analysing monthly anomalies of SWI. While in the case of the drought episode of 1999 the scarcity of water in the soil persisted until spring, in the recent episode of 2005 the deficit in greenness was already apparent at the end of summer. The impact of dry periods on vegetation was clearly observed in both arable land and forest, and it was found that arable land presented a higher sensitivity.

Persistence of negative anomalies of NDVI was also used to develop a procedure aiming to identify burned scars and assess vegetation recovery over areas stricken by wildfires. Obtained results indicated that the developed methodology is adequate to identify large burned areas. The vulnerability of land cover to wildfire was also assessed and a strong contrast was found between forest and shrubland vs. arable land and crops. The high percentage of burned pixels that were found to belong to the transitional woodland-shrub class may provide and indication of the repeated occurrence of wildfires, which may accelerate the switch of forest into shrub-woodland vegetation, with important consequences in a country where transitional woodland-shrub vegetation is the third more frequent land cover. The developed methodology based on persistent NDVI anomalies also allowed monitoring vegetation recovery in areas affected by large fires. Evidence was found that vegetation recovery may strongly depend on the meteorological conditions of the following year. In fact, vegetation recovery was especially slow in 2003 because of the following drought of 2004/2005, in particular in the case of Algarve where the effects of drought were more severe.

The main conclusions from our study may be summarized as follows:

- the impact of climate variability on vegetation dynamics, as response to precipitation and temperature conditions in winter, is well apparent in Iberian Peninsula and Northeastern Europe;
- there is strong evidence that positive (negative) values of winter NAO induce low (high) vegetation activity, over the Iberian Peninsula, in the following spring and summer seasons;
- the lagged relation between winter NAO and spring and summer NDVI may be used to build-up models of crop forecasting and long-lead fire assessment;
- the impact of climate variability on wheat yield in Portugal may be used to build-up models of wheat yield;
- drought conditions in Portugal may be adequately monitored using remote sensed information and drought severity may be assessed based on the persistence of NDVI anomalies;
- persistent anomalies of NDVI may be also used to identify burned areas and to assess vegetation recovery after large wildfires.

REFERENCES

Alley, W.M., 1984: The Palmer Drought Severity Index: Limitations and assumptions. *Journal of Climate and Applied Meteorology*, **23**, 1100–1109.

Atkinson, M.D., Kettlewell, P.S., Hollins, P.D, Stephenson, D.B. and Hardwick, N.V., 2005: Summer climate mediates UK wheat quality response to winter North Atlantic Oscillation. *Agricultural and Forest Meteorology*, **130**, 27–37.

Barnston, A.G., Livezey, R.E., 1987: Classification, Seasonality and Persistence of Low-Frequency Atmospheric Circulation Patterns. *Monthly Weather Review*, **115**, 1083-1126.

Bayarjargal, Y., Karnieli, A., Bayasgalan, M., Khudulmur, S., Gandush, C. and Tucker, C.J., 2006: A comparative study of NOAA-AVHRR derived drought indices using change vector analysis. *Remote Sensing of Environment*, **105**(1), 9-22.

Benson, B.J., and MacKenzie, M.D., 1995: Effects of sensor spatial resolution on landscape structure parameters. *Landscape Ecology*, **10**, 113-120.

Blenckner, T, Hillebrand, H., 2002: North Atlantic Oscillation signatures in ecosystems - a meta-analysis. *Global Change Biology*, **8**, 203-212.

Bogaert, J, Zhou, L, Tucker, C.J., Myneni, R.B., Ceulemans, R., 2002: Evidence for a persistent and extensive greening trend in Eurasia inferred from satellite vegetation index data. *Journal of Geophysical Research*, **107**(D11), DOI: 10.1029/2001JD00107.

Boken, V.K. and Shaykewich, C.F., 2002: Improving an operational wheat yield model using phonological phase-based Normalized Difference Vegetation Index. *International Journal of Remote Sensing*, **23**(20), 4155–4168.

Bonifacio, R., Dugdale, G. and Milford, J.R., 1993: Sahelian rangeland production in relation to rainfall estimates from Meteosat. *International Journal of Remote Sensing*, **14**, 2695–2711.

Briffa, K.R., Jones, P.D. and Hulme, M., 1994: Summer moisture variability across Europe, 1892–1991: an analysis based on the Palmer drought severity index. *International Journal of Climatology*, **14**, 475–506.

Brooks, M.L. and Pyke, D.A., 2001: Invasive plants and fire in the deserts of North America. In K. Galley and T. Wilson (Eds.), *Fire Conference 2000: The First National Congress on Fire, Ecology, Prevention and Management. Invasive Species Workshop: The Role of Fire in the Control and Spread of Invasive Species* (pp. 1-14). Tallahassee: Tall Timbers Research Station.

Buermann, W., Anderson, B., Tucker, C.J., Dickinson, R.E., Lucht, W., Potter, C.S. and Myneni, R.B., 2003: Interannual covariability in Northern Hemisphere air temperatures and greenness associated with El Niño-southern oscillation and the Arctic Oscillation. *Journal of Geophysical Research*, **108**, 4396, DOI:10.1029/2002JD002.

Bussay, A., Szinell, C., Szentimery, T., 1999: Investigation and Measurements of Droughts in Hungary. Hungarian Meteorological Service: Budapest.

Castro-Díez, Y., Pozo-Vázquez, D., Rodrigo, F.S. and Esteban-Parra, M.J., 2002: NAO and winter temperature variability in southern Europe. *Geophysical Research Letters*, **29**, DOI:10.1029/ 2001GL014042.

Cerda, A., 1998a: Changes in overland flow and infiltration after a rangeland fire in a Mediterranean scrubland. *Hydrological Processes*, **12**, 1031–1042.

Cerda, A., 1998b: Postfire dynamics of erosional processes under Mediterranean climatic conditions. *Zeitschrift für Geomorphologie*, **42**, 373–398.

Cerda, A. and Doerr, S.H., 2005: The influence of vegetation recovery on soil hydrology and erodibility following fire: an eleven year investigation. *International Journal of Wildland Fire*, **14**(4), 423–437.

Chatterjee, S., Hadi, A.S., 1986: Influential observations, high leverage points, and outliers in linear regression. *Statistical Science*, **1**(3), 379-416.

Chen, J.M. and Cihlar, J., 1996: Retrieving leaf area index for boreal conifer forests using Landsat TM images. *Remote Sensing of Environment*, **55**, 153-162.

Ciais, Ph., Reichstein, M., Viovy, N., Granier, A., Ogée, J., Allard, V., Aubinet, M., Buchmann, N., Bernhofer, Chr., Carrara, A., Chevallier, F., De Noblet, N., Friend,

A.D., Friedlingstein, P., Grünwald, T., Heinesch, B., Keronen, P., Knohl, A., Krinner, G., Loustau, D., Manca, G., Matteucci, G., Miglietta, F., Ourcival, J.M., Papale, D., Pilegaard, K., Rambal, S., Seufert, G., Soussana, J.F., Sanz, M.J., Schulze, E.D., Vesala, T. and Valentini, R., 2005: Europe-wide reduction in primary productivity caused by the heat and drought in 2003. *Nature*, **437**, 529–533.

Colwell, R.N., 1997: History and Place of Photographic Interpretation. In M.D. Bethesda (Ed.), *Manual of Photographic Interpretation* (pp. 33–48). American Society for Photogrammetry & Remote Sensing.

Cook, B.I., Mann, M.E., D'Odorico, P. and Smith, T.M., 2004: Statistical simulation of the influence of the NAO on European winter surface temperatures: Applications to phenological modeling. *Journal of Geophysical Research*, **109**(D16106), DOI:10.1029/2003JD004305.

Cracknell, A.P., 1998: Synergy in remote sensing – what's in a pixel?. International *Journal of Remote Sensing*, **19**(11), 2025-2047.

Crippen, R.E., 1987: The Regression Intersection Method of Adjusting Image Data for Band Ratioing. *International Journal of Remote Sensing*, **8**, 137-155.

Davidson, E.A. and Janssens, I.A., 2006: Temperature sensitivity of soil carbon decomposition and feedbacks to climate change. *Nature*, **440**, 165–173.

DeBano, L.F., Neary, D.G. and Ffolliott, P.F., 1998: *Fire's Effects on Ecosystems*. John Wiley and Sons, Inc., New York, 333 pp.

DeMelo, R.W., Fontana, D.C., Berlato, M.A. and Ducati, J.R., 2008: An agrometeorological-spectral model to estimate soybean yield, applied to southern Brazil. *International Journal of Remote Sensing*, **29**(14), 4013- 4028.

Denman, K.L., Brasseur, G., Chidthaisong, A., Ciais, P., Cox, P.M., Dickinson, R.E., Hauglustaine, D., Heinze, C., Holland, E., Jacob, D., Lohmann, U., Ramachandran, S, da Silva Dias, P.L., Wofsy, S.C. and Zhang, X., 2007: Couplings Between Changes in the Climate System and Biogeochemistry. In S. Solomon, D. Qin, M. Manning, Z. Chen, M. Marquis, K.B. Averyt, M. Tignor and H.L. Miller (Eds.), *Climate Change 2007: The Physical Science Basis. Contribution of Working Group I to the Fourth Assessment Report of the Intergovernmental Panel on Climate Change*

(pp. 499-587). Cambridge University Press, Cambridge, United Kingdom and New York, NY, USA. Available at: http://ipcc-wg1.ucar.edu/wg1/wg1-report.html.

Díaz-Delgado, R., Salvador, R. and Pons, X., 1998: Monitoring of plant community regeneration after fire by remote sensing. In L. Traboud (Ed.), *Fire management and landscape ecology* (pp. 315-324). International Association of Wildland Fire, Fairfield, WA.

Díaz-Delgado, R., Lloret, F., Pons, X. and Terradas, J., 2002: Satellite evidence of decreasing resilience in Mediterranean plant communities after recurrent wildfires. *Ecology*, **83**(8), 2293–2303.

Diouf, A. and Lambin, E.F., 2001: Monitoring land-cover changes in semi-arid regions: Remote sensing data and field observations in the Ferlo, Senegal. *Journal of Arid Environments*, **48**, 129 148.

D'Odorico, P., Yoo, J.C. and Jaeger, S., 2002: Changing seasons: an effect of the North Atlantic Oscillation? *Journal of Climate*, **15**, 435-445.

Drury, S., 1987: Display and enhancement of gridded aeromagnetic data of the Solway Basin. *International Journal of Remote Sensing*, **8**(10), 1433-1444.

Dube, O.P., 2007: Fire Weather and Land Degradation. In Springer Berlin Heidelberg (Ed.), *Climate and Land Degradation* (pp. 223-251). ISBN 978-3-540-72437-7. DOI 10.1007/978-3-540-72438-4

Eagleson, P., 2002: *Ecohydrology. Darwinian expression of vegetation form and function*. Cambridge University Press, Cambridge, 2002.

EEA, 2001: Sustainable water use in Europe, Part 3: extreme hydrological events: floods and droughts. Environmental Issue Report No. 21. European Environment Agency.

EPSG, 2002: Coordinate Conversions and Transformations including Formulas, Guidance Note Number 7, Petrochemical Open Software Corporation (POSC). Available at: http://www.ihsenergy.com/epsg/guid7.pdf

Estrela, M.J., Penarrocha, D. and Mill´ na, M,. 2000: Multi-annual drought episodes in the Mediterranean (Valencia region) from 1950–1996. A spatio-temporal analysis. *International Journal of Climatology*, **20**, 1599–1618.

Fang, H., Liang, S., Hoogenboom, G., Teasdale, J. and Cavigelli, M., 2008: Corn-yield estimation through assimilation of remotely sensed data into the CSM-CERES-Maize model. *International Journal of Remote Sensing*, **29**(10), 3011-3032.

Feio, M. and Henriques, V., 1986: As secas de 1980–81 e de 1982–83 e as principais secas anteriores – intensidade e distribuição regional. *Memórias do Centro de Estudos Geográficos*, **10**, 7–113.

Feio, M., 1991: Clima e Agricultura. Ministério da Agricultura, Pescas e Alimentação.

Gámiz-Fortis, S.D., Pozo-Vázquez, D., Rodrigo, F.S., Esteban-Parra, M.J. and Castro-Díez, Y., 2002: Spectral characteristics and predictability of the NAO assessed through Singular Analysis. *Journal of Geophysical Research*, **107**, 4685. DOI:10.1029/2001JD001436.

Garcia-Herrera, R., Paredes, D., Trigo, R.M., Trigo, I.F., Hernández, H., Barriopedro D. and Mendes, M.T., 2007: The outstanding 2004-2005 drought in the Iberian Peninsula: the associated atmospheric circulation. *Journal of Hydrometeorology*, (in press).

Gibb, O, Penman, H.L., Pereier, H.C. and Ratcliffe, R.A.S., 1978: *Scientific Aspects of the 1975–76 Drought in England and Wales*. The Royal Society: London.

Gilbert, E.N., 1974: Distortion in maps. SIAM Review, **16**(1), 47-62.

Gimeno, L., Ribera, P., Iglesias, R., Torre, L., Garcia, R. and Hernández, E, 2002: Identification of empirical relationships between indices of ENSO and NAO and agricultural yields in Spain. *Climate Research*, **21**, 165–172.

Gobron, N., Pinty, B. and Verstraete, M.M., 1997: Theoretical Limits to the Estimation of the Leaf Area Index on the Basis of Visible and Near-Infrared Remote Sensing Data. *IEEE Transactions on Geoscience and Remote Sensing*, **35**, 1438-1445.

Gobron, N., Pinty, B., Verstraete, M.M. and Widlowski, J.-L., 2000: Advanced Vegetation Indices Optimized for Up-Coming Sensors: Design, Performance and Applications. *IEEE Transactions on Geoscience and Remote Sensing*, **38**, 2489-2505.

Gobron, N., Mélin, F., Pinty, B., Verstraete, M.M., Widlowski, J.-L., and Bucini, G., 2001: A Global Vegetation Index for SeaWiFS: Design and Applications. In M.

Beniston and M. M. Verstraete (Eds.), *Remote Sensing and Climate Modelling: Synergies and Limitations* (pp. 5-21). Kluwer Academic Publishers, Dordrecht.

Gobron, N., Pinty, B., Mélin, F., Taberner M. and Verstraete, M.M., 2002: Sea Wide Field-of-View Sensor (SeaWiFS) - An Optimized FAPAR Algorithm - Theoretical Basis Document. EUR Report No. 20148 EN (pp. 20), Institute for Environment and Sustainability.

Gobron, N., Pinty, B., Mélin, F., Taberner M., Verstraete, M.M., Belward, A., Lavergne, T. and Widlowski, J.-L., 2005: The state of vegetation in Europe following the 2003 drought. *International Journal of Remote Sensing Letters*, **26**, 2013–2020.

Godinho, S.F., Mendes, J.C. and Reis, R.M., 1992: A Situação de Seca em Portugal iniciada no Inverno de 1991/92. *Ambiente*, **6**, 18–25.

Gouveia, C. and Trigo, R.M., 2008: Infuence of Climate Variability on Wheat Production in Portugal. In A. Soares, M.J. Pereira and R. Dimitrakopoulos (Eds.), *geoENV VI -Geostatistics for Environmental Applications* (pp.335-345). Springer.

Govaerts, Y.M., Verstraete, M.M., Pinty, B. and Gobron, N., 1999: Designing optimal spectral indices: A feasibility and proof of concept study. *International Journal of Remote Sensing*, **20**, 1853–1873.

Groisman, P.Y., Karl, T.R. and Knight, R.W., 1994: Observed impact of snow cover on the heat balance and the rise of continental spring temperatures. *Science*, **263**, 198-200.

Hagolle, O., Lobo, A., Maisongrande, P., Duchemin, B., and De Pereira, A., 2005: Quality assessment and improvement of SPOT/VEGETATION level temporally composited products of remotely sensed imagery by combination of VEGETATION 1 & 2 images. *Remote Sensing of Environment*, **94**(2), 172–186.

Hansen, J., Ruedy, R., Glascoe, J., Sato, M., 1999: GISS analysis of surface temperature change. *Journal of Geophysical Research*, **104**, 30997-31022.

Heimann, M. and Reichstein, M., 2008: Terrestrial ecosystem carbon dynamics and climate feedbacks. *Nature*, **451**, 289-292.

Henry, M.C. and Hope, A.S., 1998: Monitoring post-burn recovery of chaparral vegetation in southern California using multitemporal satellite data. *International Journal of Remote Sensing*, **19**(16), 3097–3107.

Holben, B.N., Tucker C.J. and Fan, C-J., 1980: Spectral Assessment of Soybean Leaf Area and Leaf Biomass. *Photogrammetric Engineering and Remote Sensing*, **46**, 651-656.

Holben, B.N., 1986: Characteristics of maximum-value composite images from temporal AVHRR data. International *Journal of Remote Sensing*, **7**, 1417–1434.

Holmgren, M. and Scheffer, M., 2001: El Niño as a window of opportunity for the restoration of degraded arid ecosystems. *Ecosystems*, **4**, 151-159.

Holmgren, M., Stapp, P., Dickman, C.R., Gracia, C., Grahams, S., Gutierrez, J.R., Hice, C., Jaksic, F., Kelt, D.A., Letnic, M., Lima, M., Lopez, B.C., Meserve, P.L., Milstead, W.B., Polis, G.A., Previtali, M.A., Michael, R., Sabate, S., and Squeo, F.A., 2006: Extreme climatic events shape arid and semiarid ecosystems. *Frontiers in Ecology and the Environment*, **4**, 87–95.

Hoogenboom, G, 2000: Contribution of agrometeorology to the simulation of crop production and its applications. *Agricultural and Forest Meteorology*, **103**, 137-158.

Huang, N.E., Shen, Z., Long, S.R., Wu, M.C., Shih, H.H., Zheng, Q., Yen, N.-C., Tung, C.C. and Liu, H.H., 1998: The empirical mode decomposition and the Hilbert spectrum for nonlinear and non-stationary time series analysis. Proceedings from the Royal Society of London, **545**, 903-995.

Huang, N.E., Shen, Z. and Long, S.R., 1999: A new view of nonlinear water waves: the Hilbert spectrum. *Annual Review of Fluid Mechanics*, **31**, 417-457.

Huete, A.R. and Tucker, C.J., 1991: Investigation of soil influences on AVHRR red and near-infrared vegetation index imagery. *International Journal of Remote Sensing*, **12**, 1223 1242.

Hurrell, J.W., 1995: Decadal trends in the north Atlantic oscillation: regional temperatures and precipitation. *Science*, **269**, 676–679.

Iglesias, A., Quiroga, S., 2007: Measuring the risk of climate variability to cereal production at five sites in Spain. *Climate Research*, **34**, 47–57.

Iglesias, E., Garrido, A. and Gomez-Ramos, A., 2003: Evaluation of drought management in irrigated areas. *Agricultural Economics*, **29**, 211–229.

Illera, P., Fernandez, A. and Delgado, J.A., 1996: Temporal evolution of the NDVI as an indicator of forest fire danger. *International Journal of Remote Sensing*, **17**(6): 1093–1105.

Inbar, M., Wittenberg, L. and Tamir, M., 1997: Soil erosion and forestry management after wildfire in a Mediterranean woodland, Mt. Carmel, Israel. *International Journal of Wildland Fire*, **7**(1997), 285–294.

Inbar, M., Tamir, M. and Wittenberg, L., 1998: Runoff and erosion processes after a forest fire in Mount Carmel, a Mediterranean area. *Geomorphology*, **24**(1) (1998), 17–33.

Jakubauskas, M., Lulla, K.P., and Mausel, P.W., 1990: Assessment of vegetation change in a fire-altered forest landscape. *Photogrammetric Engineering & Remote Sensing*, **56**, 371-377.

Jensen, J.R., 2005: *Introductory Digital Image Processing: A Remote Sensing Perspective*. 3rd Edition. Prentice Hall Inc., 526pp.

Jensen, J.R., 2007: *Remote Sensing of the Environment: An Earth Resource Perspective*. 2nd Edition. Prentice-Hall, Inc., Saddle River, N.J., 544 pp.

Ji, L. and Peters, A.J., 2003: Assessing vegetation response to drought in the northern Great Plains using vegetation and drought indices. *Remote Sensing of Environment*, **87**, 85-98.

Jones, P.D., Johnson, T. and Wheeler, D., 1997: Extension to the North Atlantic Oscillation using instrumental pressure observations from Gibraltar and south-west Iceland. *International Journal of Climatology*, **17**, 1433–1450.

Justice, C., Dorn, B., Hansen, M., Tucker, J., Anyamba, A., Sullivan, M. and Reshef, I., 2005: Global Agricultural Monitoring: Science Information to Inform Decision Making. U.S. Climate Change Science Program (CCSP) Workshop on Climate Science in Support of Decision Making, Arlington, Virgina, 14-16 November 2005.

Karl, T., 1986: The sensitivity of the Palmer drought severity index and Palmer's Z-index to their calibration coefficients including potencial evapotranspiration. *Journal of Climate and Applied Meteorology*, **25**, 77-86.

Karnieli, A., Shachak, M., Tsoar, H., Zaady, E., Kaufman, Y., Danin, A. and Porter, W., 1996: The effect of Microphytes on the spectral reflectance of vegetation in semi-arid regions. *Remote Sensing of Environment*, **57**, 88–96

Kaufmann, R.K., Zhou, L., Knyazikhin, Y., Shabanov, N., Myneni, R.B. and Tucker, C.J., 2000: Effect of orbital drift and sensor changes on the time series of AVHRR vegetation index data. *IEEE Transactions Geoscience and Remote Sensing*, **38**, 2584–2597.

Kaufmann, R.K., Zhou, L., Tucker, C.J., Slayback, D., Shabanov, N.V. and Myneni, R.B., 2002: Reply to Comment on 'Variations in northern vegetation activity inferred from satellite data of vegetation index during 1981-1999 by J.R. Ahlbeck. *Journal of Geophysical Research*, **107**(D11), DOI:10.1029/2001JD001516.

Keeling, C.D., Chin, J.F.S. and Whorf, T.P., 1996: Increased activity of northern vegetation inferred from atmospheric CO2 measurements. *Nature*, **382**, 146-149.

Knapp, A.K., Fay, P.A., Blair, J.M., Collins, S.L., Smith, M.D., Carlisle, J.D., Harper, C.W., Danner, B.T., Lett, M.S. and McCarron, J.K., 2002: Rainfall variability, carbon cycling, and plant species diversity in a mesic grassland. *Science*, **298**, 2202–2205.

Kogan, F.N., 1995: Application of vegetation index and brightness temperature for drought detection. *Advances in Space Research*, **11**, 91-100.

Kogan, F.N., 1997. Global drought watch from space. *Bulletin of the American Meteorological Society*, **78**, 621-636.

Kogan, F.N., 2000. Contribution of remote sensing to drought early warning. In D.A. Wilhite, M.V.K. Sivakumar and D.A. Wood (Eds.), *Early warning systems for drought preparedness and drought management: Proceedings of an Expert Group Meeting, 5–7 September, Lisbon, Portugal* (pp. 86-100). Geneva, Switzerland: WMO.

Kogan, F.N., Usa, D.C., Stark, R., Gitelson, A., Jargalsaikhan, L. and Dugarjav, C., 2004: Derivation of pasture biomass in Mongolia from AVHRR-based vegetation health indices. *International Journal of Remote Sensing*, **25**, 2889 2896.

Kutiel, P., 1994: Fire and ecosystem heterogeneity: a Mediterranean case study. *Earth Surface Processes and Landforms*, **19**, 187–194.

Lana, X., Serra, C. and Burgueño, A., 2001: Patterns of monthly rainfall shortage and excess in terms of the standardized precipitation index. *International Journal of Climatology*, **21**, 1669–1691.

Le Page, Y., Pereira, J.M.C., Trigo, R.M., DaCamara, C.C., Oom, D., and Mota, B., 2008: Global fire activity patterns (1996-2006) and climatic influence: an analysis using the World Fire Atlas. *Atmospheric Chemistry and Physics*, **8**, 1911-1924.

Li, Y., Demetriades-Shah, T.H., Kanemasu, E.T., Shultis, J.K. and Kirkham, M.B., 1993: Use of Second Derivatives of Canopy Reflectance for Monitoring Prairie Vegetation Over Different Soil Backgrounds. *Remote Sensing of Environment*, **44**, 81-87.

Lloyd-Hughes, B. and Saunders, M.A., 2002: A drought climatology for Europe. *International Journal of Climatology*, **22**(13), 1571-1592.

Los, S.O., 1998: Estimation of the ratio of sensor degradation between NOAA-AVHRR channels 1 and 2 from monthly NDVI composites. *IEEE Transactions on Geoscience and Remote Sensing*, **36**, 206-213.

Los, S.O., 1998: Linkages between global vegetation and climate: an analysis based on NOAA-Advanced Very High Resolution Radiometer Data. Doctoral Thesis, Vrije Universiteit, Amsterdam.

Lotsch, A., Tian, Y., Friedl, M.A. and Myneni, R.B., 2003: Land cover mapping in support of LAI/FPAR retrievals from EOS-MODIS and MISR: Classification methods and sensitivities to errors. *International Journal of Remote Sensing*, **24**, 1997-2016.

Lucht, W.I., Colin Prentice, W.I., Myneni, R.B., Sitch, S., Friedlingstein, P., Cramer, W., Bousquet, P., Buermann, W., and Smith, B., 2002: Climatic Control of the High-Latitude Vegetation Greening Trend and Pinatubo Effect. *Science*, **296**, 1687–1688.

MADRP, 2005: Relatório de balanço da seca. Ministério da Agricultura do Desenvolvimento Rural e Pescas, Lisboa.

Malingreau, J.P., Stephens, G. and Fellows, L., 1985: Remote sensing of forest fires: Kalimantan and North Borneo in 1982–83. *Ambio*, **14**, 314–321.

Malingreau, J.P., 1986: Global vegetation dynamics: Satellite observations over Asia. *International Journal of Remote Sensing*, **9**, 1121 1146.

Marsh, T.J., Lees, M.L., 1985: *The 1984 Drought*. Institute of Hydrology: Wallingford, UK.

Maytelaube, P., Terres, J.-M. and Doblas-Reyes, F.J., 2004: Influence of climate variability on European agriculture —analysis of winter wheat production. *Climate Research*, **27**, 135–144.

McVicar, T.R., and Jupp, D.L.B., 1998: The current and potential operational uses of remote sensing to aid decisions on drought exceptional circumstances in Australia: A review. *Agricultural Systems*, **57**, 399-468.

McVicar, T.R. and Jupp, D.L.B., 1999: Estimating one-time-of-day meteorological data from standard daily data as inputs to thermal remote sensing based energy balance models. *Agriculture and Forest Meteorology*, **96**, 219-238.

McVicar, T.R. and Jupp, D.L.B., 2002: Using covariates to spatially interpolate moisture availability in the Murray-Darling Basin: A novel use of remotely sensed data. *Remote Sensing of Environment*, **79**, 199-212.

Menzel, A., 2003: Plant Phenological Anomalies in Germany and their Relation to Air Temperature and NAO. *Climatic Change*, **57**, 243-263.

Michelsen, A., Andersson, M., Jensen, M., Kjøller, A. and Gashew, M., 2004: Carbon stocks, soil respiration and microbial biomass in fire-prone tropical grassland, woodland and forest ecosystems. *Soil Biology & Biochemistry*, **36**, 1707-1717.

Miranda, P.M.A., Valente, M.A., Tomé, A.R., Trigo, R., Coelho, M.F., Aguiar, A. and Azevedo E.B., 2006: O Clima de Portugal nos séculos XX e XXI. In Santos, F.D., Forbes K. and Moita R. (Eds.), *Climate Change in Portugal: Scenarios, Impacts and Adaptation Measures - SIAM II Project* (pp. 47-113). Gradiva, Lisbon.

Mitchell,T.D. and Jones, P.D., 2005: An improved method of constructing a database of monthly climate observations and associated high-resolution grids. *International Journal of Climatology*, **25**, 693-712.

Moik, J.G., 1980: *Digital Processing of Remotely Sensed Images*. Washington D.C., NASA, U.S. Government Printing Office, 330 pp.

Morales, A., Olcina, J. and Rico, A.M., 2000: Diferentes percepciones de la sequía en España: adaptación, catastrofismo e intentos de corrección (The different perceptions

about droughts in Spain: adaptations and correction systems, in Spanish). *Investigaciones Geográficas*, **23**, 5–46.

Myneni, R.B. and Williams, D.L., 1994: On the relationship between FPAR and NDVI. *Remote Sensing of Environment*, **49**, 200–211.

Myneni, R.B., Keeling, C.D., Tucker, C.J., Asrar, G. and Nemani, R.R., 1997. Increase plant growth in the northern high latitudes from 1981-1991. *Nature*, **386**, 698-702.

Neitsch, S.L., Arnold, J.G., Kiniry, J.R., Williams, J.R. and Kiniry, K.W., 2002: Soil and Water Assessment Tool theoretical documentation. TWRI report TR-191, Texas Water Resources Institute, College Station.

Nemani, R.R., Charles, D., Keeling, C.D., Hashimoto, H., Jolly, W.M., Piper, S.C., Tucker, C.J., Myneni, R.B. and Running, S.W., 2003: Climate-Driven Increases in Global Terrestrial Net Primary Production from 1982 to 1999. *Science*, **300**, 1560–1563.

New, M., Hulme, M. and Jones, P.D., 1999: Representing twentieth century space-time climate variability. Part 1: development of a 1961-90 mean monthly terrestrial climatology. *Journal of Climate*, **12**, 829-856.

New, M., Hulme, M. and Jones, P.D., 2000: Representing twentieth century space-time climate variability. Part 2: development of 1901-96 monthly grids of terrestrial surface climate. *Journal of Climate*, **13**, 2217-2238.

Nicholson, S.E., Davenport, M.L., and Malo, A.R., 1990: A comparison of the vegetation response to rainfall in the Sahel and east Africa, using normalized difference vegetation index from NOAA-AVHRR. *Climatic Change*, **17**, 209–241.

Nicholson, S.E., and Farrar, T.J., 1994. The influence of soil type on the relationships between NDVI, rainfall, and soil moisture in semiarid Botswana: I. NDVI response to rainfall. *Remote Sensing of Environment*, **50**, 107 120.

Nicholson, S.E., Tucker, C.J., and Ba, M.B., 1998: Desertification, drought and surface vegetation: An example from the West African Sahel. *Bulletin of the American Meteorological Society*, **79**, 815-829.

Osborn, T.J., Briffa, K.R., Tett, S.F.B., Jones, P.D., and Trigo, R.M., 1999: Evaluation of the North Atlantic Oscillation as simulated by a climate model. *Climate Dynamics*, **15**, 685–702.

Palmer, W.C., 1965: Meteorological drought. Research Paper No. 45, U.S. Department of Commerce Weather Bureau, Washington, D.C.

Paltridge, G.W. and Barber, J., 1988: Monitoring grassland dryness and fire potential in Australia with NOAA–AVHRR data. *Remote Sensing of Environment*, **25**, 381–394.

Paredes D., Trigo, R.M., Garcia-Herrera, R., Trigo, I.F., 2006: Understanding precipitation changes in Iberia in early Spring: weather typing and storm-tracking approaches. *Journal of Hydrometeorology*, **7**, 101-113.

Pausas, G.J. and Vallejo, V.R., 1999: The role of fire in European Mediterranean Ecosystems. In: E. Chuvieco (Ed.), *Remote sensing of large wildfires in the European Mediterranean basin* (pp. 3–16). Springer–Verlag (1999).

Pereira, J.S., Pereira, J.M.C., Rego, F.C., Silva, J.M.N. and Silva, T.P., 2006*: Incêndios florestais em Portugal: caracterização, impactes e prevenção*. ISA Press, Lisboa.

Pettorelli, N., Vik, J.O, Mysterud, A., Gaillard, J.-M. Tucker, C. J., Stenseth, N. C., 2005: Using the satellite-derived NDVI to assess ecological responses to environmental change. *Trends in Ecology and Evolution*, **20**, 503-510.

Phillips, I.D. and McGregor, G.R., 1998: The utility of a drought index for assessing the drought hazard in Devon and Cornwall, South West England. *Meteorological Applications*, **5**, 359–372.

Piao, S., Ciais, P., Friedlingstein, P., Peylin, P., Reichstein, M., Luyssaert, S., Margolis, H., Fang, J., Barr, A., Chen, A,. Grelle, A., Hollinger, D.Y., Laurila, T., Lindroth, A., Richardson, A.D., and Vesala, T., 2008: Net carbon dioxide losses of northern ecosystems in response to autumn warming. *Nature*, **451**, 49-52.

Pielke, R.A., 2001: Influence of the spatial distribution of vegetation and soils on the prediction of cumulus convective rainfall. *Reviews of Geophysics*, **39**, 151–177.

Pinzon, J., Pierce, J.F. and Tucker, C.J., 2001: Analysis of Remote Sensing Data Using Hilbert-Huang Transform. Proceedings from the SCI 2001 Conference, July 22-25, Orlando, Florida, SCI International.

Pinzon, J., 2002: Using HHT to successfully uncouple seasonal and interannual components in remotely sensed data. Proceedings from the SCI 2002 Conference, July 14-18, Orlando, Florida, SCI International.

Pinzon, J., Brown, M.E. and Tucker, C.J., 2004: Satellite time series correction of orbital drift artifacts using empirical mode decomposition. In N. Huang(Ed.), *Hilbert-Huang Transform: Introduction and Applications*. Chapter 10, Part II. Applications.

Pinzon, J., Brown, M.E. and Tucker, C.J., 2005: Satellite time series correction of orbital drift artifacts using empirical mode decomposition. In N. Huang (Ed.), *Hilbert-Huang Transform: Introduction and Applications* (pp. 167-186).

Qian, B., Corte-Real, J. and Xu, H., 2000: Is the North Atlantic oscillation the most important atmospheric pattern for precipitation in Europe? *Journal of Geophysical Research*, **105**, 901–910.

Reichstein, M., Papale, D., Valentini, R., Aubinet, M., Bernhofer, C., Knohl, A., Laurila, T., Lindroth, A., Moors, E., Pilegaard, K. and Seufert, G., 2007: Determinants of terrestrial ecosystem carbon balance inferred from European eddy covariance flux sites. *Geophysical Research Letters*, **34**, L01402.262.

Ricotta, C., Avena, G.C., Olsen, E.R., Ramsey, R.D. and Winn, D.S., 1998: Monitoring the landscape stability of the Mediterranean vegetation in relation to fire with a fractal algorithm. *International Journal of Remote Sensing*, **19**(5), 871–881.

Rodó, X., Baert, E. and Comin, F.A., 1997: Variations in seasonal rainfall in Southern Europe during the present century: relationships with the North Atlantic Oscillation and the El Niño-Southern Oscillation. *Climate Dynamics*, **13**, 275-284.

Rodríguez-Fonseca, B. and Castro, M., 2002: On the connection between winter anomalous precipitation in the Iberian Peninsula and North West Africa and the Summer subtropical Atlantic sea surface temperature. *Geophysical Research Letters*, **29**, DOI:1029/2001GL014421.

Rodríguez-Iturbe, I. and Porporato, A., 2004: *Ecohydrology of water-controlled ecosysytems: Soil Moisture and Plant Dynamics*. Cambridge University Press.

Rodriguez-Puebla, C., Encinas, A.H., Nieto, S. and Garmendia, J., 1998: Spatial and temporal patterns of annual precipitation variability over the Iberian Peninsula. *International Journal of Climatology*, **18**, 299-316.

Rodriguez-Puebla, C., Ayuso, S.M., Frias, M.D. and Garcia-Casado, L.A., 2007: Effects of climate variation on winter cereal production in Spain. *Climate Research*, **34**, 223-232.

Rogers, J.C., 1984: The Association between the North Atlantic Oscillation and the Southern Oscillation in the Northern Hemisphere. *Monthly Weather Review*, **112**, 1999-2015.

Rouse, J.W., Haas, R.H., Schell, J.A., Deering, D.W. and Harlan, J.C., 1974: Monitoring the vernal advancement and retrogradation (greenwave effect) of natural vegetation. NASA/GSFC Type III Final Report, Greenbelt, Md. 371 pp.

Rudolf, B. and Schneider, U., 2005: Calculation of Gridded Precipitation Data for the Global Land-Surface using in-situ Gauge Observations. Proceedings from the 2nd Workshop of the International Precipitation Working Group IPWG, Monterey, October 2004. EUMETSAT, ISBN 92-9110-070-6, ISSN 1727-432X, 231-247.

Saleska, S.R.; Miller, S.D.; Matross, D.M.; Goulden, M.L.; Wofsy, S.C.; da Rocha, H.R.; de Camargo, P.B.; Crill, P.; Daube, B.C.; de Freitas, H.C.; Hutyra, L.; Keller, M.; Kirchhoff, V.; Menton, M.; Munger, J.W.; Pyle, H.E.; Rice, A.H., and Silva, H., 2003: Carbon in Amazon forests: unexpected seasonal fluxes and disturbance induced losses. *Science*, **302**, 1554–1557.

Sáenz, J., Rodriguez-Puebla, C., Fernández, J., Zubillaga, J., 2001: Interpretation of interannual winter temperature variations over southwestern Europe. *Journal of Geophysical Research*, **106**, 20641-20651.

Sampaio, A.J., 1990: A cultura do Trigo. Ministério da Agricultura, Pescas e Alimentação.

Sannier, C.A. D. and Taylor, J.C., 1998: Real-time vegetation monitoring with NOAAAVHRR in Southern Africa for wildlife management and food security assessment. *International Journal of Remote Sensing*, **19**, 621–639.

Saura, S., 2004: Effects of remote sensor spatial resolution and data aggregation on selected fragmentation indices. *Landscape Ecology*, **19**, 197-209

Schmidt, H. and. Karnieli, A., 2000: Remote sensing of the seasonal variability of vegetation in a semi-arid environment. *Journal of Arid Environments*, **45**(1), 43-60.

Schott, J.R.; Henderson-Sellers, A., 1984: Radiation, the atmosphere and satellite sensors. In A. Henderson-Sellers (Ed.), *Satellite sensing of a cloudy atmosphere: Observing the third planet* (pp. 45-89). London, Philadelphia.

Schott, J.R., 1997: *Remote Sensing – the image chain approach*. Oxford University Press, 394 pp.

Schowengerdt, R.A., 1997: *Remote Sensing – models and methods for image processing*. 2nd Edition. Academic Press, 522 pp.

Scipal, K., 2002: Global Soil Moisture Retrieval from ERS Scatterometer Data. Doctoral Thesis, Vienna University of Technology, Austria.

Sellers, P.J., Berry, J.A., Collatz, G.J., Field, C.B. and Hall, F.G., 1992, Canopy reflectance, photosynthesis and transpiration, III. A reanalysis using improved leaf models and a new canopy integration scheme. *Remote Sensing of Environment*, **42**, 1-20.

Sellers, P.J., Los, S.O., Tucker, C.J., Justice, C.O., Dazlich, D.A., Collatz, G.J. and Randall, D.A., 1996: A revised land surface parameterization (SiB2) for atmospheric GCMs. Part 2: The generation of global fields of terrestrial biophysical parameters from satellite data. *Journal of Climate*, **9**, 706–737.

Serreze, M.C., Carse, F., Barry, R.G., Rogers, J.C., 1997: Icelandic Low cyclone activity: climatological features, linkages with the NAO, and relationships with recent changes in the Northern Hemisphere circulation. *Journal Climate*, **10**, 453–464.

Shabanov, N.V., Zhou, L., Knyazikhin, Y., Myneni, R.B., 2002: Analysis of Interannual Changes in Northern Vegetation Activity Observed in AVHRR Data during 1981 to 1994. *IEEE Transactions on Geoscience and Remote Sensing*, **40**, 115-130.

Shakesby, R.A; Coelho, C.O.A., Ferreira, A.D., Terry, J.P. and Walsh, R.P.D., 1993: Wildfire impacts on soil erosion and hydrology in wet Mediterranean forest, Portugal. *International Journal of Wildland Fire*, **3**, 95–110.

Shakesby, R.A., Wallbrink, P.J., Doerr, S.H., English, P.M., Chafer, C.J., Humphreys, G.S., Blake, W.H. and Tomkins, K.M., 2007: Distinctiveness of wildfire effects on soil erosion in south-east Australian eucalypt forests assessed in a global context. *Forest Ecology and Management*, **238**, 347-364.

Sheuyange, A., Oba, G. and Weladji, R.W., 2005: Effects of anthropogenic fire history on Savanna vegetation in North-eastern Namibia. *Journal of Environmental Management*, **75**, 189–198.

Sitch, S., Huntingford, C., Gedney, N., Levy, P.E., Lomas, M., Piao, S.L., Betts, R., Ciais, P., Cox, P., Friedlingstein, P., Jones, C.D., Prentice, I.C., Woodward, F.I., 2008: Evaluation of the terrestrial carbon cycle, future plant geography and climate–carbon cycle feedbacks using 5 Dynamic Global Vegetation Models (DGVMs). *Global Change Biology* (in the press).

Snyder, J.P., 1987: *Map Projections-A Working Manual*. U.S. Geological Survey Professional Paper 1395, Washington, D.C., U.S. Government Printing Office, 383 pp.

Stöckli, R., Vidale, P.L., 2004: European plant phenology and climate as seen in a 20-year AVHRR land-surface parameter dataset. *International Journal of Remote Sensing*, **25**, 3303-3330.

Tanré, D., Holben, B.N. and Kaufman, Y.J., 1992: Atmospheric Correction Algorithms for NOAA-AVHRR products: Theory and Application. *IEEE Transactions on Geoscience and Remote Sensing*, **30**, 231-248.

Thornes, J., 1990: The interaction of erosion and vegetation dynamics in land degradation: spatial outcomes. In J. Thornes (Ed.), *Vegetation and Erosion* (pp. 41–54). Wiley, New York.

Trabaud, L., 1981: Man and fire: impacts on Mediterranean vegetation. In F. di Castri, D.W. Goodall and R.L. Specht (Eds.), *Mediterranean-Type Shrublands* (pp. 523-537). Elsevier, Amsterdam.

Trigo, R.M. and DaCamara, C.C., 2000: Circulation Weather Types and their impact on the precipitation regime in Portugal. *International Journal of Climatology*, **20**, 1559-1581.

Trigo, R.M., Osborn, T.J. and Corte-Real, J.M., 2002: The North Atlantic Oscillation influence on Europe: climate impacts and associated physical mechanisms. *Climate Research*, **20**, 9-17.

Trigo, R.M., Pozo-Vazquez, D., Osborn, T.J, Castro-Diez, Y., Gámis-Fortis, S. and Esteban-Parra, M.J., 2004: North Atlantic Oscillation influence on precipitation,

river flow and water resources in the Iberian Peninsula. *International Journal of Climatology*, **24**, 925-944.

Tucker, C.J., 1979. Red and photographic infrared linear combinations for monitoring vegetation. *Remote Sensing of Environment*, **8**, 127-150.

Tucker, C.J., Pinzon, J.E., Brown, M.E., Slayback, D.A., Pak, E.W., Mahoney, R., Vermote, E.F. and El Saleous N., 2005: An extended AVHRR 8-km NDVI dataset compatible with MODIS and SPOT vegetation NDVI data. *International Journal of Remote Sensing*, **26**(20), 4485-4498.

Turner, M.G., 1989: Landscape ecology: the effect of pattern on process. *Annual Review of Ecology and Systematics*, **20**, 171–197.

Turner, M.G., Dale, V.H. and Gardner, R.H., 1989: Predicting across scales: theory development and testing. *Landscape Ecology*, **3**, 245–252.

Van Loon, H., and Rogers, J.C.: 1978: The seesaw in winter temperatures between Greenland and Northern Europe, Part 1: General description. *Monthly Weather Review*, **106**, 296–310.

Verstraete, M.M. and Pinty, B., 1996: Designing optimal spectral indexes for remote sensing applications. *IEEE Transactions on Geoscience and Remote Sensing*, **34**, 1254-1265.

Vicente-Serrano, S.M. and Heredia-Laclaustra A., 2004: NAO influence on NDVI trends in the Iberian Peninsula (1982-2000). *International Journal of Remote Sensing*, **25**, 2871-2879.

Vicente-Serrano, S.M., Cuadrat-Prats, J.M. and Romo, A., 2006: Early prediction of crop production using drought indices at different time-scales and remote sensing data: application in the Ebro valley (North-East Spain). *International Journal of Remote Sensing*, **27**, 511–518.

Vicente-Serrano, S.M., 2006: Spatial and temporal analysis of droughts in the Iberian Peninsula (1910–2000). *Hydrological Sciences Journal*, **51**, 83–97.

Vicente Serrano, S.M., 2007: Evaluating the Impact of drought using Remote Sensing in a Mediterranean, semi-arid region. *Natural Hazards*, **40**, 17–208, DOI 10.1007/s11069-006-0009-7.

Viedma, O., Meliá, J., Segarra, D. and Garcıa-Haro, J., 1997: Modeling rates of ecosystem recovery after fires using Landsat TM data. *Remote Sensing of Environment*, **61**, 383–398.

Vinnikov, K.Y., Robock, A., Stouffer, R.J., Walsh, J.E., Parkinson, C.L., Cavalieri, D.J., Mitchell, J.F.B., Garrett, D. and Zakharov, V.F., 1999: Global warming and Northern Hemisphere sea ice extent. *Science*, **286**, 1934-1937.

Wagner, W., Noll, J., Borgeaud, M. and Rott, H., 1999a: Monitoring Soil Moisture over the Canadian Prairies with the ERS Scatterometer. *IEEE Transactions on Geoscience and Remote Sensing*, **37**(1), 206-216.

Wagner, W., Lemoine, G., Borgeaud, M. and Rott, H., 1999b: A Study of Vegetation Cover Effects on ERS Scatterometer Data. *IEEE Transactions on Geoscience and Remote Sensing*, **37**(2), 938-948.

Walker, G.T., 1924: Correlations in seasonal variations of weather. *IX Memoirs of India Meteorological Department*, **24**, 275–332.

Wang, J., Rich, P.M. and Price, K.P., 2003: Temporal responses of NDVI to precipitation and temperature in the central Great Plains, USA. *International Journal of Remote Sensing*, **24**, 2345–2364.

Wilhite, D.A., 1993: Understanding the Phenomenon of Drought. *Hydro-Review*, **12**, 136–148.

Wilks, D.S., 1995: *Statistical methods in the atmospheric sciences: an introduction*. Academic Press, 464 pp.

Wittenberg, L., Malkinson, D., Beeri, O., Halutzy, A. and Tesler, N., 2006: Spatial and temporal patterns of vegetation recovery following sequences of forest fires in a Mediterranean landscape, Mt. Carmel Israel. *Catena*, **71**(1), 76-83.

WMO, 2006: Drought monitoring and early warning: Concepts, progress and future challenges. World Meteorological Organization, 26 pp.

Wolf, P.R., 1983: *Elements of Photogrammetry*. 2nd edition, McGraw-Hill, 628 pp.

Wu, J., Shen, W., Sun, W. and Tueller, P.T., 2002: Empirical patterns of the effects of changing scale on landscape metrics. *Landscape Ecology*, **17**, 761–782.

Zhang, X., Wang, X.L. and Corte-Real, J., 1997: On the relationships between daily circulation patterns and precipitation in Portugal. *Journal of Geophysical Research*, **102**, 13495–13507.

Zhao, M., Heinsch, F.A., Nemani, R.R. and Running, S.W., 2005: Improvements of the MODIS terrestrial gross and net primary production global data set. *Remote Sensing of Environment*, **95**, 164–176.

Zhou, L., Tucker, C.J., Kaufmann, R.K., Slayback, D. Shabanov, N.V. and Myneni, R.B., 2001: Variations in northern vegetation activity inferred from satellite data of vegetation index during 1981 to 1999. *Journal of Geophysical Research*, **106**, 20069-20083.